TREATMENT-RESISTANT OPHTHALMOPLEGIA IN MYASTHENIA GRAVIS: EXTRAOCULAR MUSCLE PATHOLOGY, THE ROLE OF TGFβ1 AND THE DERIVATION OF INDUCED PLURIPOTENCY TOWARDS 'DISEASE-IN-A-DISH' MODELING.

Dr Robyn Marié Rautenbach
RTNROB001

Thesis presented for the degree of

MSc (MEDICINE)

In the Department of Medicine & Human Biology

Faculty of Health Sciences

UNIVERSITY OF CAPE TOWN

February 2016

Supervisor: Associate Professor Jeannine Heckmann

Co-supervisor: Dr Robea Ballo

DECLARATION

I, Robyn Marié Rautenbach, hereby declare that the work on which this dissertation is based is my original work (apart from the normal guidance from my supervisor/s and except where acknowledgements indicate otherwise) and that neither the whole work nor any part of it has been, is being, or is to be submitted for another degree in this or any other university.

I empower the university to reproduce for the purpose of research either the whole or any portion of the contents in any matter whatsoever.

Signed by candidate

February 2016

ACKNOWLEDGEMENTS

This thesis is dedicated to my husband and son, Mark and Joey - you are EVERYTHING to me!

I would like to acknowledge and express my gratitude to the following people or parties for their unfailing support throughout this endeavour:

- **The Discovery Foundation** for their financial support of this locally- and internationally-relevant project.
- My supervisor, **Associate Professor Jeannine Heckmann,** for her patience and dedication to this work. This thesis would not have been possible without her robust MG patient database, and her dedication to these patients. I am so grateful for the many ideas she formulated and for her help throughout the writing of this thesis.
- My co-supervisor **Dr Robea Ballo**, for all her invaluable advice and assistance throughout the project, for the hours spent together in tissue culture with our stem cells, and for performing the quantitative PCR experiments on my stem cells.
- **Histopathology laboratory, NHLS, Red Cross War Memorial Childrens' Hospital – Associate Professor Komala Pillay, Mr Ebrahim Dollie**, **Mrs Sue Ford** and **Mrs Colleen Jackson** for assisting with the processing and reporting of extraocular muscle tissue for histopathology and electron microscopy. **Komala,** for always being available to review important aspects of the histopathology and offering guidance on the reporting and context of these findings.
- **Associate Professor Sharon Prince** and the **members of the T-box laboratory** particularly for their help and guidance with western blot experiments, and for just always being available.
- **Dr Elizabeth van der Merwe** for her assistance refining and optimising the protocol for extraocular muscle tendon-derived myofibroblast ICC experiments and for helping with the fluorescent and confocal microscopy of these cells.

- **Professor Anthony Murray** for his clinical and surgical insights into these interesting cases.
- My co-researches in the **Neurology Research Group**, particularly **Dr Melissa Nel** for teaching me all that she already knew about the laboratory environment, and for her help processing skin and extra-ocular muscle biopsy samples and establishing and maintaining these precious cells in culture. Special thanks too to **Jennifer Auret** and **Joy-Mari Buys** who taught and assisted me with certain Western blot experiments.
- The members of the **UCT Stem Cell Initiative**, particularly **Dr Lauren Watson** for her assistance with immunocytochemistry for my induced pluripotent stem cells, and **Danielle Smith** for helping to propagate my induced pluripotent stem cells on feeder-free substrates in order to fully characterise these cells.
- **Mrs Toni Wiggins** for her assistance in teaching me general tissue culture principles and techniques, and for helping with cell counts for growth curves on occasions when I wasn't able to perform the count(s) myself.
- **Cytogenetics laboratory, NHLS, GSH** – Theresa and her team who performed the karyotyping for iPS cell characterisation.
- **Dimakatso Gumede** for her assistance with the real-time quantitative PCR experiments on my stem cells (in conjunction with Dr Robea Ballo).
- The members of the various 6th floor laboratories, the **Kidson lab**, the **Prince (T-box) lab**, and the **Redox lab** - the entire group was incredibly supportive and gave wonderful technical advice in times of need.
- I'd like to extend enormous gratitude to my incredible family, and my friends, colleagues and employers, who supported me throughout this project.

TABLE OF CONTENTS

LIST OF FIGURES

LIST OF TABLES

LIST OF ABBREVIATIONS

%	percentage
C	Celsius
α	alpha
β	beta
µg	microgram
µl	microlitre
µm	micrometre
µM	micromolar
ACh	acetylcholine
AChR	acetylcholine receptor
ATPase	adenosine triphosphatase
bFGF	basic fibroblast growth factor
BCA	bicichoninic acid
BSA	bovine serum albumin
cDNA	complementary DNA
cm	centimetre
CO_2	carbon dioxide
Col1A2	collagen -∝2 type 1
COX	cytochrome oxidase
CR1	complement receptor 1
CRP	complement regulatory protein
CS	control sera
CT	computerised tomography
Daf	mouse decay accelerating factor
DAF	human decay accelerating factor
DAPI	4', 6-Diamidino-2-Phenylindole
dH_2O	distilled water
ddH_2O	double distilled water
DMEM	Dulbecco's modified eagle's medium
DMSO	dimethyl sulfoxide

DNA	deoxyribonucleic acid
EAMG	experimental autoimmune myasthenia gravis
EB	embryoid body
EDTA	ethylenediaminetetra-acetic acid
EHS	Engelbreth-Holm-Swarm
EM	electron microscopy
EOM	extraocular muscle
FBS	fetal bovine serum
FCS	fetal calf serum
g	gram/gravity
G	guanine
H&E	haematoxylin & eosin
H_2O	water
HCl	hydrogen chloride
HDF	human dermal fibroblast
hES	human embryonic stem-cell
HRP	horseradish peroxidase
ICC	immunocytochemistry
IF	immunofluorescence
IFNγ	interferon gamma
IL	interleukin
iMEF	inactivated mouse embryonic fibroblast
Inc	incorporated
iPS	induced pluripotent stem-cell
KCl	potassium chloride
kDa	kilo Dalton
KH_2PO_4	monopotassium phosphate
LM	light microscopy
LPS	levator palpebrae superioris
LR	lateral rectus
LRP4	lipoprotein receptor-related protein 4

M	molar
MAC	membrane-attack complex
MAPK	mitogen-activated protein kinase
MCM	MEF conditioned medium
MEF	mouse embryonic fibroblast
mg	milligram
MG	myasthenia gravis
MGS	treatment-naïve MG patient sera
ml	millilitre
mm	millimetre
mM	millimolar
MMC	mitomycin C
mRNA	messenger ribonucleic acid
miRNA	micro ribonucleic acid
MOI	multiplicity of infection
MR	medial rectus
MRI	magnetic resonance imaging
mtDNA	mitochondrial deoxyribonucleic acid
MuSK	muscle-specific tyrosine kinase
MyHC	myosin heavy chain
NaCl	sodium chloride
Na_2HPO_4	disodium phosphate
ng	nanogram
NHLS	National Health Laboratory Service
nm	nanometre
NMJ	neuromuscular junction
OP-MG	ophthalmoplegic phenotype of myasthenia gravis
PAGE	polyacrylamide gel electrophoresis
PBS	phosphate buffered saline
PBST	1x PBS/0.1% Tween
PCR	polymerase chain reaction

PFA	paraformaldehyde
P/S	penicillin-streptomycin
q-PCR	quantitative PCR
rhTGFβ1	recombinant human transforming growth factor beta 1
RIPA	radio immuno precipitation assay
RNA	ribonucleic acid
rpm	revolutions per minute
RSA	South Africa
RT	room temperature
Rx	treatment
SDS	sodium dodecyl sulphate
SDS-PAGE	SDS-polyacrylamide gel electrophoresis
SeVdp	Sendai viral vector
SMA	smooth muscle actin
SNP	single nucleotide polymorphism
SOP	standard operating procedure
STIR	short tau inversion recovery
TBST	1 x TBS/0.1% Tween
TGFβ	transforming growth factor beta
TNFα	tumour necrosis factor alpha
T-SNMG	triple seronegative myasthenia gravis
U	unit
UK	United Kingdom
USA	United States of America
UV	Ultra-violet

ABSTRACT

Myasthenia gravis (MG) is an autoimmune disease in which pathogenic antibodies target specific neuromuscular junction proteins, most frequently acetylcholine receptors (AChR). Among those without detectable AChR-antibodies, a subgroup of patients has antibodies directed against muscle-specific tyrosine kinase (MuSK). In MG the pathogenic antibodies result in failure of neuromuscular transmission with consequent fatiguable skeletal muscle weakness. MG frequently affects the extraocular muscles (EOMs) early in the course of the disease, resulting in diplopia and ptosis, which is usually reversible with treatment. A treatment-resistant ophthalmoplegia and ptosis occurs as a complication of MG in a distinct subset of cases referred to as OP-MG.

The EOMs are highly specialised muscle tissue with a unique physiological and immunological microenvironment with a large satellite cell niche, a distinct muscle fibroblast population, different transcriptional and cellular signaling pathways and fewer intrinsic complement regulatory proteins to protect them against antibody-activated complement-mediated damage. We hypothesised that in OP-MG, there is a differential response of the EOMs to the underlying MG disease process(es) on a genetic and molecular level, resulting in abnormal myofibre homeostasis.

We aimed to report descriptive clinical-pathological data pertaining to EOM function and histopathological and ultrastructural EOM tissue analysis of a patient with OP-MG versus that of a non-MG control (both consented to EOM donation at ocular realignment surgery). EOM tissue from an OP-MG individual with AChR- and MuSK-antibody negative MG, demonstrated predominantly myopathic pathology and ultrastructural evidence of mitochondrial stress. The OP-MG EOM findings differ from the control EOM, which showed normal muscle histopathology in a patient undergoing strabismus surgery for a sensory exotropia in a non-seeing eye (loss of retinal stimulus for fusion) and a similar duration of deviation. These OP-MG findings

appear to better correlate with previously reported histology/ultrastructure in limb muscle in MuSK-positive MG rather than AChR-positive MG.

We next focussed on transforming growth factor beta-1 (TGFβ1) as a critical cytokine involved in muscle repair. An auto-induction pathway in muscle allows TGFβ1 expression to influence the transdifferentiation of satellite cells into myofibroblasts or myoblasts. In orbital fibroblasts, TGFβ1 has also been shown to upregulate decay accelerating factor (DAF), a complement regulatory protein expressed at lower levels in EOMs than other muscles, which should protect against complement-mediated injury. We established OP-MG and control-MG phenotype-specific dermal fibroblast cell lines and performed immunoblotting to evaluate TGFβ1-induced Smad3 phosphorylation and Daf expression in mouse myotubes. We demonstrated repression of phosphorylated-Smad3, a marker of the canonical TGFβ1 pathway, in OP-MG versus control MG fibroblasts after treatment with TGFβ1. We also demonstrated that TGFβ1 significantly upregulates Daf expression levels in mouse myoblasts. Taken together, these results suggest that OP-MG fibroblasts (and possibly myofibroblasts) are likely to be more susceptible to complement-mediated damage and abnormal myofibrogenesis due to their altered response to TGFβ1 stimulation and secondary DAF upregulation.

Finally we investigated the feasability of establishing an *in vitro* disease model for MG or OP-MG by reprogramming dermal fibroblasts into disease phenotype-specific induced pluripotent stem (iPS) cells. We successfully generated and characterised iPS cells for one individual. However, this process was very labour-intensive, cost-inefficient and time-consuming, taking approximately four months to establish pluripotency in a single patient and thereby limited its further application(s).

In conclusion, the EOM ultrastructural findings of an OP-MG case are novel and show similar findings to those described in limb skeletal muscle of MuSK-positive MG patients. The TGFβ1 pathway appears to be differentially regulated in OP-MG compared to control-MG cases and this may impact DAF upregulation in the EOMs in MG patients. Finally, our group is exploring an alternative method of establishing a 'disease-in-a-dish' model that is more cost-effective and practically feasible than the iPS cell route.

CHAPTER 1

LITERATURE REVIEW

1.1 MYASTHENIA GRAVIS

Myasthenia gravis (MG) is an uncommon, treatable neurological disorder of autoimmune etiology, in which pathogenic antibodies target specific neuromuscular junction (NMJ) proteins or receptors, most frequently acetylcholine receptors (AChR). This results in failure of neuromuscular transmission with consequent fatiguable muscle weakness, often initially involving the ocular muscles and manifesting with intermittent blepharoptosis and diplopia. Ultimately the disease generalises in most cases, and may result in weakness of the bulbar, neck, limb and respiratory muscles (Silvestri & Wolfe 2012).

The worldwide incidence of MG ranges from 1.7-21.3 cases per million per year and the prevalence is estimated to be between 15-179 cases per million (Carr et al. 2010). The average annual incidence of AChR antibody positive MG in South Africa for 2011-2012 was reported to be 8.5 cases per million (Mombaur et al. 2015), which is comparative to the pooled worldwide incidence rate of 7.3 cases per million reported in a large systematic review (Carr et al. 2010). South African data for adults with AChR antibody positive MG showed similar age and gender distribution to comparative reports from Norway, Greece, Canada and the United Kingdom (Mombaur et al. 2015).

In the juvenile population in South Africa, ocular MG was reported to present at an earlier mean age of 5.1 years versus generalised MG which presented in older children with a mean age of 10.2 years. Both of these groups of juvenile MG (ocular and generalised) achieved a remission rate of at least 45% with immunosuppressive therapy, but almost a quarter of children of African genetic ancestry developed a treatment-resistant ophthalmoplegia as a complication of generalised MG (Heckmann et al. 2012). Although adult myasthenic patients with generalised MG

also developed treatment-resistant ophthalmoplegia it was less frequent (Heckmann et al. 2007).

The objective of therapy in MG is to return patients to normal function as quickly as possible, while limiting undesired adverse effects and costs. Most patients can return to productive lives and a generally favourable prognosis with treatment (Vincent & Drachman 2002). The mortality of MG has been significantly reduced with modern therapeutic approaches, but remains significant with an overall in-hospital mortality rate of 2.2–4.5% reported in the USA (Alshekhlee et al. 2009).

Current treatment strategies for MG can be subdivided into having two main objectives:

1. Increasing the amount of the neurotransmitter acetylcholine (ACh) available for post-synaptic membrane receptor-binding at the NMJ.
2. Decreasing the number of circulating auto-antibodies which target the post-synaptic membrane ACh-receptors, thereby making more receptors available for effective neurotransmission.

Acetylcholine-esterase inhibitors prevent the breakdown of ACh in the synaptic cleft, ensuring that it is available for receptor binding for longer periods of time and in higher concentrations. Measures for reducing the numbers of circulating antibodies include (Vincent & Drachman 2002):

- Immunosuppressant therapy – to inhibit the production of auto-antibodies against AChRs and consequent immune complexes. These include corticosteroids and steroid-sparing agents such as azathioprine or methotrexate (Heckmann et al. 2011).
- Plasmapharesis – to remove circulating AChR auto-antibodies and immune complexes from the circulation; a temporary measure employed in times of myasthenic crisis, peri-operatively and in severe refractory cases.
- Intravenous immunoglobulin – a temporary measure to bind circulating anti-AChR auto-antibodies thereby inhibiting their binding and consequent internalisation and/or blockade, as well as neutralising cytokines and other

inflammatory mediators and preventing activation of the complement pathway (Peter et al. 2014).

- Thymectomy – removal of the thymus gland in the presence of a thymoma and/or thymic hyperplasia and AChR antibody positive generalised MG may result in the improvement of symptoms and signs of MG to a variable degree over a period of months or years.

The neuromuscular junction and MG

The pathogenic antibodies in AChR-antibody positive myasthenia gravis are targeted at the alpha subunit of the AChR, which is located on the post-synaptic muscle membrane of the neuro-muscular junction (NMJ). The NMJ is the area of contact between the terminal nerve endings and the muscle fibres. The terminal end of the axon contains synaptic vesicles that are filled with the neurotransmitter acetylcholine (ACh), which is released when the action potential arrives at the axon terminal. Acetylcholine molecules diffuse across the synapse and bind to the AChR located on the crests of the postsynaptic folds of the NMJ. Upon receptor-binding, the AChR pores open with the influx of cations and consequent depolarisation along the muscle membrane. This results in the activation of voltage-gated Na^+ channels in the clefts generating an action potential that causes the muscle to contract (Guyon et al. 1998).

AChR antibodies have been shown to reduce the number of functional AChRs available for effective neuro-muscular impulse conduction by several mechanisms (Silvestri & Wolfe 2012):

- Accelerated internalisation and degradation of AChR molecules by cross-linking two adjacent AChRs with anti-AChR antibody.
- Complement activation and damage of the endplate and the post-synaptic membrane.
- Loss of AChRs at the damaged endplate junctional folds with consequent reduction of surface area available for insertion of newly-synthesised AChRs.
- Direct blockade due to binding of auto-antibody to AChR.

The concept of 'safety margin' or 'safety factor' is important in explaining the pathophysiology of MG. Normally there is an excess of ACh quanta released from the presynaptic membrane, and an excess of post-synaptic AChRs available for consequent binding to ensure optimal neuromuscular transmission. Any negative alteration in the ratio of ACh molecules to ACh-receptors will result in a decreased probability of interaction between the ACh molecule and its receptor, and this will reduce the 'safety margin/factor'. A reduction in the 'safety margin/factor' thereby predisposes to failure of neuromuscular transmission, resulting in fatiguability and weakness of the muscle (Vaphiades et al. 2012).

Subtypes of MG according to autoantibodies

Approximately 85% of MG cases have detectable serum levels of anti-AChR antibodies, the remaining 15% are termed seronegative and may have auto-antibodies directed at other receptors located at the NMJ (Silvestri & Wolfe 2012). A loss of 60% of AChRs is necessary for the manifestation of MG weakness (Jacob et al. 2009). A variable proportion of these patients have antibodies to the muscle-specific tyrosine kinase (MuSK); these antibodies are directed against the extracellular domain of MuSK and are shown to inhibit agrin-induced AChR clustering in muscle myotubes. MG patients with MuSK antibodies appear to have more prominent oculobulbar weakness, frequent respiratory crises, and often have a variable response to treatment (Sanders et al. 2003).

The presence of anti-low density lipoprotein receptor-related protein 4 (LRP4) antibodies have been reported in a variable proportion of patients negative for AChR and MuSK antibodies. This subgroup of MG may have distinct clinical features, including mild disease at presentation and a prompt and adequate response to pyridostigmine, a cholinesterase inhibitor, therapy (Zouvelou et al. 2013). More recently agrin, an extracellular matrix proteoglycan released by motor neurons which is critical for NMJ formation and maintenance, was identified as another target for auto-antibodies in MG. Anti-agrin antibodies were found in two of four triple seronegative MG cases in one reported series (Zhang et al. 2014). Another published series reported five agrin antibody-positive MG cases; in these cases the anti-agrin antibodies were always detected in combination with auto-antibodies

against MuSK, LRP4, or AChRs (Gasperi et al. 2014).

Presently, using the current techniques of radioimmunoassay and cell-based assays, there remains a proportion of MG patients who do not have antibodies against AChR, MuSK or LRP4. These are referred to as triple-seronegative myasthenia gravis (T-SNMG). Our group has shown that patients with moderate to severe generalised MG (with/without ocular involvement) and are AChR antibody negative, are more likely to have MuSK positive MG if they have African genetic ancestry and T-SNMG if they were Caucasian (Huda et al. 2016).

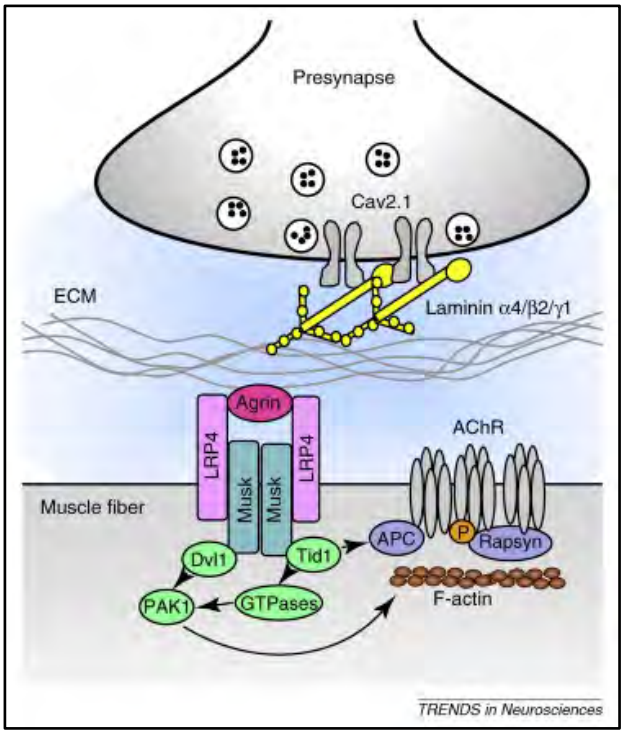

Figure 1.1 Structure of the neuromuscular junction and its various membrane-bound receptors and proteins. Vesicles at the terminal end of the axon release acetylcholine (Ach), which diffuses across the synaptic cleft and attaches to the acetylcholine receptors (AChRs) on the postsynaptic membrane leading to the generation of an action potential with consequent muscle contraction. (Dityatev et al. 2010)

Histology of muscles in MG

Histopathological changes in muscle are principally classified as either neurogenic, due to a loss of nervous stimulation to the muscle, or myopathic, due to an intrinsic abnormality of the muscle. Signs of neurogenic muscle pathology include grouped

muscle fibre atrophy (type I or type II), small angulated muscle fibres, fibre type grouping with 'target' formations representing re-innervated fibres, and nuclear clumping. Myopathic conditions result in identifiable histopathological features including a wide variation in muscle fibre size, degeneration (necrosis) & regeneration, centrally-located nuclei, inflammation with vascular changes, fibrosis and the accumulation of abnormal material or inclusions (Dubowitz et al. 2013).

Histopathologcial alterations in limb muscle biopsy samples taken from patients with MG display the following characteristic changes (Shah et al. 2015):

- The NMJs of MG patients have approximately 30% fewer AChRs than healthy individuals.
- There is simplification of the pattern of post-synaptic membrane folding at the NMJ.
- A larger gap exists between the axon terminal of the nerve and the post-synaptic muscle membrane.

Oosterhuis and Bethlem reported neurogenic changes with and without lymphocytic infiltrations in muscle biopsies of MG patients, even in the absence of clinical muscle atrophy (Oosterhuis & Bethlem 1973). These findings must be carefully regarded since this report was published prior to the availability of antibody serotyping and at a time when MG therapies were limited, and there was significant potential for undertreatment.

Reports suggest distinct features evident on skeletal muscle histopathology and electron microscopy in the different serological types of MG, particulary AChR positive MG and anti-MuSK MG. In AChR-antibody positive cases the pathogenic process is primarily complement-mediated damage to the motor endplate and its resultant consequences.

Anti-AChR positive MG is associated with marked myofibre atrophy (particulary type II fibres) and myofibrillar disarray, both consistent with neurogenic/neuropathic disease (Padua et al. 2006; Martignago et al. 2009; Cenacchi et al. 2011). Padua et al described the muscle histology in 11 cases of AChR negative MG. They observed similar histological features to those seen in AChR positive MG in seven of the 11

cases; an increased variability in muscle fibre diameter and non-specific atrophy, while the remaining four biopsies showed normal muscle features (Padua et al. 2006).

In contrast to these patients, MG cases with anti-MuSK antibodies demonstrate myopathic changes and frequent mitochondrial abnormalities on limb muscle biopsies (Rostedt Punga et al. 2006; Martignago et al. 2009; Cenacchi et al. 2011). In cases with both AChR and MuSK antibodies, muscle displayed a pathological intermyofibrillar network, atrophy, cytochrome oxidase (COX)-negative fibres, and 'ragged red fibres' (Rostedt Punga et al. 2006). Mitochondrial dysfunction of various causes is characterised by the accumulation of diseased mitochondria under the plasma membrane of skeletal muscle fibres resulting in an irregular contour and the apprearance of 'ragged red fibres' on modified Gomori trichrome staining (Dubowitz et al. 2013).

Reported histopathological and ultrastructural data is sparse, but in summary the available literature describes predominantly neurogenic features in AChR positive MG limb skeletal muscle versus features resembling a mitochondrial myopathy in MuSK positive MG cases.

1.2 THE EXTRAOCULAR MUSCLES AND THEIR SUSCEPTIBILITY TO MYASTHENIA GRAVIS

The extraocular muscles are classified as skeletal muscle, but they are specifically modified for their unique actions and are therefore distinct from their limb and trunk skeletal muscle counterparts. The extraocular muscles comprise six small, specialised, voluntary muscles that control the movement of each eyeball within the socket, and function in conjunction with another small skeletal muscle responsible for elevating the upper eyelid.

EOM tissue is highly-specialised in order to finely regulate small amplitude and high velocity eye movements, and therefore have very small resultant fusional tolerances which explains why patients with MG often present with ocular symptoms (diplopia) before noting any other muscular weakness.These small muscles have a discrete

layered organisation and constitute a unique muscle allotype with 6 distinct fibre types classified according to their location, innervation pattern and fatigue-resistance properties. EOM fibres have higher firing frequencies and faster contractile properties with shorter relaxation times, and their motor units are smaller, in order to vary forces by tiny increments. Adult EOMs contain multiply-innervated fibres with en-grappe endplates facilitating innervation at multiple points along the length of each muscle fibre; this type of innervation is uncommon in other mammalian skeletal muscles and accounts for the faster contractile properties of EOMs. EOMs are highly vascular and posess abundant mitochondria allowing for their high fatigue resistance and 'fast twitch' capabilities (Kaminski et al. 2003; Yu Wai Man et al. 2005; Fischer et al. 2005). The EOMs are highly dependent on oxidative metabolism via glucose-based aerobic metabolism (Fischer et al. 2005). Almost all known isoforms of myosin heavy chain (MyHC) are expressed in EOM fibers, with developmental MyHC isoforms that persist almost exclusively in adult EOMs (Yu Wai Man et al. 2005).

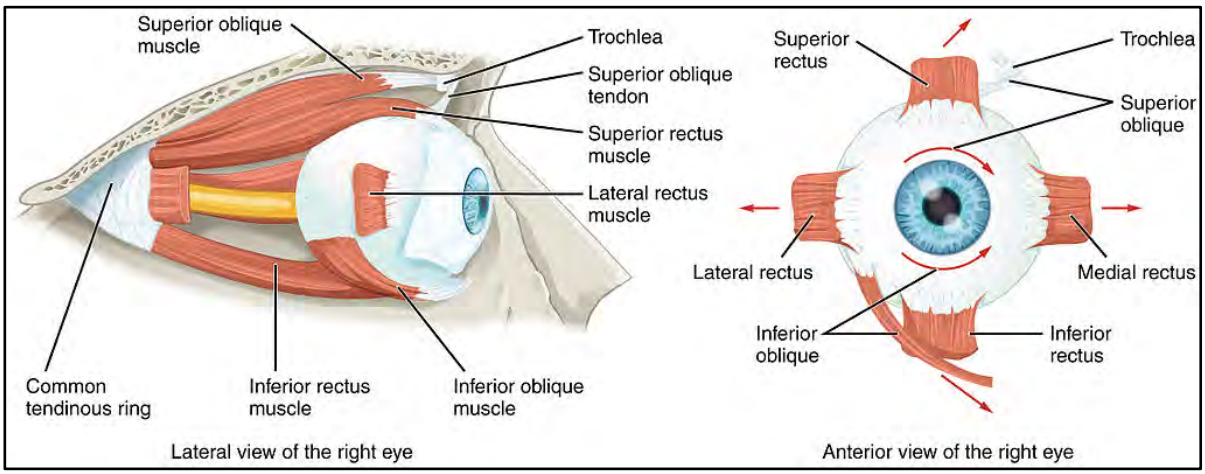

Figure 1.2 The extra-ocular muscles - lateral view & anterior view of the right eye. The four rectus muscles (superior, medial, inferior and lateral) and their tendinous insertions into the sclera can be seen in the anterior view (right), while the two oblique muscles (superior and inferior) are better demonstrated in the lateral view (left).
(Downloaded from http://www.medicalinstitution.com/extraocular-muscles)

The neuromuscular junctions of EOMs display poor postsynaptic membrane folding and fewer AChRs than those in skeletal muscles, with a resultant reduction in the

'safety factor' at the NMJ. Fetal and adult AChR isoforms are expressed in EOM; the fetal AChR has a longer open time and lower conductance, which affects the time course and amplitude of the endplate potential. This fetal isoform is unique to EOM and was previously postulated be a specific immunological target in MG (Kaminski et al. 1996; Kaminski et al. 2003; Yu Wai Man et al. 2005). This theory has however been discredited on the grounds of concomitant eyelid involvement; the levator palpebrae superioris is the dominant upper eyelid muscle and does not have fetal AChRs (Kaminski et al. 1995).

EOM tissue undergoes continuous remodeling by means of repair and regeneration throughout life, even when uninjured, via a niche of muscle progenitor cells known as satellite cells. These are located under the basal lamina of the myofibres (Yu Wai Man et al. 2005; Fischer et al. 2005). The EOMs have a unique physiological and immunological microenvironment with a large satellite cell niche, a distinct muscle fibroblast population (Kusner et al. 2010), different transcriptional and cellular signaling pathways and lower expression levels of certain intrinsic complement regulatory proteins to protect them against complement-mediated damage (Kaminski et al. 2003). EOMs differentially express immune-related genes, suggesting that their susceptibility and response to autoimmune disorders differs from that of skeletal muscle (Porter et al. 2001).

Decay accelerating factor (*DAF* or *CD55*), a membrane-bound complement regulatory protein gene, is expressed at low levels in EOM, while the complement factor H-related protein (a circulating complement regulator) gene is expressed at high levels in EOM (Kaminski et al. 2003). Studies using an experimentally acquired myasthenia gravis (EAMG) mouse model have demonstrated that in keeping with an increased immune response and gene transcripts in EOM compared with other muscles after induction of EAMG, an inflammatory cell infiltrate was also more prominent in EOMs on histopathology. These findings led the authors to conclude that EOMs have a divergent response to EAMG compared with other muscles (Zhou et al. 2014). These anatomical and physiological features of EOM may explain why they are preferentially or differentially affected by this disease.

Dysthyroid disease also preferentially, and almost exclusively, affects the extra-ocular muscles. However, this does not appear to be attributable to the muscle allotype, but is instead largely ascribed to the disease process that specifically targets orbital fibroblasts. Enlargement of the EOMs occurs due to an abnormal accumulation of glycosaminoglycans and fluid in the orbital soft tissues that is detected by specialised magnetic resonance imaging (MRI) techniques (Hoh et al. 1994). The pathogenic mechanism underlying thyroid-associated ophthalmopathy is attributed to circulating B and T lymphocytes, directed against an antigen expressed on both thyroid follicular cells and on orbital fibroblasts (Lehmann et al. 2008). The hypothesis that the orbital fibroblasts are the principal target in thyroid-associated ophthalmopathy is further supported by the intact and undisturbed sarcomeric organisation of extra-ocular muscle fibres in these cases (Porter & Baker 1996).

Treatment-resistant ophthalmoplegia as a complication in MG

In 2007, Heckmann et al. reported racial differences in the clinical manifestations of MG in a South African cohort. In this multiracial sample they found that Black subjects were significantly more likely than Whites to develop a treatment-resistant ophthalmoplegia and ptosis (18% versus 2%). Thirteen of the 14 patients with this ophthalmoplegic phenotype (OP-MG) had generalised disease and anti-AChR antibodies (Heckmann et al. 2007). In a paper reporting the characteristics of juvenile MG among South Africans, it was found that younger children developed ocular MG while older children developed generalised MG with a mean age of 5.1 years versus 10.2 years respectively. There was no racial variation with respect to AChR antibody status, maximum severity of disease, or use of immunosuppressive therapy. However, a significant number of children of African genetic ancestry (23%) developed partial or complete ophthalmoplegia as a complication of generalised MG (Heckmann et al. 2012). While these two subgroups of MG patients develop this complication more frequently, it does also develop in adults and among Caucasians (Heckmann et al. 2007); unpublished observations and personal communications - J Heckmann, South Africa; J McConville, Ireland; J Verschuuren, Netherlands).

Imaging of extraocular muscles in MG

Magnetic resonance imaging (MRI) is superior to computerised tomography (CT) for

imaging the orbital soft tissues and the EOMs, but CT scans provide sufficient detail to comment on gross features of EOMs - such as size, volume, shape, and thickening of the EOM tendinous insertion. Conventional MRI is ideal for discerning soft tissue pathology according to its hydrogen content, but it is unable to discriminate between fat and water in tissues, which both appear bright on T1- and T2-weighted images. Specialised techniques, such as short tau inversion recovery (STIR), can be employed with MRI to selectively supress the signal from fat in order to better visualise water/fluid in the orbital soft tissues and EOMs (Hoh et al. 1994).

Okamoto et al. identified bilateral EOM atrophy on orbital CT in seven cases of long-standing ophthalmoplegia, attributable to MG in three cases and to mitochondrial myopathy in the remaining four cases. In this report it was not possible to differentiate these two entities with CT and MRI alone since the appearance of the EOMs on neuro-imaging was too similar (Okamoto et al. 1996). In patients with chronic progressive external ophthalmoplegia (CPEO), a myopathic condition, digital measurements of the EOMs on MRI had statistically significantly smaller volumes than those of control subjects. It is thought that the variation in the degree of EOM atrophy in this condition is influenced by the duration of the ophthalmoplegia and the underlying mitochondrial defect (Carlow et al. 1998). However, in a study assessing the specific diagnostic findings of CPEO on high-resolution orbital MRI, CPEO was associated with minimal EOM volume reduction, despite clinically severe EOM weakness when compared to patients with oculomotor paralysis. Therefore denervated EOMs, following neurogenic paralysis, demonstrated a statistically significant volume reduction when compared to normal and CPEO groups. One subject with MG (EOM involvement was not specified) was imaged and analysed in this study, and no internal abnormalities in the EOMs were observed on high-resolution MRI compared to normal volunteers (Ortube et al. 2006). Chan and Orrison reported a single case of long-standing treatment-resistant ophthalmoplegia in a MuSK positive MG patient demonstrating severe atrophy of almost all the EOMs on MRI. Only the inferior oblique muscle appeared spared, with the affected muscles taking on the appearance of ‘ribbon-like’ bands after the loss of their fusiform muscle belly (Chan & Orrison 2007).

There are very few reports on the radiological appearance of the EOMs in MG, with little/no consistency and a broad spectrum of findings ranging from normal EOM appearance with normal muscle volume, to marked atrophy of almost all the EOMs.

Histology of extraocular muscles in MG

Pathological changes of EOMs in MG are poorly reported for the following reasons:

- EOM tissue is relatively inaccessible and therefore seldom ascertained.
- The long tendinous insertions of EOMs require large muscle resections in order to obtain representative samples of muscle tissue.
- EOM resection is seldom indicated for ocular realignment in MG patients, since the majority of EOM paralysis is reversible and responsive to conventional medical therapy.

There is currently very little existing literature describing the histopathological features of MG in extraocular muscles, and only a few reports detailing the characteristic changes in limb skeletal muscle specimens of MG cases. Gratton et al. reported a single case of AChR positive MG with severe ophthalmoplegia and ptosis requiring ocular re-alignment surgery after the ophthalmoplegia failed to respond to pyridostigmine, prednisone and azathioprine therapy. Histology of this patient's superior rectus muscle demonstrated atrophy with complete replacement of EOM by connective tissue/fibrosis (Gratton et al. 2014).

1.3 THE ROLE OF THE COMPLEMENT SYSTEM IN MYASTHENIA GRAVIS

The complement pathway is a cascade of biochemical reactions composed of multiple serum and membrane proteins, which serves to protect the body. It does this through a number of processes including cell lysis of pathogens, enhancement of phagocytosis by opsonization with complement fragments, and the attraction of inflammatory cells (Kohl 2006).

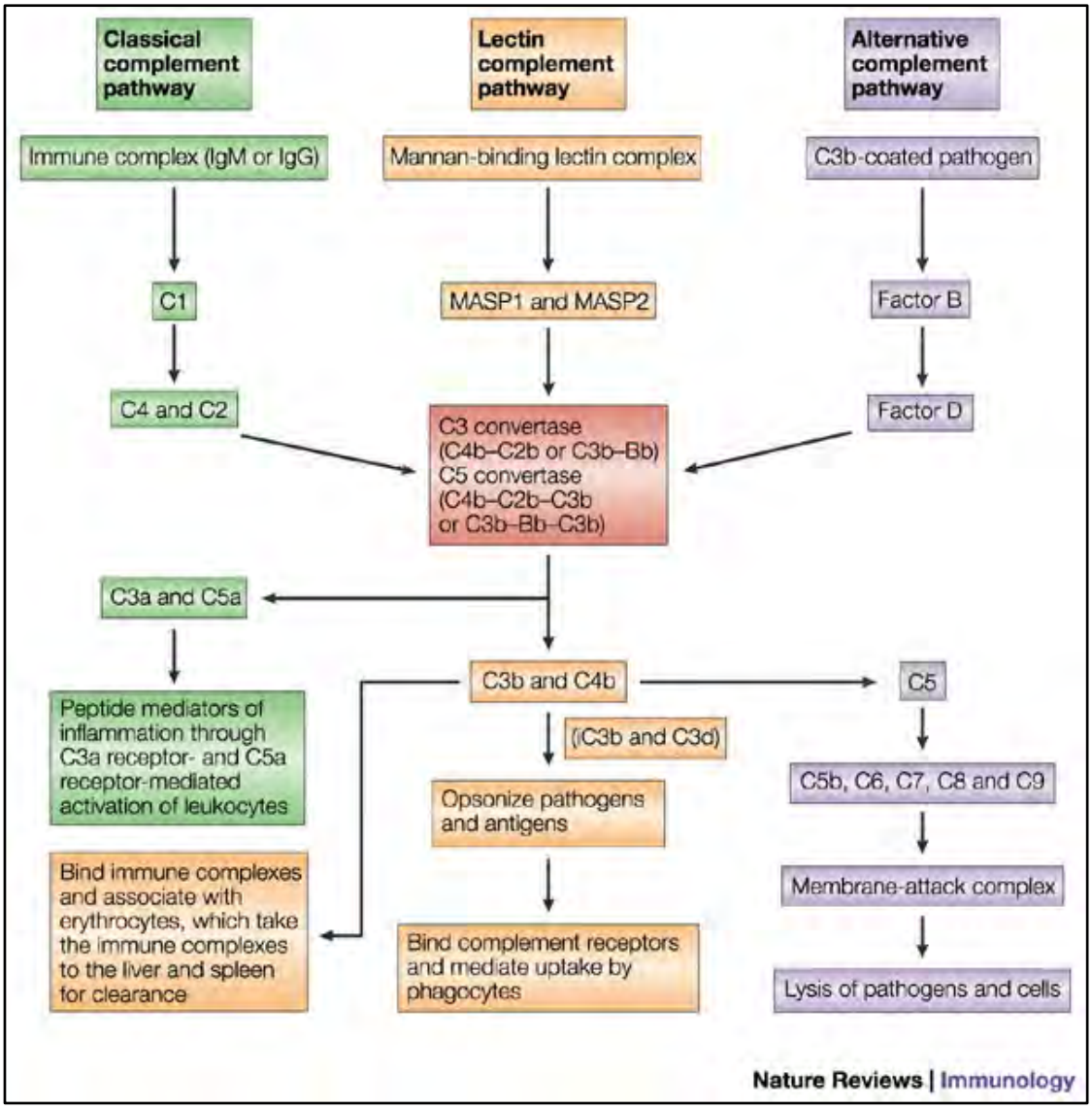

Figure 1.3 The classical, lectin and alternative pathways are involved in the complement system. The classical pathway is the most relevant in Myasthenia Gravis because of its activation by auto-antibodies to the acetylcholine receptors (AChRs). All three pathways converge on complement C3 and complement C5, resulting in their cleavage and activation of the membrane-attack complex (MAC) with consequent cell lysis. (Carroll 2004)

Activation of complement leads to the formation of proteolytic enzymes that mediate the cleavage of complement proteins into fragments, followed by a series of activation steps and the generation of a number of proteins which lead to the formation of the membrane-attack complex (MAC) that produces cell lysis. In MG, the assembly of the MAC via complement activation by the AChR-pathogenic antibodies, causes architectural changes at the endplate and postsynaptic muscle membrane, and thereby contributes to failure of neuromuscular transmission (Soltys

et al. 2008). There is substantial evidence for the role of complement-mediated damage at the NMJ and muscle motor endplate in myasthenia gravis (Tüzün et al. 2011). Complement activation fragments complement C3, complement C9 and the MAC have been found at the NMJs in MG patients (Nakano & Engel 1993), and the complement C3 component was demonstrated at the motor end-plate of animals with experimental autoimmune MG (Sahashi et al. 1980; Soltys et al. 2008).

In AChR positive MG, most of the pathogenic antibodies are IgG1, which are known to fervently activate the classical complement pathway with consequent destruction of the postsynaptic muscle membrane. However, anti-MuSK antibodies are predominantly IgG4 and have a lower pathogenicity at the motor endplate due to poor activation of the complement pathway (Rostedt Punga 2011).

There is differential expression of complement regulatory genes in EOM (Kaminski et al. 2003) and EOMs express less membrane-bound complement regulatory proteins than limb muscles (Soltys et al. 2009). This could provide yet another explanation for the susceptibility of EOMs to MG, since they have reduced protective mechanisms against complement-mediated tissue injury (Kaminski et al. 2003; Soltys et al. 2008).

Decay-accelerating factor (DAF)

It is critical for the human body to exercise control over the complement system in order to avoid damage to self-tissues by means of activated autologous complement. This protective role is performed by complement regulatory proteins (CRPs), which are ubiquitously expressed on the surface membrane of most cell types (Kim & Song 2006). Decay-accelerating factor (DAF or CD55) is a 70 kDa membrane CRP that regulates complement by inhibiting the assembly of, and accelerating the dissociation of complement C3 and complement C5 convertases (Walport 2001). DAF has been shown to be primarily regulated at a transcriptional level (Thomas & Lublin 1993), but there is evidence suggesting that its expression can be regulated by cytokines such as interleukin 1 and 6 (IL-1, IL-6), tumour necrosis factor alpha (TNF-α) and interferon gamma (IFN-γ) (Cauvi et al. 2006). However, there is still much about the molecular mechanisms governing DAFs regulation that remains unknown.

Porter et al. demonstrated that DAF is expressed at lower levels in EOMs compared to other skeletal muscles (Porter et al. 2001). In addition, during experimental autoimmune MG, DAF is downregulated in EOMs (Kaminski et al. 2004; Kaminski et al. 2004), thereby rendering them more susceptible to complement-mediated damage. However, in orbital fibroblasts, DAF expression has been shown to be significantly up-regulated by transforming growth factor beta-1 (TGFβ1). It is thought that this TGFβ1-mediated up-regulation of DAF should serve to prevent complement-mediated injury to orbital fibroblasts in the course of orbital inflammatory disease (Cocuzzi et al. 2001).

The treatment-resistant ophthalmoplegia that develops in a subgroup of MG cases as described above (Heckmann et al. 2007) associates with a functional single nucleotide polymorphism (SNP) of the regulatory region of *DAF c.-198 C>G* (rs28371586). Based on these results, we postulated that during the course of autoimmune MG, this SNP may result in inadequate DAF upregulation and consequent increased susceptibility to complement-mediated damage to the EOMs during critical periods of the immune response or in response to prednisone therapy (Heckmann et al. 2010; Auret et al. 2014). Interestingly, the *DAF/CD55* 5` region (promoter sequence) was predicted to have a Smad-protein binding element involved in TGFβ1 signaling (Wenzel et al. 2005).

Due to our group's interest in the possible role of TGFβ1 in the regulation of the DAF promoter region, I assessed Daf levels in reponse to TGFβ1 treatment in mouse myoblasts as a proxy for human skeletal muscle.

1.4 TRANSFORMING GROWTH FACTOR BETA-1 (TGFβ1)

The transforming growth factor beta (TGFβ) superfamily of multifunctional cytokines is responsible for the regulation of a number of cellular responses and figures prominently involved in the development and homeostasis of most human tissues. TGFβ plays a central role in cell proliferation and differentiation, as well as embryonic development, angiogenesis and maintenance of the extra-cellular matrix (Kubiczkova et al. 2012). It is important to emphasize that the downstream effects of

this signalling cascade are often tissue-specific. Given its multifaceted effects in different tissues, deregulation of TGFβ signalling cascades can result in an array of developmental defects and/or diseases. Several members of the TGFβ family, and particularly TGFβ1 have been shown to play vital roles in regulating muscle growth, repair and atrophy (Burks & Cohn 2011).

TGFβ1 is a prominent pro-fibrotic cytokine, which when stimulated results in the production of extracellular matrix components. TGFβ1 is activated by peptides liberated during injury in order to activate normal wound healing and tissue repair. TGFβ1 receptor activation at the cell surface results in an intracellular cascade via phosphorylation of latent cytoplasmic transcription factors called Smad proteins. TGFβ1 binding results in the activation of type II and type I receptors, which directly phosphorylate Smad2 and/or Smad3 to initiate signal transduction via the canonical cascades. Activated Smad-complexes translocate to the nucleus and bind defined elements on DNA resulting in the transcriptional regulation of target genes (Kubiczkova et al. 2012; Leask & Abraham 2004). The TGFβ1-Smad signalling pathway is tightly regulated and sensitive to alterations in cellular conditions. Overproduction of TGFβ1 can result in excessive deposition of scar tissue and fibrosis, and has been implicated in fibrosis of various tissues and organs (Blobe et al. 2000).

TGFβ1 can also signal via induction of the non-canonical pathways including mitogen-activated protein kinase (MAPK). The mechanisms of MAPK activation by TGFβ1 and the subsequent biological consequences are cell-type specific. MAPK may also modulate TGFβ1-induced Smad signals and phosphorylate Smad proteins independent of TGFβ1, providing a degree of crosstalk between the canonical and non-canonical TGFβ1 pathways (Burks & Cohn 2011).

During myogenesis, the spatial and temporal expression of TGFβ1 in the developing connective tissue correlates to the fibre type composition of the surrounding myotubes. Myotubes formed before the expression of TGFβ1 develop into slow fibres, while fast fibres develop from myoblasts adjacent to connective tissue expressing TGFβ1. In mature adult muscle, TGFβ1 negatively affects skeletal muscle repair and regeneration by inhibiting the proliferation of satellite cells, the fusion of

myofibres, and the expression of some muscle-specific genes. TGFβ1 may also induce the transformation of myoblasts into myofibroblasts following muscle injury (Burks & Cohn 2011).

Myogenesis is regulated by a variety of interactive signal transduction pathways, some of which exhibited differential gene/protein regulation in mouse EOM and mouse limb muscle myoblasts. For example, the expression of MAPK pathway transcripts were higher in mouse limb muscle compared to mouse EOMs. TGFβ1 signalling pathway transcripts were also differentially expressed between mouse limb muscles and EOMs at gene and protein levels (Porter et al. 2006).

In muscle cell repair and regeneration, TGFβ1 has been shown to act independently or through auto-induction, and inhibit perimysial satellite cell activation, impair myocyte differentiation, and promote the transformation of myoblasts into myofibroblasts. Excessive production of TGFβ1 can induce myoblasts to express TGFβ1 in an autocrine manner, thereby up-regulating this pro-fibrotic pathway resulting in muscle fibrogenesis and inhibition of myocyte differentiation (Burks & Cohn 2011).

While TGFβ1 commonly causes severe fibrosis in many different tissues including skeletal muscle, the systemic administration of TGFβ1 has been found to result in severe cachexia and muscle atrophy (Mendias et al. 2012). This study demonstrated that TGFβ1 dramatically affects the contractile properties of skeletal muscles, causing a significant reduction in the force-generating capacity of otherwise healthy muscle tissue. These results indicate that even in the absence of physical muscle injury, TGFβ1 can directly induce muscle fibre atrophy in a satellite cell-independent manner. Here we postulated that TGFβ1 levels, in response to MG-induced EOM complement-mediated damage, was adversely affecting muscle fibre regeneration resulting in the profound weakness of the EOMs observed in MG patients with severe treatment-resistant ophthalmoplegia.

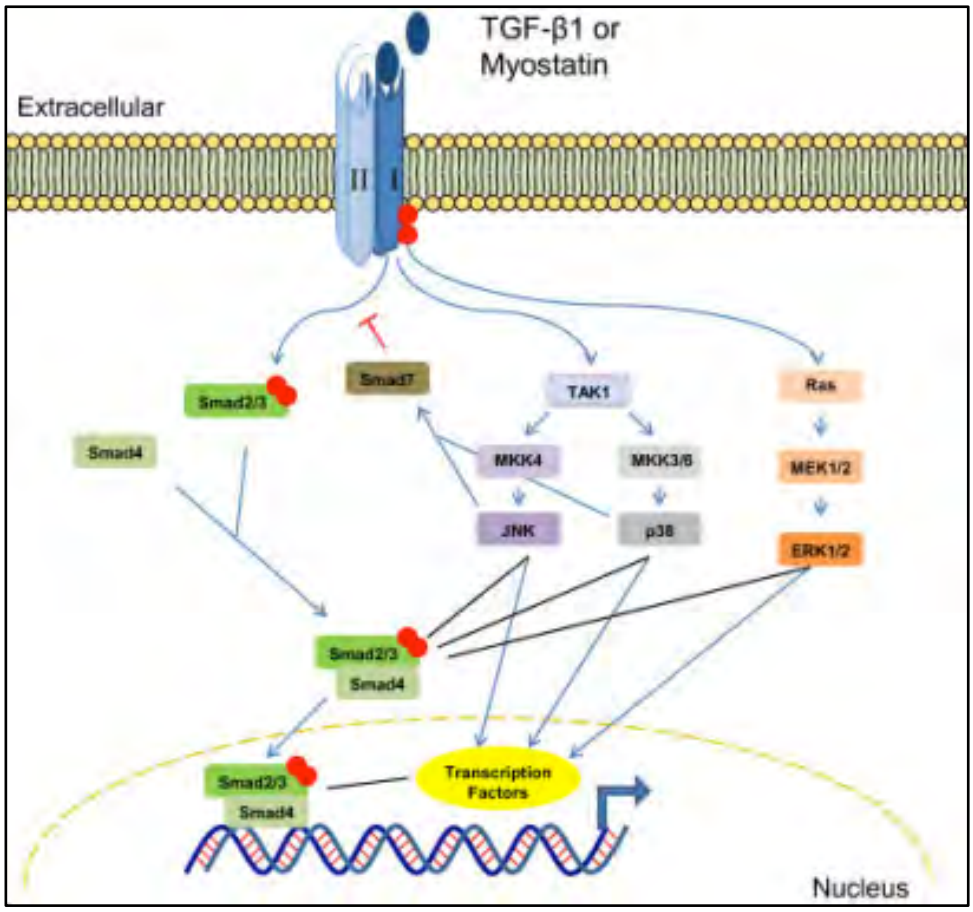

Figure 1.4 The TGFβ or Myostatin pathway demonstrating crosstalk between the canonical (Smad) & non-canonical TGFβ1 and myostatin pathways. (Burks & Cohn 2011)

Crosstalk between TGFβ1 and complement activation has been reported to augment injury in the case of pulmonary fibrosis. The deleterious profibrotic effect of complement C5, which generates complement C5a and C5b, is reportedly dependent on TGFβ1. It is apparent that complement C3a and complement C5a significantly suppress the expression of the TGFβ1 inhibitor, Smad7. Both complement C3a and complement C5a robustly activate p38 MAPK, with similar effects to the activation of the TGFβ-Smad pathway.

Genetic mapping of the *TGFB1* gene has shown that it has a highly polymorphic and functional regulatory region that likely impacts the pathogenesis of numerous TGFβ1-related/mediated diseases (Shah et al. 2006). Recently our group demonstrated the association of a functional African-specific polymorphism *TGFB1*

c.-387 C>T (rs1146316) among South Africans of African-genetic ancestry with juvenile MG complicated by treatment-resistant ophthalmoplegia (Nel et al. 2016).

Due to the fact that TGFβ1 is up-regulated in injured muscle, we propose that complement-mediated damage at the motor end-plate in MG may result in aberrant muscular repair responses in susceptible individuals thereby contributing to the treatment-resistant ophthalmoplegia in juvenile MG. Therefore, in this work we explored the effect of TGFβ1 on Smad pathway activation in the pathogenesis of treatment-resistant ophthalmoplegia in this subset of MG patients.

1.5 'DISEASE-IN-A-DISH' MODELING

Improved *in vitro* models of disease are valuable and necessary in order to investigate the pathogenesis of diseases on a molecular or cellular level, and provide a means of assessing various therapies. In order for these models to be representative, they should ideally be patient-specific and disease phenotype-specific. The more specific and more representative the model of disease, the more accurate the deductions that can be made and explored.

Human induced pluripotent stem (iPS) cells, are created from adult rather than embryonic tissues and represent a breakthrough in stem cell science (Takahashi & Yamanaka 2006; Takahashi et al. 2007). Human iPS cells are generated from somatic cells, that are genetically reprogrammed into an embryonic stem-cell-like state. iPS cells and human embryonic stem (hES) cells are pluripotent, which refers to the ability of the cells to differentiate into any or all of the three germ layers and self-renew (Stadtfeld & Hochedlinger 2010; Plath & Lowry 2011).

To convert a somatic cell into an iPS cell, a very small skin sample is taken from the patient, and a patient-specific skin fibroblast cell culture is then established *in vitro* (Takahashi & Yamanaka 2006). The fibroblast is then reprogrammed by reactivation of the embryonic regulatory genes and deactivation of the differentiation-specific genes. This phenomenon was first demonstrated by Takahashi and Yamanaka, who showed that the ectopic expression of four key transcription factors; Oct3/4, Sox2, Klf4 and c-Myc, reactivates endogenous pluripotency genes in mouse and human

fibroblasts resulting in cells with all the properties of embryonic stem cells (Takahashi & Yamanaka 2006; Takahashi et al. 2007). The iPS cells survive endless passaging and can be grown *en masse in vitro* providing a limitless supply of cells for differentiation into the particular cell type of interest for therapeutic or non-therapeutic purposes.

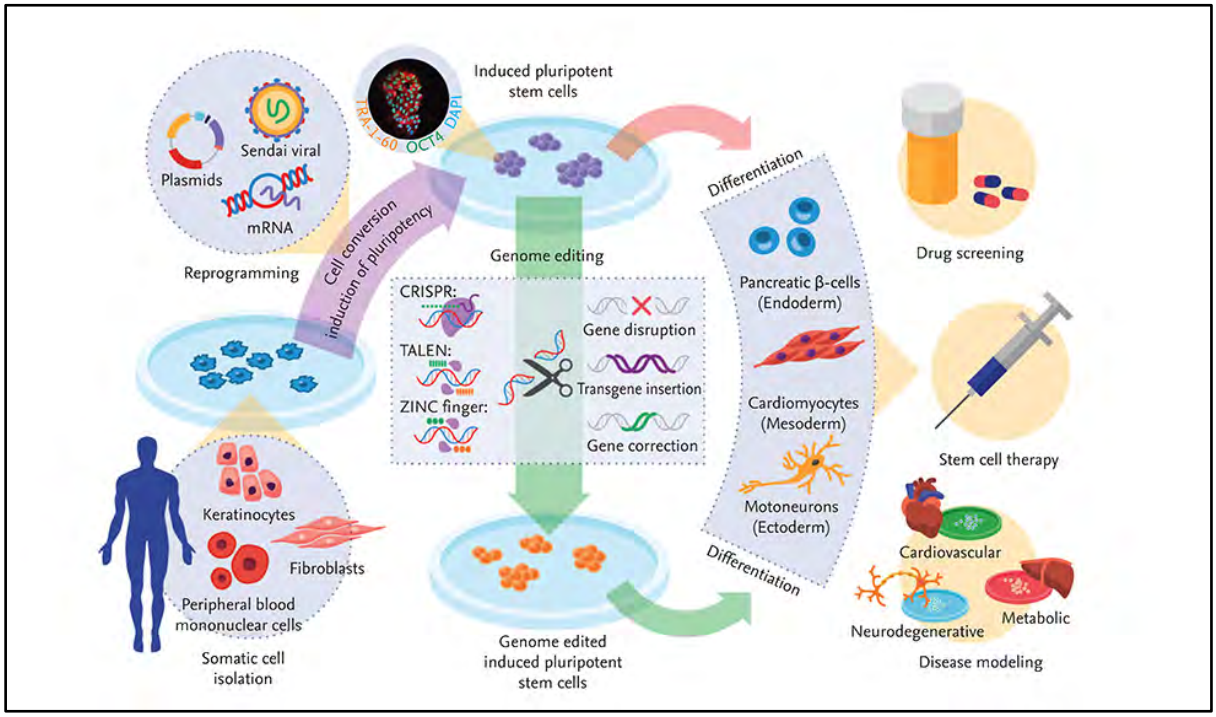

Figure 1.5 Human induced pluripotent stem (iPS) cell generation, differentiation and applications - including 'disease-in-a-dish' modeling. This figure demonstrates the generation of patient-specific iPS cells after reprogramming somatic cells with a viral vector loaded with critical regropramming genes. Thereafter the iPS cells can be differentiated into cells from any of the embryonic germ layers; endoderm, mesoderm, ectoderm. The applications of these patient-specific iPS cells include drug screening, stem cell therapy and disease modeling. (Downloaded from http://www.synapse.koreamed.org)

The availability of patient-specific iPS cell lines provides unprecedented opportunities to elucidate disease mechanisms *in vitro*, to carry out drug screening and toxicology studies, and to advance cell replacement therapy in regenerative medicine (Colman & Dreesen 2009a; 2009b). Reprogramming of fibroblasts from patients with Mendelian and complex genetic disorders allows the establishment of disease-specific iPS cell lines. To study the disease mechanism, a key issue is

whether the affected cell type derived from iPS cells can recapitulate the disease phenotype in culture.

Induction of lineage-specific differentiation is achieved by providing appropriate environmental factors, such as culture media, substrates or cytokines. Thus far several groups have demonstrated myogenic differentiation from hES cells by means of both the formation of three-dimensional cell aggregates called embryoid bodies (EBs), and a two-dimensional protocol for generating myogenic precursors (Mahmood et al. 2010; Barberi et al. 2007). Recently Awaya et al. reported a novel culture system that induces homogenous myogenic mesenchymal cells from both human ES and iPS cells. These myogenic mesenchymal cells exhibited stable long-term engraftment in injured muscles of immunodeficient mice *in vivo* and were reactivated upon subsequent muscle damage, increasing in number to reconstruct damaged muscles (Awaya et al. 2012).

It is widely accepted that EOM is a functionally discrete and a more specialised allotype of skeletal muscle (Kaminski et al. 2003; Yu Wai Man et al. 2005; Porter & Baker 1996). Extra-ocular muscles also have a distinct embryonic lineage compared to somite-derived muscles, and arise from progenitors that originate in cranial paraxial and prechordal mesoderm (Kang & Krauss 2010). Transcriptional regulation in EOMs is distinct from that in somite-derived muscles; Tbx1 and Pax3 appear to be dispensable, while Pitx2 is the critical upstream activator of myogenesis in EOMs and directly targets and activates transcription of the Myf5 and MyoD promoters (Kang & Krauss 2010; Zacharias et al. 2011). Numerous transcriptional and functional differences have been reported in stem cell populations isolated from EOMs and limb muscles. The muscle-derived stem cell population (satellite cells) is reported to be fifteen times greater in EOM versus limb muscle (Pacheco-Pinedo et al. 2009), and these myogenic precursor cells appear to be resistant to both oxidative stress and mechanical injury, and actively proliferate throughout life (Kallestad et al. 2011). All of these factors make the establishment of a completely representative *in vitro* disease model with EOM-specific myocytes very challenging.

Never the less, iPS cell technology and patient-derived ‘disease-in-a-dish’ models have the potential to significantly increase our understanding of the underlying

disease. This is of particular importance and relevance in the case of MG patients with treatment-resistant ophthalmoplegia, since diseased EOM tissue is not available or accessible for scientific study.

1.6 PROBLEM IDENTIFICATION

A severe treatment-resistant ophthalmoplegia (OP-MG) was first identified and described as a distinct complication of MG by Heckmann et al. in 2007. These patients are defined as having non-fatiguable, constant ophthalmoplegia and blepharoptosis of variable degrees, arbitarily defined as ranging from partial (involving ≥6 EOMs) to complete (involving all 12 EOMs) with unilateral or bilateral eyelid involvement. This group of patients have generalised MG, are predominantly AChR antibody positive, and are most frequently of African or recent African (mixed) genetic ancestry (Heckmann et al. 2007).

This phenotype often, but not always, has its onset in childhood or adolescence; resulting in long-term morbidity and functional visual impairment (Heckmann et al. 2012). We hypothesise that the phenotype is the result of a pathogenic process whereby the extra-ocular muscles have an altered and potentially abnormal response to immune-mediated MG. Our hypothesis is further supported by the resistance of the ophthalmoplegia to proven conventional immunosuppressive therapy, which appears to effectively treat the generalised component of disease in this subset of MG patients (Heckmann et al. 2007).

HYPOTHESIS

In this subset of myasthenia gravis patients with treatment-resistant ophthalmoplegia (OP-MG), there is a differential response of the extra-ocular muscles to the underlying disease process(es) on a genetic and molecular level, possibly due to abnormal myofibre homeostasis.

1.7 OBJECTIVES AND AIMS

My initial objective in this project was to investigate the feasibility of creating a 'disease-in-dish-model' for OP-MG using iPS cells, since this exciting and novel aspect of stem cell science had recently become available/possible in our laboratory. During this time I also had access to unique clinical material in the form of extraocular muscle, and therefore included the descriptive clinical and histopathological features of this material as an additional component in this thesis. To expand my knowledge and exposure to laboratory techniques, I learnt and performed other molecular biology techniques, such as immunoblotting and immunocytochemistry. These techniques were employed to investigate TGFβ1 expression in various cell lines, and contributed to other work on OP-MG published by our group in 2015.

The broad objective of this research is to explore the cellular and molecular mechanism(s) responsible for the development of the treatment-resistant ophthalmoplegia, with the following specific aims:

Specific Aims

1. To report descriptive clinical-pathological data, particularly pertaining to EOM function and the findings of histopathological and ultrastructural EOM tissue analysis, of patients with OP-MG versus that of non-MG control patients.
2. To assess TGFβ1-Smad expression in disease phenotype-specific cell lines and mouse myotubes.
3. To generate disease phenotype-specific induced pluripotent stem cells by reprogramming dermal fibroblasts obtained from MG and/or OP-MG patients.

CHAPTER 2

MATERIALS AND METHODS

This study was approved by the University of Cape Town Health Sciences Faculty Research Ethics committee (HREC 257/2012, 121/2013) and all individuals (or their parents if < 18 years of age) signed informed consent to participate.

2.1 DESCRIPTIVE CLINICAL-PATHOLOGICAL DATA STUDY

2.1.1 Clinical data

Three patients with a clinical diagnosis of OP-MG were referred for ophthalmological assessment. All OP-MG patients had the classical features of MG-associated fatigable weakness and at least one of the following; pyridostigmine responsiveness and/or >10% decremental response in compound muscle action potentials to repetitive nerve stimulation. All patients had a therapeutic response to immunosuppressive treatment in non-ocular muscles. OP-MG has been defined as (Heckmann et al. 2012):

- Complete OP-MG - all 12 EOMs show either no movement or only brief microsaccades (75-100% weakness) and frequent eyelid involvement with bilateral ptosis.
- Partial OP-MG - >50% of the EOMs show loss of motility (75-100% weakness), with or without eyelid involvement.
- Control MG - well characterised MG patients followed for many years without the development of the OP-MG phenotype.

After obtaining consent from patients known to the dedicated myasthenia gravis clinic at Groote Schuur Hospital, these patients' medical records were reviewed to retrieve data pertaining to the following:

- The extent and duration of MG; particulary their clinical phenotype with reference to presence or absence, and degree of treatment-resistant ophthalmoplegia.
- The medical records were reviewed for the results of any tests to determine the serological type of MG (anti-AChR/anti-MuSK/anti-LRP4 antibodies), thyroid biochemical results, and any orbital and extra-ocular muscle imaging perfomed on these MG patients.
- The clinical findings of the patients' ophthalmological examinations – particulary their ocular motility examination, including forced duction or traction test and active force generation test findings.
- The intra-operative findings of MG patients undergoing ocular re-alignment surgery.

2.1.2 EOM tissue samples

Informed consent

Permission to conduct this study was obtained from the University of Cape Town Health Sciences Faculty Research Ethics committee (HREC 257/2012, 121/2013) (*Appendix A.1)*. Two MG patients with complete OP-MG and 3 non-MG control patients undergoing ocular re-aligment surgery gave voluntary informed consent to donate excess EOM tissue excised at surgery (*Appendix A.1)*.

Collection and storage of EOM tissue samples

Fresh EOM tissue was collected in ice cold saline in theatre immediately after the tissue was excised by the surgeon. This tissue was then transported on ice to the laboratory without delay. In the laboratory the EOM tissue was soaked in 4% paraformaldehyde (PFA)/ phosphate-buffered saline (PBS) for 2 hours. Thereafter the tissue was washed thoroughly with PBS to remove the PFA, before being allowed to soak in 30% sucrose in 1x PBS for a few hours or overnight; as a means of tissue cryoprotection. The following morning the tissue was pinned to a small piece of cork and 'flash' frozen in iso-pentane cooled in liquid nitrogen in order to eliminate freezing/ice crystal artefact. The frozen tissue sample was transferred to a labelled cryovial, and stored at -80°C until all the collected samples were ready for further

processing and analysis. These frozen muscle biopsies were later transported on dry ice to the National Health Laboratory Service (NHLS) histopathology facility at Red Cross War Memorial Childrens' Hospital, where they were once again stored at -80°C until processed. While the NHLS technicians were responsible for the processing of these EOM samples, I was present in the histopathology laboratory at the time and therefore directly observed the processing, staining and reporting of these EOM sections for histology and ultrastructural analysis. *(Appendix A.3)*

2.1.3 Processing of EOM tissue samples for histopathology

Dubowitz et al. recommend that all histological, histochemical and immunohistochemical studies be performed on frozen material, preferably prepared as soon as possible after removal (Dubowitz et al. 2013). Frozen sections are preferred since fixation and wax-embedding may distort the myofibre architecture and certain biochemical studies are not possible on material processed in this manner. Unfortunately we were only able to perform a very limited panel of immunohistochemical studies on our muscle sample(s) due to one cryoprotected OP-MG sample having been misplaced and the other OP-MG sample had been processed and wax-embedded in 2012, with the residual portion of this EOM not adequately cryoprotected in the intervening 30 months to allow for further analysis. It was not possible to perform histochemical stains for the oxidative enzymes, particularly cytochrome oxidase (COX) since this enzyme reaction is very sensitive to even brief fixation and can only yield reliable results in frozen sections. Quantification of the degree of change in fibre sizes in relation to fibre types by means of the 'lesser diameter' principle, and atrophy and hypertrophy factors was not possible since transverse sections could not be obtained for all samples and the specific fibre types could not be reliably identified by means of adenosine triphosphatase (ATPase) staining or immunolabelling for myosin isoforms. For light microscopy, transverse sections of muscle yield more information than longitudinal sections.

Freezing and cutting of EOM tissue samples

The orientation of the muscle biopsy specimen was checked using a stereoscopic microscope before the biopsy was cut into pieces no greater than 5mm x 4mm and orientated to produce cross-sections of the muscle fibres. In the case of the EOM samples, the biopsy specimens were very small and could not always be orientated to yield a cross-sectional slice of tissue.

The EOM specimen was orientated as upright as possible onto a drop of Tissue-Tek® O.C.T™ Compound (#4583, Sakura Finetek Europe BV, The Netherlands) on a small square of cork. A small container of iso-pentane was cooled in liquid nitrogen until a thick ice rim formed around the inside of the iso-pentane container. The cork, holding the muscle sample, was held with a forceps and lowered into the iso-pentane and vigorously agitated from side to side for a few seconds. Thereafter the frozen muscle biopsy sample was frozen onto a labelled chuck with Tissue-Tek® O.C.T™ Compound using liquid nitrogen, wrapped in parafilm and stored at -80°C until it was sectioned.

These frozen sections were cut in a cryostat, consisting of a rotary microtome enclosed in a cold cabinet kept at approximately -25°C. Once the sections were cut, a rapid haematoxylin and eosin (H&E) stain was performed to ensure that it was an adequately representative section of muscle tissue.

Haematoxylin and Eosin (H&E) staining

H&E staining has the ability to clearly demonstrate a number of different tissue structures. The haematoxylin component stains the cell nuclei blue/black, while the eosin stains the cell cytoplasm and most connective tissue fibres in varying shades and intensities of pink, orange and red.

Once the frozen sections were cut to an approximate thickness of 7-8µm, they were immediately fixed in methanol for a few seconds. Thereafter the sections were rinsed with water, stained with haematoxylin (*Appendix A.3*) for 10-15 seconds while being agitated, and rinsed with water again. The section was covered in Scott's tap water substitute (*Appendix A.3*) until it turned blue (approximately 5 seconds). Sections were stained in a stock solution of eosin (2 parts)/phloxine (1 part) for 10-

15 seconds, rinsed with water, and dehydrated in an ascending series of alcohols before being mounted. The section was finally clarified with xylene to prevent traces of water causing turbidity, and mounted in Entellan™ rapid mounting medium (#107961, Merck Millipore, Germany).

Modified Gomori Trichrome staining

The term 'trichrome' refers to a number of techniques used to selectively demonstrate muscle, collagen fibres, fibrin and erythrocytes. This modified Gomori's technique is preferred when using fresh frozen muscle biopsy specimens in the processing NHLS histopathology laboratory. Nuclei appear grey/black, connective tissue (collagen) stains green, and cytoplasm stains red.

Appropriately cut frozen sections were allowed to air dry for at least 10 minutes. They were then stained with Gladsdon's haematoxylin for 1-2 minutes, before being rinsed with running water until they turned blue. Thereafter the sections were stained with Gomori solution (*Appendix A.3)* for a period of 10-15 minutes. The sections were rinsed with water and differentiated in a 0.2% solution of acetic acid if deemed necessary, before being dehydrated in graded alcohols, clarified with xylene and mounted in Entellan™ rapid mounting medium.

Oil Red O staining

The most common method of demonstrating lipids in tissue is with frozen crystat sections, while the Oil Red O method is mainly used for lipid demonstration in cytology specimens – fat appears red and nuclei stain blue. The term 'lipid' is used to describe all naturally occurring fats and fat-like substances; these can be seen as droplets within the cells or bound to other tissue components.

Cryostat-cut frozen sections were air-dried, and then washed in distilled water (dH_2O) before the Oil Red O working solution (*Appendix A.3*) was applied for 7-10 minutes. Differentiation was performed by means of 3-4 submersions in 70% iso-propyl alcohol. The section was then washed in water, and the nuclei counter-stained with haematoxylin for approximately 1 minute. Thereafter the section was subjected to Scott's tap water substitute (*Appendix A.3*) until it turned blue, and mounted in glycerine jelly.

Immunohistochemistry for fast & slow myosin (*Appendix A.3*)

The mounted sections were dewaxed in xylene and then hydrated using absolute alcohol to 70% alcohol. The sections are then immersed in water, followed by ethylenediaminetetra-acetic acid (EDTA) at pH 8. Whilst in the latter, the slides are placed in the pressure cooker for 2 minutes and then placed in 1x PBS for transportation. Immunohistochemistry was performed with antibodies against fast and slow myosin (Novocastra, UK, Dilution 1:40).

2.1.4 Processing of EOM tissue samples for electron microscopy (EM)

Fixation and processing of EOM tissue samples for EM

A small fragment of muscle tissue was taken from the specimen for electron microscopic examination. Care was taken to ensure that this thin slice of tissue displayed longitudinally-orientated muscle fibres. This fragment was transferred into a small tube containing a fixative of 3% gluteraldehyde in 0.2M sodium cacodylate buffer (*Appendix A.3*). Tissue sections to be examined by the transmission electron microscope need to be cut to a thickness of approximately 15nm, compared to the 5-8μm sections required for light microscopy. In order to cut these ultra-thin sections, four small (<0.25mm) pieces of tissue were sampled from each specimen and processed to a resin (Spurr resin Premix Kit, TAAB, UK), and then polymerized at 60°C to harden (*Appendix A.3*).

Cutting and staining sections for EM

The resin-embedded tissue blocks were trimmed until the tissue was correctly orientated for sections to be cut. Initially thicker (0.5μm) sections of tissue were cut with the ultratome. These thicker sections were then stained with 1% Toluidine Blue (Merck, Germany) in sodium tetraborate (Merck, Germany), allowed to dry on a hot plate, and then rinsed with water and dried again. The 'thick' sections are used as a visual reference to ensure that it is an appropriately representative tissue section with all the structures of interest visible. An area approximately a fifth the size of the original thick tissue section was selected for the subsequent ultra-thin sections. The ultra-thin (15nm) sections were cut from the hardened resin block using an ultratome. These thin sections were then floated from the ultratome knife with

dH_2O and picked up on wet 3mm copper grids, before being transferred to filter paper in a petri dish. The ultra-thin sections for EM were stained with uranyl acetate (6.25g/100ml dH_2O) for 10 minutes, washed with dH_2O, and then stained with lead citrate (*Appendix A.3*) for 6 minutes. After rinsing with dH_2O again, the grids containing the sections were transferred onto blotting paper and allowed to dry.

2.1.5 Viewing and analysis of EOM tissue samples

Extraocular muscle sections were viewed with an Olympus BX-41 light microscope for histopathological analysis, and digital images were captured and edited using Dino-eye with Dinocapture 2.0 software. Ultrastructural analysis was performed using a Joel (JEM-1011) transmission electron microscope located in unit D7 at Groote Schuur Hospital. ITEM analysis software by Olympus Software Imaging Solutions version 5 (build 1187) was used to analyse the EM sections and capture digital images.

Histopathological and ultrastructural analysis and interpretation was performed by viewing between two and five sections of muscle at different levels of magnification for these small EOM samples. The EOM samples were reported according to the following modified template applicable to all muscle samples (*Appendix A.3*):

Morphology

- Variation in myofibre size
- Atrophic fibres
- Variation in myofibre shape
- Position and number of nuclei
- Necrotising fibres
- Regenerative fibres
- Increased endomysial connective tissue
- Inflammatory infiltrate

Special stains

- Modified Gomori Trichrome
- Oil red O

Histochemistry

Not possible on our EOM samples (see explanation above)

Immunohistochemistry

- Slow and fast myosin

Ultrastructural analysis of myofibres

- Sarcolemma
- Myofibrils & cytoskeleton
- Nucleus
- Mitochondria
- Membrane systems
- Deposits & particles
- Other unusual structures

2.2 STUDIES ON PHENOTYPE-SPECIFIC FIBROBLASTS, MYOFIBROBLASTS & C2C12 MOUSE MYOBLASTS

To assess the TGFβ1-Smad3 signalling pathway in phenotype-specific fibroblasts, myofibroblasts and mouse myoblasts we performed the following experiments using immunoblotting and immunocytochemistry techniques.

2.2.1 Culture & maintenance of patient-specific dermal fibroblasts & EOM myofibroblasts

Phenotype-specific human dermal fibroblast (HDF) cultures were established from fresh full-thickness skin biopsy samples, approximately 4mm in diameter, using the explant culture method. The dermal biopsies were minced with sterile blades in the laminar flow cabinet and the cells were cultured under coverslips in 35mm cell culture dishes in DMEM (Highveld Biological, RSA) with 10% FBS (Biochrom, Germany), 100U/ml penicillin and 100µg/ml streptomycin. Fibroblasts emerged after 4-7 days and when these cultures were confluent, they were subcultured and cryopreserved with 10% DMSO in liquid nitrogen at passage 2. Each fibroblast cell line was subjected to testing for Mycoplasma contamination prior to cryopreservation (*Appendix A.4)*.

Perimysial myofibroblast cultures were established by preparing excised EOM tendon in the same manner described above for the skin biopsies. Fibroblast and myofibroblast cultures independently isolated from different individuals were maintained as monolayers in the abovementioned medium at 37°C and 95% air, 5%CO_2 and 65% humidity. Medium was replaced every 2-3 days and all cultures were routinely subjected to Mycoplasma tests and only Mycoplasma-free cells were used in experiments.

2.2.2 Culture & maintenance of C2C12 mouse myoblasts

Mouse myoblast C2C12 cells were cultured in the same medium and conditions as the human dermal fibroblasts (section 2.2.1), but were allowed to differentiate into myotubes by switching from growth medium (DMEM + 10% FBS + 1% P/S) to differentiating medium (DMEM supplemented with 2% horse serum and 1% P/S) approximately 6 days before the stimulation experiment. Medium was replaced every 2-3 days and all cell cultures were routinely subjected to Mycoplasma tests and only Mycoplasma-free cells were used in experiments *(Appendix A.4)*.

2.2.3 Mycoplasma testing

Cells grown on a coverslip in antibiotic-free medium for at least 5 days were washed with 1x PBS before being fixed in a 1:3 mixture of glacial acetic acid and methanol for 5 minutes. Thereafter the fixative was discarded and the coverslip with the cells allowed to air-dry at RT for 3-5 minutes. Once dried, the DNA was stained with Hoechst 33258 (0.5µg/ml) (*Appendix A.4*) for 6-10 minutes and kept in the dark, then washed briefly with 1x PBS to remove excess stain. The coverslip was then mounted on a glass microscope slide with mounting fluid at pH 5.5 (*Appendix A.4*). Once the mounting fluid had dried, the cells were viewed by means of fluorescence microscopy using the DAPI filter. In Mycoplasma negative cells, Hoechst 33258 staining is limited to the nucleus; while cells infected with Mycoplasma display both nuclear and cytoplasmic staining.

2.2.4 Preparation of cells for stimulation experiments

Fibroblasts from subpassages 4-8 were used for all experiments. For each sample, approximately 2 x 10^5 human dermal fibroblasts from the individual cell lines of

interest were plated (in each well of a 6-well plate) 2-3 days before the scheduled experiment. It was determined in a prior experiment that this volume of cells per well, ensured a 85-90% confluent monolayer culture after approximately 48 hours and yielded sufficient cellular protein for western blot experiments.

C2C12 cells were plated at a density of 1-1.5 x 10^5 per 6cm cell culture dish, depending on whether the cells were likely to be in culture for more or less than 9 days. Prior to any treatments, the C2C12 cells were serum-starved by changing to a differentiation medium containing only 0.5% horse serum from day 6 of differentiation. TGFβ1 treatment followed 16-24 hours after serum-starvation *(Appendix A.4 & A.5)*.

2.2.5 Stimulation experiments with homologous sera & recombinant human TGFβ1 (rhTGFβ1)

Phenotype-specific fibroblast stimulation with homologous sera & rhTGFβ1

In order to assess whether there was a differential response in autocrine TGFβ1 pathway activity between the different phenotype-specific HDF cell lines in response to stimulation with sera and rhTGFβ1, we conducted the following experiments.

Sera from healthy controls and newly diagnosed AChR-antibody positive MG patients were collected, allowed to clot at RT for 4 hours and centrifuged in a swinging bucket rotor centrifuge at 1900xg for 10 minutes at 4°C. The supernatant serum was recovered and aliquoted under sterile conditions, before being stored at -20°C.

Patients selected for sera donation had generalised MG with substantial extraocular mucle involvement and were treatment-naïve (newly diagnosed or 1 individual known with MG but defaulted treatment for ≥5 months). The active MG sera, containing a unique 'cocktail' of cytokines and mediators, were used to stimulate phenotype-specific cells in an attempt to replicate the biological environment present at a cellular level in this disease. Sera samples were expected to be heterogenous between samples in terms of their autoantibody and cytokine profile. For this reason they were stored in batches to enable sera from a single donor (homologous) to be used in each separate experiment (and for all related repeats) to minimize experimental variability.

Twenty four hours prior to treating the individual dermal fibroblast cultures, the serum concentration of the growth medium was reduced from 10% to 0.5% FBS. Thereafter, the subconfluent fibroblast cultures were stimulated with the following treatments for 1 hour; no treatment (vehicle only), 10% pooled control serum from two normal donors 1:1, 10% treatment-naïve MG serum (obtained from a newly diagnosed AChR-antibody positive individual with generalised MG and concomitant ocular muscle involvement), rhTGF-β1 (#240-B, R&D Systems, USA) at a concentration of 5ng/ml (diluted in 4mM HCl containing 1mg/ml of bovine serum albumin). Aliquots of sera stored at -20°C were thawed and 10% dilutions of MG and control sera were prepared in medium with 0.5% FBS, and then heated to 80°C for 5 minutes in order to activate latent native TGFβ1 (Brown et al. 1990). Thereafter the sera were allowed to cool to room temperature before being administered to the cell cultures as outlined in **Figure 2.2.1** (*Appendix A.5)*.

CONTROL -MG (HDF)	**No treatment**	**Control serum (10%)**	**MG serum (10%)**	**rhTGFβ1 (5ng/ml)**
PARTIAL / COMPLETE OP-MG (HDF)	**No treatment**	**Control serum (10%)**	**MG serum (10%)**	**rhTGFβ1 (5ng/ml)**

Figure 2.2.1 Demonstrates the phenotype-specific human dermal fibroblast (HDF) cell lines (control MG/OP-MG) and the treatments for stimulation experiments.

C2C12 mouse myotube stimulation with rhTGFβ1

In order to evaluate Daf levels in response of to variable doses and periods of rhTGFβ1 stimulation, we performed the following western blot experiments in 6 day differentiated C2C12 mouse myotubes.

The C2C12 6 day differentiated myotubes were subjected to the following treatments; no treatment, rhTGFβ1 10ng/ml x 1 day, rhTGFβ1 10ng/ml x 2 days, rhTGFβ1 1ng/ml x 3 days, rhTGFβ1 1ng/ml x 5 days **(Figure 2.2.2)**. The medium (differentiation medium with 0,5% horse serum) and rhTGFβ1 (1ng/ml) was refreshed on day 3 in the C2C12 cells being subjected to 5 days of rhTGFβ1 treatment (*Appendix A.5)*.

C2C12 6-day differentiated mouse myotubes		
No rhTGFβ1	**rhTGFβ1 (10ng/mg) x 1 day**	**rhTGFβ1 (10ng/ml) x 2 days**

C2C12 6-day differentiated mouse myotubes		
No rhTGFβ1	**rhTGFβ1 (1ng/ml) x 3 days**	**rhTGFβ1 (1ng/ml) x 5 days**

Figure 2.2.2 Demonstrates the C2C12 mouse myotubes and the rhTGFβ1 treatments (different doses & durations) for stimulation experiments.

2.2.6 Western blot analysis

Phenotype-specific fibroblast stimulation with heterologous sera & rhTGFβ1 and resultant phosphorylation of Smad3

Subconfluent cultured fibroblasts were harvested by trypsinisation with trypsin-EDTA (Biowest, France). Cells were rinsed with ice-cold 1x PBS solution, then harvested whole cell extracts were incubated in radio immuno precipitation assay (RIPA) lysis buffer, containing proteinase and phosphatase inhibitors (*Appendix A.6*), on ice for a minimum of 30 minutes, centrifuged at 12 000 rpm for 20 minutes at 4°C, and the protein-rich supernatants recovered. Protein concentrations for each cell extract were determined using the bicichoninic acid (BCA) Protein Assay Kit (Pierce, USA) with bovine serum albumin (BSA) as the standard. Aliquots of protein were then stored at -80°C until further use (within 24 hours). Equal amounts of protein lysates (35μg or 40μg) were solubilised in RIPA buffer, heated at 75°C for 10 minutes, and separated in 1.5mm thick 8% or 10% SDS-polyacrylamide gels using running buffer (*Appendix A.6*). Molecular weight markers were used to monitor protein separation. Proteins were electrotransferred to a Hybond ECL nitrocellulose membrane (Amersham Biosciences, UK) using transfer buffer, and equal protein loading was monitored with Ponceau S stain and anti-p38 MAPK as the loading control. **Figure 2.2.3** demonstrates the sequence of protein loading and consequent banding pattern.

To reduce non-specific binding, nitrocellulose membranes were blocked in 1x TBS/0.1% Tween (*Appendix A.6*) containing 5% non-fat dry milk powder for 1 hour at RT for phosphorlyated-Smad3 (p-Smad3). Membranes were incubated at 4°C overnight with primary rabbit monoclonal antibodies against phospho-Smad3 (#9520, Cell Signalling Technology, USA) at a dilution of 1:1000 in 5% BSA (Roche,

USA) in 1x TBS/0.1% Tween. To detect p38 MAPK (loading control and 'house keeping protein'), membranes were soaked in a solution of 5% non-fat dry milk powder in 1x PBS/0.1% Tween for 1 hour at RT to reduce non-specific binding. Thereafter the membrane was washed with 1x PBS/0.1% Tween, before being incubated with rabbit polyclonal anti-p38 MAPK antibodies (M0800, Sigma, USA) at a dilution of 1:5000 in 1x PBS/0.1% Tween overnight at 4°C. Following overnight incubation with the primary antibodies and subsequent washes, the membranes were incubated with horseradish peroxidase (HRP)-conjugated secondary anti-rabbit antibodies (BioRad, USA) at a dilution of 1:4000 in 5% non-fat dry milk powder in 1x PBS/0.1% Tween for 1 hour at RT. Membranes were again washed in PBS/0.1% Tween and the proteins of interest visualised by enhanced chemiluminescence using one of the following kits; SuperSignal® West Dura Extended Duration substrate (Thermo Fisher Scientific™, USA), SuperSignal® West Pico Chemiluminescent Substrate (Thermo Fisher Scientific™, USA), WesternBright™ ECL HRP substrate (Advansta, USA). For all detection solutions a total of 1ml of the substrates A and B detection reagents (ratio 1:1) were added to the membrane for 1-2 minutes before the membrane was sandwiched between acetate sheets in a cassette and exposed to X-ray film. The film was immersed in developer until bands became visible, rinsed under running water and immersed in fixing solution for a minimum of 5 minutes. Thereafter the film was rinsed in running water and allowed to air-dry.

1	2	3	4	5	6	7	8	9
Molecular weight marker	HDF – CONTROL MG				HDF – PARTIAL / COMPLETE OP-MG			
	No treatment	Control serum (10%)	MG serum (10%)	rhTGFβ1 (5ng/ml)	No treatment	Control serum (10%)	MG serum (10%)	rhTGFβ1 (5ng/ml)

Figure 2.2.3 Demonstrates the manner in which the molecular weight marker and phenotype-specific human dermal fibroblast (HDF) cell lysates from sera & rhTGFβ1 stimulation experiments were loaded for western blotting.

The expression of protein bands on the developed film was quantified as the densitometry value analysed by UN-SCAN-IT gel 6.1 software and normalised to the appropriate 'house-keeping' protein (p38 MAPK) using Microsoft® Excel® for Mac 2011 version 14.4.6 (141106).

Stripping the nitrocellulose membrane

Membranes probed for more than one protein (p-Smad3 and p38 MAPK) were immersed in pre-heated stripping buffer (*Appendix A.6*) for 30 minutes at 50°C. This was followed by 2 x 10 minute and 2 x 5 minute washes with 1 x PBS/0.1% Tween, after which standard western blotting procedure was once again followed to detect the protein of interest.

C2C12 mouse myotube stimulation with rhTGFβ1 and resultant Daf levels

Approximately 1.5 x 10^5/ml C2C12 cells, cultured for protein analysis, were plated in 6cm cell culture dishes. Differentiated myotubes were harvested by trypsinisation as previously described. Whole cell extracts from C2C12 cells were prepared under reducing conditions using RIPA lysis buffer (*Appendix A.6*) and stored on ice for 30 minutes. Equal amounts of protein (30μg) were prepared and loaded in each lane, after heating at 100°C for 5 minutes. **Figure 2.2.4** demonstrates the loading pattern of protein and consequent band sequence.

The cellular protein was resolved on a 1.5mm thick 8% SDS-PAGE gel and then transferred electrophoretically to a Hybond ECL nitrocellulose membrane as previously described in section 2.2.1.6. The membrane was carefully cut to separate the Daf bands (at 70 & 100kDa) from the p38 MAPK band (at 38-40kDa), to allow the membranes to be separately probed for Daf and p38 MAPK. The primary antibodies and appropriate dilutions were: rabbit polyclonal Daf antibody (sc-9156, Santa Cruz Biotechnologies, USA) diluted 1:200 in 1x PBS/0.1% Tween. The remainder of the processes are identical to those described above.

1	2	3	4	5	6	7
Molecular weight marker	C2C12 myotubes			C2C12 myotubes (technical repeat)		
	No rhTGFβ1	rhTGFβ1 x 1 day	rhTGFβ1 x 2 days	No rhTGFβ1	rhTGFβ1 x 1 day	rhTGFβ1 x 2 days
	No rhTGFβ1	rhTGFβ1 x 3 days	rhTGFβ1 x 5 days	No rhTGFβ1	rhTGFβ1 x 3 days	rhTGFβ1 x 5 days

Figure 2.2.4 Demonstrates the manner in which the molecular weight marker and C2C12 mouse myotube cell lysates from rhTGFβ1 stimulation experiments were loaded for western blotting.

2.2.7 Immunoflourescence microscopy for smooth muscle actin & collagen in EOM myofibroblasts

In order to assess whether there was a differential response in myofibroblast differentiation after rhTGFβ1 stimulation in the phenotype-specific EOM myofibroblast cell lines, we performed immunofluorescence microscopy for the differentiation products α-smooth muscle actin (α-SMA) and collagen-∝2 type 1 (Col1A2).

Phenotype-specific human myofibroblasts were derived from EOM tendon explant cell cultures and maintained as for dermal fibroblasts as described in section 2.2.1. Due to the derivation of these cells from extraocular muscle tendinous insertion, there was some uncertainty as to the exact cell phenotype isolated in explant cell culture, fibroblast or myofibroblast. Care was therefore taken to compare the basal cell morphology prior to any experiments, and the morphology of the cells after equivalent periods of exposure to rhTGFβ1 and vehicle (no rhTGFβ1).

To evaluate the growth of the comparative phenotype-specific myofibroblasts, an equal number (5 x 10^4) of control (MG189) and MG (MG64) cells were seeded in duplicate 35mm tissue culture dishes. A growth assessment was conducted over a period of 14 days with cell counts performed using a haemocytometer as described previously (Prince et al., 2003) on days 1, 4, 7, 10, 14 and medium was replenished on days 4, 8 and 12.

To evaluate the response of these comparative phenotype-specific cells to TGFβ1, we treated the cells with rhTGFβ1 at a concentration of 1ng/ml (diluted in 4mM HCl containing 1mg/ml of bovine serum albumin) or vehicle (supplemented DMEM) for 96 hours, as demonstrated in **Figure 2.2.5** (*Appendix A.5*). The cells were then rinsed thoroughly with 1xPBS, before being fixed with 4% PFA/PBS for 15 minutes. After further 1xPBS rinses, the cells were permeabilised with 100% ice-cold methanol for 10 minutes, and rinsed thoroughly with 1xPBS again. The cells were then blocked with one of two blocking solutions; 20% donkey serum in 0.1% Triton-X, or 1% BSA in 0.1% Triton-X (*Appendix A.7*). The myofibroblast cultures were then incubated with primary antibodies at optimal dilutions at 4°C overnight (**Figure 2.2.5**). The primary

antibodies and their dilutions were as follows; anti-α-SMA mouse monoclonal antibodies (ab7817, Abcam, UK) 1:100, anti-Col1A2 goat polyclonal antibodies (sc-8786, Santa Cruz Biotechnology, USA) 1:50. After rinsing with 1xPBS, the cells were incubated with secondary HRP-conjugated anti-mouse and anti-goat antibodies (Jackson ImmunoResearch Laboratories Inc., USA) for 2 hours in the dark at RT (*Appendix A.7*). Thereafter the cells were counter-stained with Hoechst 33258 (0.5μg/ml) for 5 minutes. After the final 1xPBS rinses, the coverslips with monolayer cell cultures were mounted onto glass slides using Mowiol® mounting medium (Hoechst, Germany) containing n-propyl gallate (Sigma, USA) to prevent the signal from fading (*Appendix A.7*) and allowed to dry at RT in the dark overnight. Negative controls were cells treated as above, but the primary antibody was excluded.

α-smooth muscle actin					
OP-MG EOM-derived Myofibroblasts			**Non MG EOM-derived Myofibroblasts**		
Experimental **Control** **No rhTGFβ1**	**rhTGFβ1** **x 96 hrs**	**Control** **No 1° Ab**	**Experimental** **Control** **No rhTGFβ1**	**rhTGFβ1** **x 96 hrs**	**Control** **No 1° Ab**

Collagen ∝2 type 1					
OP-MG EOM-derived Myofibroblasts			**Non MG EOM-derived Myofibroblasts**		
Experimental **Control** **No rhTGFβ1**	**rhTGFβ1** **x 96 hrs**	**Control** **No 1° Ab**	**Experimental** **Control** **No rhTGFβ1**	**rhTGFβ1** **x 96 hrs**	**Control** **No 1° Ab**

Figure 2.2.5 Demonstrates the phenotype-specific extraocular muscle (EOM)-derived myofibroblasts and the stimulation experiment treatments for immunocytochemistry for ∝-smooth muscle actin & collagen ∝2 type 1.

The cells were visualised by fluorescence microscopy using a Zeiss Axiovert 200M fluorescent microscope (Zeiss, Germany) with the following filters:

- DAPI – excitation BP 365/12, emission LP 387
- Alexa488 – excitation BP 450-490, emission LP/BP 515-565
- Cy3 – excitation BP 546/12, emission LP 590

Confocal fluorescence microscopy was performed with an LSM 510 Meta with NLO microscope (Zeiss, Germany), using the 20x objective and 1-3x zoom.

All images were acquired using the same intensity and photodetector gain to allow quantitative comparisons of relative levels of immunoreactivity between samples. Images were edited and optimised using Axiovision 4.7, ImageJ, and Zen 2009 Light Edition software.

2.2.8 Statistical analysis

Densitometric readings of the protein bands expressed on the developed film (obtained by the method described in section 2.2.6) were imported into, and fold activation in arbitrary units was calculated by first normalising each band to p38 MAPK as background expression, and then to the untreated control. Mean and standard deviations were calculated with pooled data from these western blot experiments. The two-tailed T-test was performed on pooled data to calculate the relevant changes between cell lines and treatment groups, and p-values <0.05 were considered statistically significant.

Cell counts were conducted on each cell line (duplicate parallel cultures for each line) on days 1, 4, 7, 10 and 14. Microsoft® Excel® for Mac 2011 version 14.4.6 (141106) was used to determine the average cell number/density on the respective days, and these average/mean values were plotted to generate a growth curve for each cell line. A two-tailed T-test was performed to compare cell numbers between the two cell lines on day 4 and day 10. Doubling time of each cell line was calculated by means of an online doubling time calculator (Roth V 2006 Doubling Time Computing, available from http://www.doubling-time.com/compute.php).

2.3 GENERATION OF MG &/OR OP-MG PHENOTYPE-SPECIFIC PATIENT-DERIVED INDUCED PLURIPOTENT STEM CELLS

Due to the paucity of muscle tissue, particularly EOM tissue, available for study in patients with MG, one of my objectives was to establish phenotype-specific induced pluripotent stem cells for a potential 'disease-in-a-dish' model. Here I describe the method(s) I employed and the difficulties encountered during this process.

Two individuals in regular attendence at the myasthenia gravis clinic at Groote Schuur Hospital were selected as being representative of the control MG and partial OP-MG phenotypes (see section 2.1.1 for definitions). Following the informed consent process, a 4mm full-thickness skin biopsy was taken by a doctor (myself or Dr Melissa Nel) and transported in cell culture medium to the tissue culture laboratory, and cultured as described below. The participants consented to their cells being utilised for MG-based research to be undertaken by the Neurology Research Group at the University of Cape Town, subject to approval by the institutional Human Research Ethics committee (*Appendix A.1*). Cells from these individuals were utilised for the experiments described here. All samples have been de-identified to protect anonymity.

2.3.1 Creation of MG phenotype-specific patient-derived iPS cells from HDF

Skin biopsies and dermal fibroblast isolation

Described in section 2.2.1.

Preparation of inactivated mouse embryonic fibroblast feeder cells (iMEFs)

A standard cell culture method employed for the derivation, maintenance and culture of induced pluripotent stem cells is to co-culture them with fibroblasts (murine or human) capable of conditioning the culture environment, and thereby supporting the pluripotency and proliferative potential of these cells. Feeder cells perform this function by secreting growth factors and extracellular matrix components to enable cell attachment and proliferation. Primary mouse embryonic fibroblasts (MEFs) were utilised for our induced pluripotent stem cell co-cultures, local primary outbred MEFs isolated from 14.5 day old embryos (BALB/c strain) and commercially obtained MEFs (MEF(CF1) ATCC® SCRC-1040, USA). As described in section 2.2.3, all cell cultures (HDF and MEFs) were routinely subjected to Mycoplasma tests and only Mycoplasma-free cells were used to generate feeder cells (MEFs) and stem cells.

It is essential to mitotically inactivate fibroblast-feeder cells so that they do not overgrow the stem cell culture. The inhibition of mitosis can be achieved by irradiating the MEFs or by treating them with a cytostatic agent, such as mitomycin

C. In this state the cells are metabolically active and provide secreted factors, extracellular matrix components and cellular contact to keep the stem cells from differentiating and maintaining a normal karyotype without proliferating and thereby overgrowing the stem cell colonies. Mitomycin C (MMC) inhibits DNA synthesis and nuclear division, and exposure to MMC at 10μg/ml for 2-3 hours is sufficient to mitotically inactivate MEFs. MMC must be handled with caution and disposed of appropriately due to its toxic and potentially carcinogenic properties. The same process for inactivation of MEFs with mitomycin C was applied to both local primary outbred MEFs (E14.5) and commercially obtained MEFs (ATCC®), and both lines of MEFs were inactivated at passage 6 (*Appendix A.8*).

Reprogramming of human dermal fibroblasts (Figure 2.3.2)

Low passage (p2-p4) patient-specific human dermal fibroblasts (MG7 & MG822) were seeded into 35mm wells (6-well plate) at cell densities of 1.5 x 10^5 and 1.75 x 10^5 cells/well. Cells were allowed to settle and adhere to the surface of the well, while being maintained in human derived fibroblast (HDF) medium (*Appendix A.8*). Twenty four to 48 hours later the wells with cells at 80-90% confluency were selected to be infected with the Sendai viral vector (SeVdp), and the medium was changed to HDF medium without antibiotics.

The reprogramming gene-loaded Sendai viral vector (SeVdp) was a kind gift from Professor Mahito Nakanishi from the Research Center for Stem Cell Engineering, National Institute of Advanced Industrial Science and Technology, Japan. The SeVdp viral vector is not pathogenic to human or animal cells since the cells carrying the SeVdp do not generate any virus-like particle(s) due to the functional deletion of genes coding for the structural proteins M, F, and HN from the vector genome. The vector is loaded with the reprogramming genes; *KLF4, OCT3/4, SOX2, c-MYC* – allowing the simultaneous transfer of the reprogramming genes on a single common vector into a somatic cell and thereby providing enhanced efficacy. This SeVdp vector exhibits sustained infectious ability without cytotoxicity, and even after infection of a differentiated cell and after cell division it persists in the cytoplasm of the infected cell. This vector allows the expression of exogenous reprogramming

genes for 10-20 days, the period required for the completion of the reprogramming process, therefore enabling complete reprogramming with a single vector/construct of multiple genes. The reprogramming gene-loaded Sendai viral vector can be removed from the cells by adding a small interfering RNA (siRNA), or by integrating a target sequence for microRNA (miRNA) into an *L*, *NP*, or *P* gene-noncoding region of the SeVdp. The SeVdp is silenced via the endogenous miRNA pathway by targeting the mir-302a binding site, this miRNA is selectively expressed in embryonic stem cells and fully reprogrammed iPS cells (Nakanishi & Otsu 2012). This technique has the advantage of being able to automatically remove the reprogramming gene-loaded SeVdp vector without the need for externally introducing siRNA. Consequently the iPS cell is genetically identical to the parent differentiated cell used to generate the iPS cell, and since there is no foreign exogenous DNA in the cell at the end of the procedure, the cell's potential for self-renewal is enhanced (Nishimura et al. 2011; Nakanishi & Otsu 2012). The vector that was used to generate iPS cells in this project incorported the mir302 target sequence.

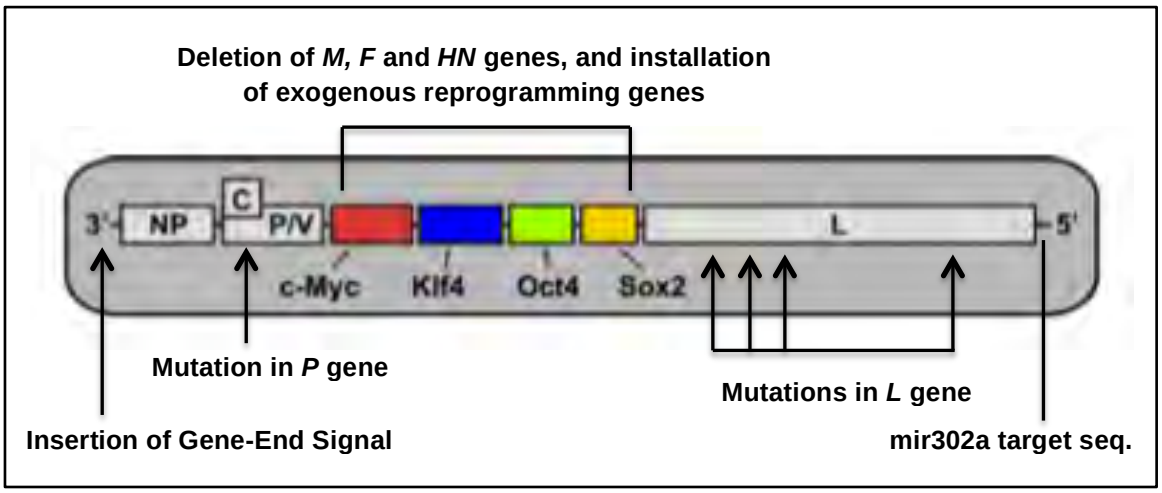

Figure 2.3.1 The genomic structure of the defective and persistent reprogramming gene-loaded Sendai virus vector [SeVdp (KOSM)302L]. SeVdp has mutations in the *L* and *P* genes, which are resposible for low cytotoxicity and for defective induction of interferon (IFN). The *M*, *F* and *HN* genes are deleted and replaced with the reprogramming genes; *c-MYC, KLF4, OCT4* and *SOX2.* The mir302 target sequence is added to the *L* gene-noncoding region of the Sendai viral vector to ensure silencing of the viral vector in the cell. (Nishimura et al. 2011)

The multiplicity of infection (MOI) is a virological term used to describe the ratio of infectious virus particles to the number of target cells. The SeVdp viral vector that we received and used has 1 x 10^6 to 3 x 10^7 cell infectious units per 1ml, providing an MOI of 3-10 when you infect 1-1.5 x 10^5 cells with 50µl of SeVdp (this is the recommended MOI for the reprogramming of adherent cells such as fibroblasts). Seventy-five microlitres (75µl) of the SeVdp virus (equivalent to a minimum MOI of 5) was added to the selected wells of HDF (1.5 x 10^5 cells) in a dropwise manner, then mixed in the medium by gently shuffling the 6-well plate from side to side. Thereafter the cells and virus were allowed to stand in the laminar flow cabinet at RT for 2 hours, before being incubated at 37°C and 5% CO_2 overnight.

The iPS cells were generated in feeder-dependent culture using commercially obtained MEFs (ATCC®, USA) inactivated with mitomycin C (*Appendix A.8*). The SeVdp-infected fibroblasts were viewed under the light microscope to ensure cell adherence and viability. Thereafter the SeVdp-infected cells(1.6 x 10^4 cells/well) were transferred to iMEFs (plated the previous day) with 1ml of warm HDF medium and returned to the incubator at 37°C and 5% CO_2. Again, full class II biosafety precautions, as described in *Appendix A.8* were observed when working with the SeVdp virus.

In order to check the seeding efficiency of these cells, a further 1.6 x 10^4 cells/ml were plated in a well or cell culture dish without iMEFs. This served as a plating control, as it is not possible to distinguish between the MEF and HDF cells when in co-culture.

Culture of induced pluripotent stem cells

As mentioned previously, human stem cells (both hES cells and iPS cells) can be successfully established and maintained in co-culture with murine or human fibroblast feeder cells. Significant progress has been made in the development of feeder-free culture systems to support human stem cells, thereby eliminating feeder cells completely and reducing or removing non-human products in the culture. Culture in feeder-free systems is achieved by feeder cell conditioned media or other specialised media, and a matrix-coated tissue culture surface such as Matrigel®

(Valamehr et al. 2011; Villa-Diaz et al. 2013).

Basic fibroblast growth factor (bFGF) plays a central role during prenatal development and postnatal growth and regeneration of a variety of tissues by promoting cellular proliferation and differentiation. It is a critical component of hES cell culture medium – as it is a growth factor necessary for the cells to remain in an undifferentiated state, although the mechanisms by which it does this are poorly understood (Liu et al. 2006). It is crucial to add fresh bFGF, aseptically on a daily basis, to the pre-warmed media prior to adding to the cells.

Selective Rho-asssociated kinase (ROCKi) inhibition by means of Y-27632 dihydrochloride (Sigma-Adrich®, USA) has been shown to markedly decrease dissociation-induced apoptosis, and thereby increases cloning efficiency and facilitates subcloning of stem cells (Watanabe et al. 2007). ROCKi was always added to medium upon thawing of cells and when enzymatically passaging iPS cells in order to reduce cell death.

Since stem cells are almost always in culture in excess of 3 months, stem cells are often cultured and maintained in media supplemented with antibiotics (penicillin and streptomycin). The use of prophylactic antibiotics in these culture media may however make detection of any breach in sterility more difficult and may mask potential Mycoplasma infections. Daily visual inspection of cell morphology is highly recommended for proper growth and for the removal of any differentiating colonies via manual dissection.

The iPS cells were initially maintained in feeder-dependent culture using mitomycin C inactivated MEFs (iMEFS). Good quality iMEFs are vital to prevent problems such as poor colony support, failure to seed after passage, and improper seeding with resultant differentiation. The density of the feeder cells plays a critical role in ensuring the delivery of sufficient growth factors to maintain the iPS cells in an undifferentiated state without depleting the nutrients in the co-culture environment, which in turn would diminish the iPS cell colonies' capacity for growth. iMEFS are reliable in culture for up to 10 days, thereafter the co-cultures require supplementation of growth factors, cytokines and nutrients via MEF-conditioned

medium (MCM). The iPS colonies formed on iMEFS are uniformly shaped with well-delineated edges, therefore making it easy to identify colonies and signs of differentiation.

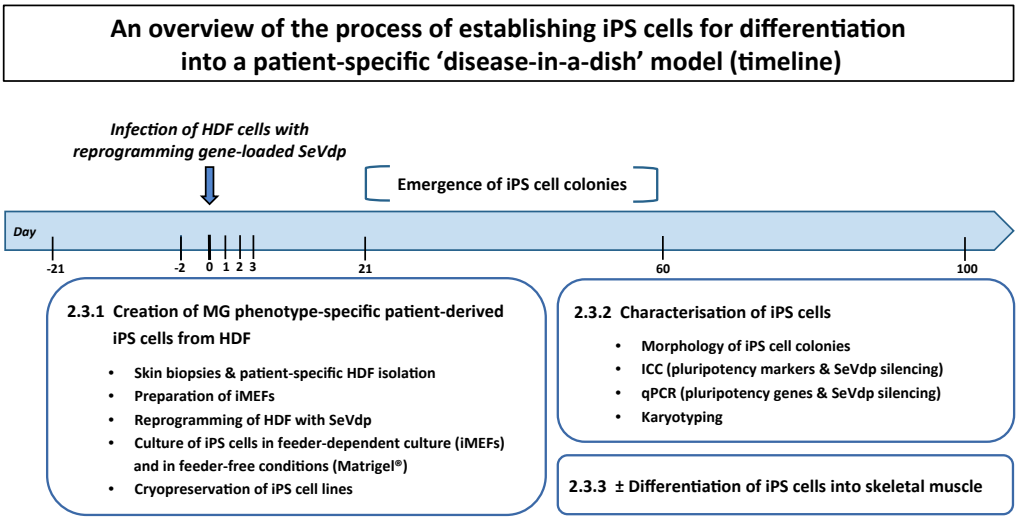

Figure 2.3.2 An overview of the process of establishing induced pluripotent stem (iPS) cells – represented as a timeline.

While awaiting the emergence of iPS cell-like colonies on the pO-plate containing the reprogrammed fibroblasts on iMEFs, the hES medium with P/S and bFGF (hES++) was replaced every second day for the first 6-8 days. After approximately 10 days, the hES++ medium was substituted with MEF-conditioned medium supplemented with P/S and bFGF (MCM++) every second day (*Appendix A.8*). When iPS cell colonies were identified, colonies with tightly-packed morphology and a distinct edge were selected for 'picking' (manual passaging) as seen in **Figure 2.3.3**. Initially only 1 colony per well was selected, and the colony was labeled by marking the lid. The colony was named as follows; for patient MG822, the first colony was MG822.1 and the second MG822.2, etc. These colonies (passage 1) were transferred to their own individual, labeled 6-well plate.

Manual passaging was performed using a 26-guage insulin needle to dissect the colonies into small patches under the stereoscopic microscope (Nikon SMZ-2T, Japan) at a setting of 1.5-2, while working in the laminar flow cabinet. These patches of cells were transferred to one gelatinised well of iMEFs in hES++ medium (split in a ratio of 1 colony : 1 well) with a 5ml pipette. Each clone in each new well was propagated by numerous subpassages, always in a one colony to one well ratio. Early colonies with promising morphology were subcultured repeatedly until later mature colonies were abundant and had better morphology with well-defined borders and no differentiation. During the expansion of iPS cells any areas of partially differentiated colonies were teased away and removed before passage.

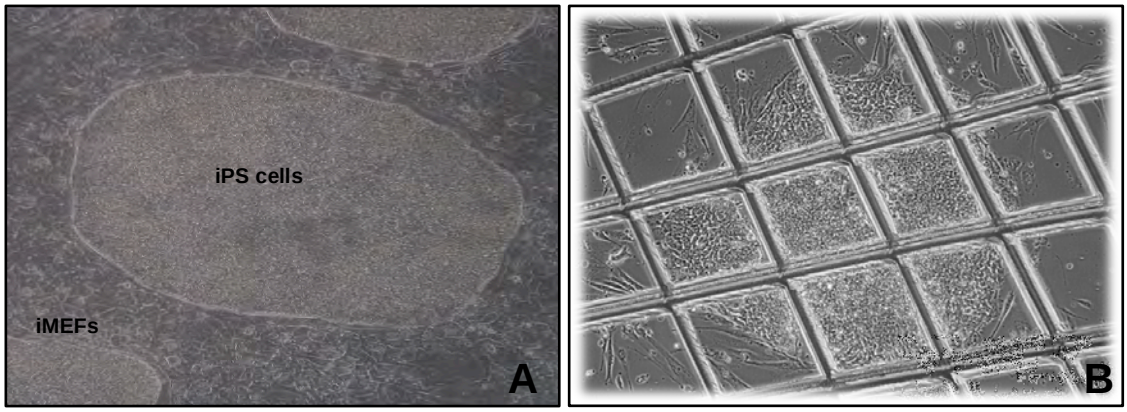

Figure 2.3.3 (A) The appearance of induced pluripotent stem (iPS) cell colonies (MG822.7 p4) in co-culture with inactivated mouse embryonic fibroblasts (iMEFs). (B) Manual passaging of iPS cell colonies into patches with a 26-gauge insulin needle. [20x magnification]

Depending on the downstream application or experiment, iPS cell colonies were either cultured in feeder-dependent culture (iMEFs) or adapted to feeder-free conditions (Matrigel® with Essential8™ or mTeSR™1 medium). iMEFs for feeder-dependent culture were prepared 1 day prior to passaging iPS cell colonies and labelled with the date to ensure that feeder layers more than 3 days old were never used. Optimum iMEF cell densities per 35mm ($10cm^2$ growth area) well were as follows; ATCC® iMEFs initally plated at a density of 3×10^5 cells/well and then later adjusted to 1.5×10^5 cells/well, and outbred E14.5 iMEFs at 3×10^5 cells/well. While in co-culture, 50% of the hES++ medium was replaced with fresh medium every day,

and manually passaging onto fresh iMEFs every 4-5 days. iPS cell clones were frozen down or discarded on a weekly basis or when appropriate.

Under feeder-free conditions, the iPS cells were grown on hES-qualified Matrigel® matrix (Corning Life Sciences, USA) in Essential 8™ medium (#A1517001, Gibco™, Life Technologies, USA) or mTeSR™1 complete kit for hES maintenance (#5857, Stemcell Technologies, Canada). Matrigel® is the trade name for a gelatinous protein mixture secreted by Engelbreth-Holm-Swarm (EHS) mouse sarcoma cells that resembles the complex extracellular environment of many tissues. It is therefore used by cell biologists as an acellular substrate for culturing cells, particularly human embryonic and induced pluripotent stem cells (Hughs et al. 2010; Benton et al. 2009). Once suffient undifferentiated iPS cell colonies were established on iMEFs, approximately half of the colonies in culture were enzymatically passaged with TrypLE™ Express onto Matrigel® (prepared as per manufacturer's instructions) and subcultured 3-4 times until there were suffient cells for karyotyping, RNA extraction for qPCR, and genomic DNA extraction (*Appendix A.8*).

Thawing of cryopreserved iPS cells

When thawing frozen iPS cells, iMEFs were prepared as per usual by plating iMEFs in gelatin-coated wells in MEF medium (ATCC® iMEFs 1.2-1.5 x 10^5 cells/well & outbred E14.5 iMEFs 3 x 10^5 cells/well). After 24 hours, when iMEFs were adherent, the MEF medium was removed and the cells were rinsed well with 1ml of pre-warmed Knockout™ DMEM. This was then replaced with 2ml of pre-warmed hES++ and Y-27632 dihydrochloride (10µl/ml) and incubated at 37°C for 2 hours. The iPS cell pellet was thawed and centrifuged in Knockout™ DMEM at 1500 rpm for 3-5 minutes, and the supernatant was discarded. The iPS cell pellet was resuspended in pre-warmed hES++ medium from the prepared wells in a ratio of 1:1 from each well. The cell suspension was split 20%:80% between the wells (as we were not always certain how many cells were frozen in each vial, and it allowed us to plate at two different cell densities), gently rocked from side to side, and placed in the incubator at 37°C and 5% CO_2. Depending on the adherence of the cells, a 50% hES++ medium change was performed 1 or 2 days after thawing and plating the cells.

Cryopreservation of iPS cells

iPS cell clones selected to be cryopreserved (from iMEFS and Matrigel®) were washed and trypsinised with 0.5ml of TrypLE™ Express for 3-5 minutes. Then 4.5ml of 1x PBS was added to dilute out the TrypLE™ Express, before this cell suspension was transferred to a 15ml tube and centrifuged at 1200 rpm for 5 minutes. The supernatant was discarded and the cell pellet was resuspended in ice cold basal medium (KODMEM), before an equal volume of 2x iPS cell freezing medium (*Appendix A.8*) was added. The iPS cells were then frozen in aliquots of 1ml per cryovial at -80°C for the first 24 hours in a Nalgene™ Cryo 1°C freezing container, and then transferred to liquid nitrogen stores thereafter.

2.3.2 Characterisation of iPS cells

In order to determine whether the reprogrammed dermal fibroblasts were pluripotent and resembled human embyonic stem cells, the iPS cell lines were subjected to validation by means of various tests.

Morphology of iPS cell colonies

Undifferentiated iPS cells grow as compact colonies, and exhibit high nucleus-to-cytoplasm ratios with prominent nucleoli. These iPS cell colonies maintain a distinct border on feeder cells, making it easier to identify early differentiation.

Immunocytochemistry for pluripotency protein markers & SeVdp

Immunocytochemistry (ICC) was perfomed on the iPS cell colonies to demonstrate the presence of pluripotency protein markers, thereby proving that the cells were in fact reprogrammed and possessed stem cell qualities. iPS cells were cultured and prepared for immunocytochemistry (*Appendix A.7 & A.8*) to confirm the expression of three selected pluripotency markers (OCT4, TRA-1-60, and NANOG). iPS cells were analysed as colonies grown in co-culture with iMEF feeders, and the feeder cells acted as an internal negative control (showing no expression of the pluripotency markers).

The iPS cells were passaged ontol iMEF-lined coverslips in the wells of a 12-well plate ($4cm^2$ growth area) in hES++ medium and left undisturbed at the back of the

incubator at 37°C and 5% CO_2. The hES++ medium was only replaced after 36-48 hours, and then daily thereafter. The iPS cell colonies were allowed to expand and were only processed for ICC after 3-5 days. The immunocytochemistry processes and antibodies are described in greater detail in *Appendix A.7.*

In addition to confirming the expression of pluripotency markers, ICC using an antibody raised against the SeVdp vector (a kind gift from Professor Mahito Nakanishi, Japan) was used to verify that the viral vector had been eliminated from the regrogrammed cells. The SeVdp vector contained a microRNA (miRNA) target binding site designed to be targeted by mir-302a, a miRNA selectively expressed in embryonic stem cells (Nakanishi et al, 2012). Therefore fully reprogrammed iPS cells would silence the SeVdp through this endogenous miRNA pathway. iPS cells cultured as colonies on iMEFs were fixed and processed for ICC, and fluorescence levels were compared to that of newly-infected dermal fibroblasts. The ICC for SeVdp was done in conjunction with the ICC for pluripotency markers and described in more detail in *Appendix A.7*.

The iPS cells were then viewed with the flourescence microscope detailed in section 2.2.7. Efforts were made to use the same exposure times for each filter across multiple slides/images, in order to more accurately compare different experiment conditions and positive & negative controls. Images were edited and optimised using Axiovision 4.7 and ImageJ software.

Quantitative polymerase chain reaction (q-PCR) for pluripotency genes & SeVdp

The expression of selected pluripotency genes (*OCT4, SOX2, NANOG*) and the silencing of the ectopic reprogramming genes of the SeVdp in the iPS cells was confirmed by quantitative PCR (q-PCR). Three 35mm wells of each iPS cell line were cultured in feeder-free conditions until confluent. The cells were lifted enzymatically and centrifuged at 1500rpm for 5 minutes to form a cell pellet, which was either stored at -80°C until needed or immediately subjected to RNA isolation. Total RNA was extracted from cells using the High Pure RNA isolation kit (Roche, USA). The quality and concentration of RNA was determined by spectrophotometry using a NanoDrop® ND-1000 spectrophotometer (Agilent Technologies, Germany). Only

samples exhibiting an A260/A280 ratio equal to or above 1.8 were selected and stored at -80°C for further applications. Reverse transcription of RNA was performed according to the manufacturer's instructions using M-MLV reverse transcriptase (Promega, USA). Quantitative real-time PCR was conducted on the StepOnePlus™ (Thermo Fisher Scientific, USA) using PowerUp™ SYBR® Mastermix (Life Technologies, USA). PCR reactions containing 1X PowerUp™ SYBR® Mastermix, and 0.4µM of each PCR primer set (designed using the Primer-BLAST open source software available at http://www.ncbi.nlm.nih.gov/tools/primer-blast) to a total volume of 8µl were aliquoted into a 0.1ml MicroAmp® Fast 96-well reaction plate (Applied Biosystems, USA). Two microlitres of a 1:2 dilution of cDNA were added per well to give a final reaction volume of 10µl. The supplier's software was used to set up the required cycling parameters. A comparative $\Delta\Delta C_p$ program was selected with a total of 40 cycles and a melting temperature of 60°C. PCR cycle parameters were: denaturation (10 minutes at 95°C), annealing and amplification for 40 cycles (15 seconds at 95°C; 1 minute at 60°C), melting step (15 sec at 65°C) and a cooling step (30 sec at 40°C). Each DNA sample was quantified in duplicate and a negative control without cDNA template was run with every assay to assess the overall specificity. Melting curve analysis was carried out to ensure product specificity and data was analysed using the $2^{-\Delta\Delta C_T}$ method of relative quantification (*Appendix A.9*). Relative mRNA expression levels were normalised to β-glucuronidase (GUSB) for each reaction. Primers used to amplify the target genes were purchased from IDT technologies, USA, and GUSB was purchased from Qiagen, USA (QT00046046). Microsoft Excel software was used to calculate the mean and standard deviation $2^{-\Delta\Delta C_T}$ for each gene of interest.

Karyotyping

In addition to standard pluripotency tests, it was necessary to confirm the genomic integrity and the absence of induced genetic aberrations in the iPS cells after the reprogramming and culture processes. This was achieved through karyotype analysis with Giemsa-banding. iPS cells, and the original dermal fibroblast used to derive the iPS cell lines, were cultured in feeder-free conditions and a confluent 25cm^2 flask of

cells was transferred to the Cytogenetics Laboratory of the National Health Laboratory Service (NHLS) at Groote Schuur Hospital for the analysis.

A technique of suspension harvest is employed for fibroblasts, as this method is cost-effective and produces good quality metaphase cells. In this method the dividing cells in culture are halted in metaphase by the addition of Colcemid™ (N-desacetyl-N-methylocolchicine) which prevents spindle formation, thereby ensuring that the chromosomes remain condensed, and makes the cell walls more permeable. Hypotonic potassium chloride is added to swell the cells. Methanol/acetic acid fixative is used to precipitate the proteins, which can then be washed away. Slides are prepared by dropping cells onto clean, cold slides. The cells break open on the slide to release the chromosomes, and heat is then applied to encourage the chromosomes to spread, thereby facilitating counting and analysis.

Chromosomes are more easily identified when they have been banded, each chromosome has a particular banding pattern unique to its chromosome number. Alterations in banding pattern allows the identification of deletions, insertions and translocations. Chromosomes can be classified using their banding information by means of the International System for Human and Cytogenetic Nomenclature (ISCN). The technique of trypsin Giemsa(G)-banding was used in our case(s). The addition of trypsin is thought to collapse the chromosome structure, and this process is then halted by the protein in FBS and the cold buffer. The stain then binds preferentially to different areas of the DNA forming the appearance of light and dark bands. Dark bands are rich in adenine (A) and thymine (T) and replicate late in the S phase, and they do not seem to have many active genes. Depending on the stage of mitosis at which the chromosome is banded, one can see from 400 to 850 bands.

For the analysis, at least 5 metaphase spreads from the slides produced from each harvest were counted and the analysis was split between 2 technologists. The slides were first analysed for numerical and structural abnormalities, thereby determining the karyotype of 2 metaphase spreads (one from each culture if a duplicate culture was set up).

2.3.3 Differentiation of iPS cells

Due to the high cost and labour-intensiveness of establishing pluripotent stem cells in one individual (MG822) and the lack of an efficient and specific differentiation protocol for extraocular muscle, we did not to proceed with differentiation at this stage. These iPS cell clones (at various subpassages) were cryopreserved in their confirmed pluripotent state for later differentiation if and/or when appropriate.

CHAPTER 3

RESULTS

3.1 DESCRIPTIVE CLINICAL-PATHOLOGICAL DATA STUDY

In this section I describe the clinical and (histo)pathological features of EOM from MG patients compared to control EOM from non-MG patients. All EOMs for histopathological analysis were obtained from patients undergoing ocular re-alignment surgery who consented to the donation of the excised EOM tissue for the purposes of this study (*Appendix A.1*).

3.1.1 Clinical data

Myasthenia gravis with treatment-resistant ophthalmoplegia (OP-MG) cases

The clinical records of three South African MG patients with severe treatment-resistant ophthalmoplegia (OP-MG) were reviewed as they were referred for consideration for ocular re-alignment surgical procedures. I will refer to them as OP-MG. Two of these patients were women of mixed ancestry with generalised MG of early childhood-onset (MG86, aged 2 years & MG64, aged 4 years), and both had detectable serum AChR antibodies. In both, MG was diagnosed within a year of symptoms and they were initially started on pyridostigmine and prednisone therapy. The remaining MG case (MG82, age at onset 45 years) was a white woman, with generalised disease of approximately five years duration, and was found to have triple seronegative MG (T-SNMG) without detectable AChR, MuSK or LRP4 antibodies in her sera by radioimmunoassay and cell-based assays (Huda, et al. submitted 2016). Her MG was diagnosed within six months of symptom onset based on the characteristic clinical picture, decremental response on muscle repetitive nerve stimulation studies and a positive response to intramuscular neostigmine. This patient also had Crohn's disease diagnosed at age 28, and a strong family history of autoimmune disease (mother with psoriasis and sister with rheumatoid arthritis). She was treated with pyridostigmine, prednisone and methotrexate as a steroid-sparing agent (Heckmann et al. 2011).

Thyroid disease was excluded in all three cases by biochemical measurements and STIR sequence MRI assessments of the orbits and EOMs. No mitochondrial DNA (mtDNA) deletions were detected in all three cases on serum screening using long-range PCR covering the 'hot spot' region for mtDNA deletions, as reported by Heckmann et al. in 2007.

All three OP-MG patients had variable degrees of upper eyelid involvement resulting in blepharoptosis. There was little/no detectable function in the levator palpebrae superioris muscles (responsible for lifting/elevating the upper eyelid), and the orbicularis oculi muscles (responsible for closing the eyelids) were also weak bilaterally. Ocular motility was poor in all directions of gaze, with almost complete ophthalmoplegia (100% pareses) in most directions. In directions where some movement was present (≤ 25% movement), saccades were described as slow.

Two patients (MG64 & MG82) had a visible deviation of one or both eyes and consequent diplopia due to visual axis malalignment. In both of these cases the eye/s were deviated laterally (exotropia) and inferiorly (hypotropia). On forced duction testing, no resistance to movement was encountered in any direction, thereby eliminating mechanical restriction as a potential cause of the severely limited extraocular motility. Active force generation testing revealed marked paresis with virtually no clinically detectable power in all EOMs, with the superior rectus muscle (responsible for globe elevation) being affected the most severely in both cases.

The two cases with juvenile onset OP-MG (MG64 & MG86) also had pseudoproptosis attributable to large globes, both cases had long axial lengths (>26mm) and refractive errors in keeping with axial myopia. Orbital imaging was valuable in excluding a condition known as 'heavy eye syndrome', where the enlarged globe herniates between the lateral rectus (LR) and the superior rectus (SR) muscles, as a cause of the manifest deviation. Taken together, the two juvenile onset treatment-resistant cases (MG86 & MG64) had additional clinical features demonstrating anatomical variation in globe stucture and/or position.

Figure 3.1.1 Photograph of an MG patient with severe treatment-resistant ophthalmoplegia (OP-MG). The right eye is deviated laterally (exotropia) & inferiorly (hypotropia), and minimal/no blepharoptosis is evident. Photograph courtesy of Professor Anthony Murray and with permission from the patient.

All patients underwent orbital and extra-ocular muscle imaging by means of MRI, and contrasted CT scanning in two of the three cases. No increase or decrease in EOM volume or EOM displacement was noted on CT or MRI of the orbits in all three patients (see discussion and **Figure 3.1.2**).

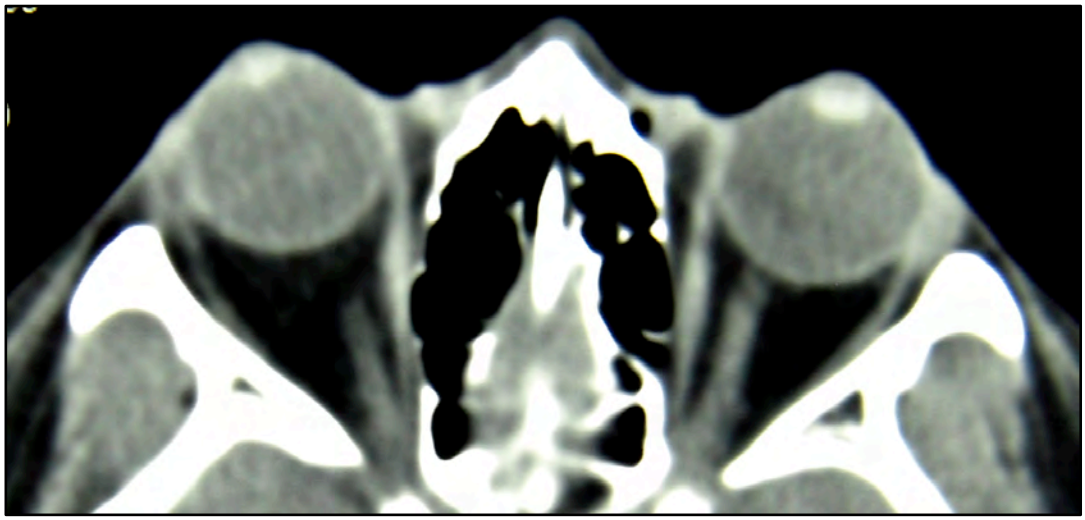

Figure 3.1.2 An axial CT scan image of the orbits of an MG patient with treatment-resistant opthalmplegia (OP-MG) demonstrating normal globes & normal volume of the horizontal rectus muscles. This saggital view is at the level of the optic nerves, with both lateral rectus muscles (temporal orbit) and medial rectus muscles (nasal orbit) visible. Image courtesy of Professor Anthony Murray.

One of the AChR positive MG cases and the T-SNMG case required ocular realignment surgery to alleviate intractable diplopia after years of stable disease on treatment. During the surgical procedure, the surgeon again performed forced duction testing and found no resistance to movement in any direction. The surgeon also noted that the EOM tissue (being recessed and resected) was very friable and required additional sutures to resecure it to the sclera (personal communication Prof Anthony Murray).

These cases participated in previous *DAF* and *TGFβ1* gene association studies; all three possessed wild type alleles (C/C) for the *DAF* regulatory region c.-198 C>G variant (Heckmann et al. 2010). The two juvenile onset cases (MG64 & MG86) were evaluated for the African-specific *TGFB1* promoter SNP c.-387 C>T (Nel et al. 2016); MG64 was wild type (C/C) while MG86 had the high-risk allele (T/C) that associated with juvenile MG treatment-resistant ophthalmoplegia.

Control cases

The clinical records of three non-MG patients who consented to the donation of excess EOM excised at realignment surgery were reviewed. Two of these control patients were of mixed ancestry and one was an indigenous black African. Two patients were undergoing realigment surgery after having developed a lateral deviation in a non-seeing eye due to the loss of a sensory stimulus for fusion, fixation and alignment. The other case was healthy with normal vision and no abnormality of ocular motility, but undergoing surgery to correct a decompensated infantile strabismus. All three had normal eyelid muscle function and full ocular motility with no resistance on forced duction testing and no weakness on active force generation testing. Only one patient had other medical conditions in the form of diabetes mellitus and hypertension; this sample was only utilised for EOM-derived myofibroblast explant cultures and not for comparative histopathological purposes. The ages of the control patients at the time of EOM donation were as follows; MG189 = 56 years old, C8 = 32 years old, C9 = 20 years old.

3.1.2 EOM tissue samples

EOM tissue samples were obtained from two OP-MG cases (MG82 and MG64). Unfortunately the EOM sample of MG64 (medial rectus muscle) was misplaced in the laboratory freezer where it was being stored at -80°C for later processing, and could not be located. Prior to storing this sample, the tendinous portion (1-2mm) of the EOM was excised and explant cultures of OP-MG EOM perimysial myofibroblasts were established for future use. The excised EOM (medial rectus muscle) of MG82 was processed for histopathology in 2012 and the remaining EOM tissue stored at -80°C until January 2015, when we performed additional frozen section stains and prepared samples for EM from this residual EOM sample.

Three non-MG (MG189, C8, C9) individuals donated their excised EOM tissue. One sample (MG189) was a very small section (4-5mm) of the lateral rectus (LR) muscle and therefore comprised only tendon, making it unsuitable for histopathology. Instead it was used to establish a comparative control EOM perimysial myofibroblast culture. The remaining two samples comprised a section of LR muscle approximately 7mm in length (C9), and a medial rectus (MR) muscle section of 6.5mm (C8). These samples were sucrose-protected, 'flash' frozen with iso-pentane and cryopreserved for a period of approximately 20 months prior to processing and staining. Both of these samples were processed for histopathology and EM, but the LR muscle section (C9) again comprised mostly tendon and therefore did not demonstrate suffiently-representative muscle tissue for a good comparison.

3.1.3 EOM histopathology (Table 3.1.1)

Comparative histopathological examinations were performed on the medial rectus muscle samples of one OP-MG case (MG82) and one control case (C8). The EOM histology slides from 2012 were prepared in a different manner (wax-embedded formalin-fixed sections and stains) to those prepared by means of frozen section in 2015. The formalin-fixed EOM section slides prepared in 2012 were of a better quality than the frozen section slides prepared in 2015, due mainly to the fact the residual EOM sample used for the frozen sections comprised mostly peri-tendinous muscle and was therefore less representative. Both the OP-MG and control EOM samples were very small pieces of tissue and could not be orientated vertically when

frozen, thus resulting in small longitudinal sections of muscle as opposed to the preferred transverse sections obtained in the formalin-fixed sections. The abovementioned factors resulted in a dissimilar appearance of the comparative section slides of the OP-MG case and the control sample. The slides from both individuals were therefore assessed according to published reference norms of histological findings in skeletal and extra-ocular muscle tissue. The systematic approach used to analyse and report the histopathological findings (described in detail in section 2.1.5) was modified since fewer tissue sections were possible from these very small EOM samples.

On H&E staining, the OP-MG EOM sections (**Figure 3.1.3**) showed increased myofibre size variation with splitting of the myofibres. Compared to normal, there was more abundant adipose tissue and collagen representing muscle fibre atrophy and replacement fibrosis. Nuclear clumping, a change seen in severe atrophy and commonly in longstanding denervation, was seen in some of the OP-MG EOM sections. The control sample showed myofibres with normal morphology, and were tightly packed with scanty connective tissue between the fibres and no obvious atrophy (**Figure 3.1.4B** and **Figure 3.1.5B**). Control EOM was noted to have an increased number of internal nuclei, but this was within normal limits for adult EOM (<10%), and may have been over-estimated since this is better evaluated on transverse muscle sections which were not available for our control case. No H&E stained section of the control EOM is shown here, as this slide(s) displayed artefactually separated muscle fibres with no associated collagen and adipose deposition, this finding was therefore attributed to the mechanical separation of fibres during the cutting of these sections (see supplementary figure in *Appendix A.3*).

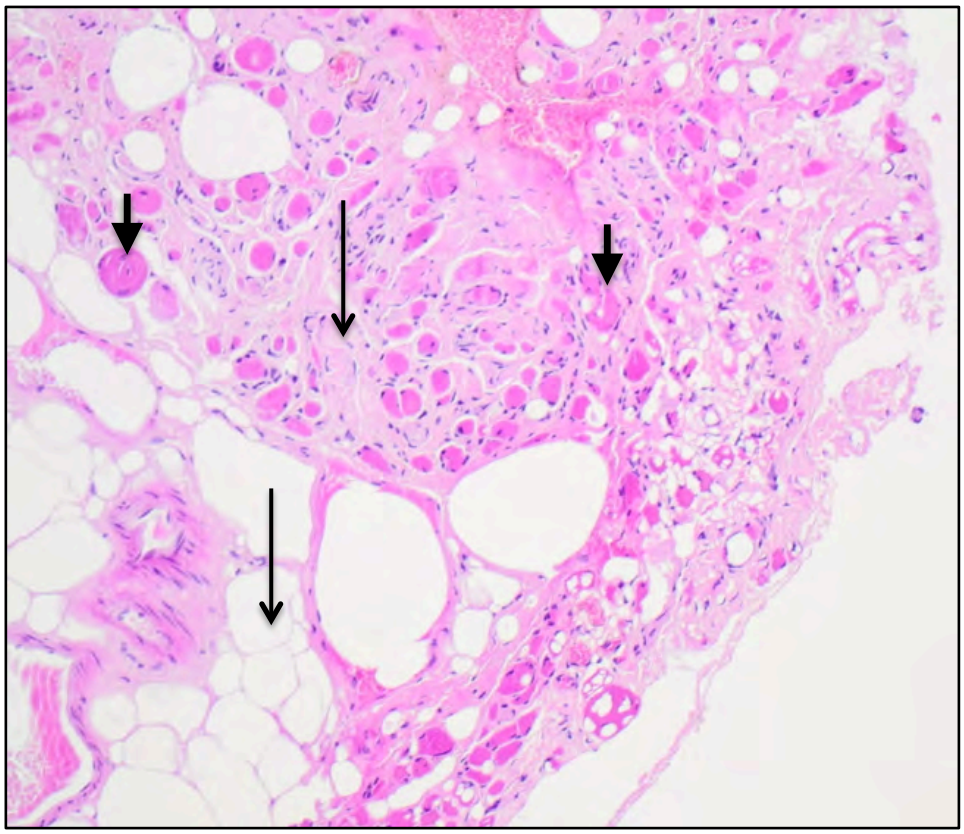

Figure 3.1.3 Haematoxylin & Eosin staining of EOM tissue section of an MG patient with treatment-resistant ophthalmoplegia (OP-MG) demonstrating increased myofibre size variation, myofibre whorling & splitting (short arrows), and abundant adipose & collagen (long arrows) between the muscle fibres. [200x magnification]

The modified Gomori trichrome stain (**Figure 3.1.4**) demonstrated dense connective tissue comprised mostly of collagen (light green), with no obvious mitochondrial aggregates and no 'ragged red fibres' in the OP-MG patient (**A**). In the control sample (**B**), tightly-packed myofibres with very little collagen can be seen, and no abnormal mitochondrial aggregates or 'ragged red fibres' were observed.

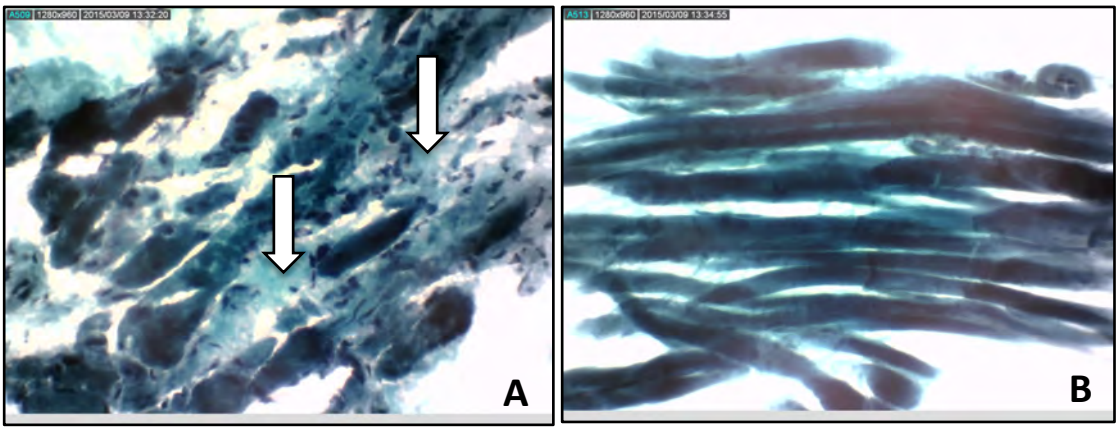

Figure 3.1.4 Modified Gomori Trichrome staining of EOM tissue sections. (A) OP-MG – demonstrating abundant dense connective tissue/collagen (arrows), and no 'ragged red' fibres. (B) Control – demonstrating tightly-packed myofibres with little collagen and no 'ragged red' fibres. [100x magnification]

On Oil Red O staining (**Figure 3.1.5**), no increased sarcoplasmic lipid was seen inside the myofibres, but abundant lipid (dark pink/red) was seen outside and in between the muscle fibres of the OP-MG patient (arrows) in image (**A**). No abnormal lipid was observed inside or outside the muscle fibres in the control EOM sample (**B**).

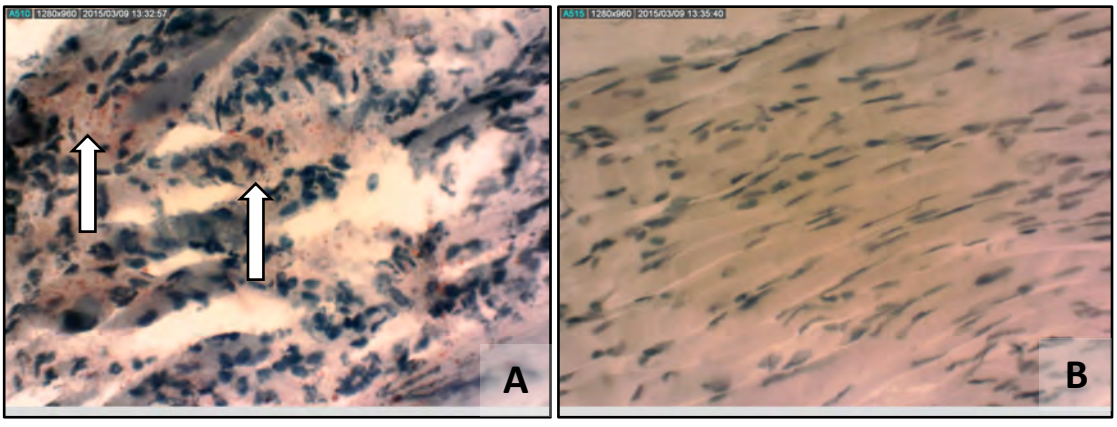

Figure 3.1.5 Oil red O staining of EOM tissue sections of (A) OP-MG EOM demonstrating abundant lipid between myofibres (arrows), and (B) Control EOM with tightly packed myofibres and no lipid between the myofibres. [100x magnification]

As mentioned previously in section 2.1.3, it was only possible to perform very limited immunohistochemistry on the archived wax-embedded formalin-fixed EOM sections from 2012. Immunohistochemistry for slow (type I) and fast (type II) myosin can only be performed on cross-sections of muscle, therefore only the OP-MG patient's formalin-fixed EOM sections could be subjected to this investigation, since the control patient's EOM sections were longitudinal in nature. Fast myosin, which stains type II fibres, only stained very focally on the OP-MG EOM sections, while the slow myosin (type I) did not stain at all. This does suggest that there is an even mixture of type I and type II fibres, and that no fibre type predominates in the OP-MG EOM sample. These immunohistochemistry slides were of poor quality, most likely related to technical factors during the processing (dewaxing, rehydration, permeabilisation) of these EOM sections prior to antibody incubation. The slides are not shown here, but can be viewed in *Appendix A.3*.

Table 3.1.1 Summarised comparison of the histopathological findings of the medial rectus muscles from an OP-MG patient & a control (non-MG) patient.

OP-MG EOM		CONTROL EOM
• Increased myofibre size variation • Splitting & whorling of myofibres • Abundant adipose tissue & collagen between muscle fibres • Nuclear clumping	**Haematoxylin & Eosin**	• Tightly packed myofibres with normal morphology • No obvious myofibre atrophy • Scanty CT between fibres • Increased number of centrally located nuclei (<10%)
• Abundant collagen between myofibres • Normal mitochondrial aggregates • No 'ragged red fibres'	**Modified Gomori Trichrome**	• Little/no collagen between myofibres • Normal mitochondrial aggregates • No 'ragged red fibres'
• Abundant lipid outside/ between myofibres • No abnormal sarcoplasmic lipid	**Oil Red O**	• No lipid outside myofibres • No abnormal sarcoplasmic lipid

The histopathological features observed in the EOM of the OP-MG patient can be best summarised as myopathic muscle pathology. The increased variation in muscle fibre diameter, abundance of connective tissue, and increased number of central nuclei may be features of normal peritendinous muscle tissue or myopathic features. Since these findings were evident in this patient's formalin-fixed EOM slides containing non-tendinous muscle (2012) and in the EOM frozen section samples from residual peritendinous muscle (2015), it is likely to be pathological. The findings in this OP-MG case were consistent with those reported by Gratton et al. (2014) in a case of AChR postive MG with treatment-resistant ophthalmoplegia; demonstrating non-specific atrophy and marked replacement fibrosis with abundant adipose and collagen deposition in EOM tissue (no ultrastructure is reported in this case). The control EOM demonstrated normal muscle morphology. It is noteworthy that the control EOM sample showed no atrophy or other pathological features after having been frozen for approximately 20 months prior to processing, compared to the OP-MG EOM samples that were frozen for approximately six and 30 months, respectively.

3.1.4 EOM ultrastructure (Table 3.1.2)

The OP-MG EOM (**Figure 3.1.6A**) demonstrated predominantly myopathic changes, with loss of the normal structural myofibrillar pattern and resultant Z-band streaming (wavy band appearance). Significant atrophy could be seen with sarcolemmal wrinkling and folding, with an increased amount of collagen deposition between myofibres. There were large subsarcolemmal aggregates of swollen mitochondria, but the mitochondria appeared structurally normal with no paracrystalline inclusion ('parking lot') bodies observed on high-power magnification. Lipid droplets were present between myofibres, but not within the sarcoplasm, and there was no excessive glycogen present. We did not observe any changes specific to neurogenic pathology, such as angulated fibres and group fibre atrophy, but chronic denervation or muscle disuse of any cause may result in the replacement of muscle fibres by connective tissue. The most striking findings in the OP-MG extraocular muscles were myopathic changes with myofibrillar disarray and mitochondrial abnormalities, but no ragged red fibres or 'parking lot' bodies.

The control patient demonstrated normal muscle ultrastructure with a normal myofibrillar pattern consisting of discrete and linear bands. There was no atrophy and no increased collagen, lipid or glycogen. There were normal mitochondria in central aggregates within the muscle fibres, and sparing of the subsarcolemmal space(**Figure 3.1.6B**).

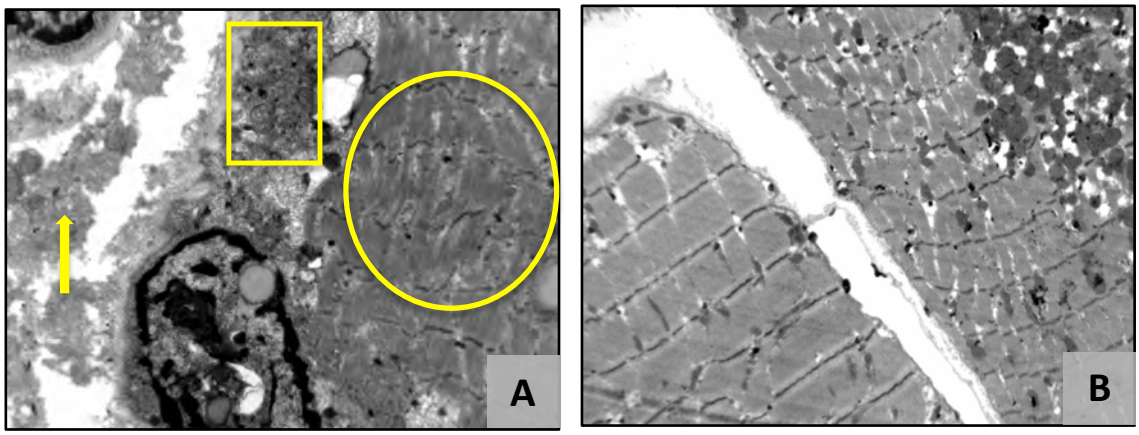

Figure 3.1.6 Electron microscopy of EOM tissue sections. (A) OP-MG – myofibrillar disarray with Z-band streaming (circle), abundant collagen deposition (arrow), sub-sarcolemmal aggregates of swollen mitochondria (rectangle/box). [7000x magnification] **(B) Control – normal myofibrillar pattern, no sarcolemmal membrane changes, central accumulations of normal mitochondria (not involving the sub-sarcolemmal space).** [3000x magnification]

The ultrastructural changes that we observed in the OP-MG are novel for EOM, and reflect those reported in limb skeletal muscle in various subtypes of MG. AChR positive MG is associated with a broad spectrum of muscle pathology, including marked myofibre atrophy and myofibrillar disarray with Z-line streaming (Padua et al. 2006; Martignago et al. 2009; Cenacchi et al. 2011). In seronegative MG with anti-MuSK antibodies, cases demonstrated myopathic changes and frequent mitochondrial abnormalities with/without 'ragged red fibres' on limb muscle biopsies (Rostedt Punga et al. 2006; Canacchi et al. 2011). While in cases with both AChR- and MuSK-antibodies, muscle displayed a pathological intermyofibrillar network, atrophy, cytochrome oxidase (COX)-negative fibres, and 'ragged red fibres' (Rostedt Punga et al. 2006).

Table 3.1.2 Summarised comparison of the EOM ultrastructural (electron microscopic) findings of an OP-MG patient & a control (non MG) patient.

OP-MG EOM		CONTROL EOM
• Myofibrillar disarray (Z-band streaming) • Atrophy (sarcolemmal folding) • Increased collagen • Swollen mitochondria in subsarcolemmal aggregates • No crystalline inclusions in mitochondria • Increased lipid between myofibres (not within myofibres) • No excessive glycogen	**Electron microscopy**	• Normal myofibrillar pattern • No atrophy • No collagen • Normal mitochondria in central aggregates within myofibres • No excessive lipid • No excessive glycogen

3.1.5 Clinical-pathological correlation (Table 3.1.3)

Equivalent samples of medial rectus muscle (6.5mm) were obtained from both these patients (OP-MG and non-MG control) approximately 3-4 years after the onset of the ocular malalignment. The clinical-pathological correlation shows that the EOM from this non-myasthenic individual demonstrated normal muscle morphology with no atrophy evident on histopathological and electron microscopic analysis, which corresponds to the absence of clinically-detectable EOM paresis in this control patient with a sensory exotropia. The OP-MG EOM sections demonstrated extensive non-specific myopathic features; myofibrillar disarray, marked atrophy with increased connective tissue, and abnormal subsarcolemmal mitochondrial accumulations were the most striking features on ultrastructural analysis. The histopathological and ultrastructural findings in the OP-MG case correlate well with this individual's clinical findings of severe EOM weakness, with no resistance or restriction on forced duction testing and no active force generation in almost all the EOMs.

Despite a similar period of ocular malaligment in these two cases, the actual degree, duration, and mechanism of muscle 'inactivity' is not similar, since the control case has a subclinical reduction in tonic innervation of the MR muscle with normal ocular motility (normal motor unit in this EOM). The non-MG control has a manifest

deviation due to the loss of the visual stimulus for fusion and vergence in this eye, with a resultant centrally-governed reduction in tonic innervation to the paired agonist-antagonist muscles of this eye. Another potential confounder is the age differential between these two cases (OP-MG = 54 years old, and non-MG control = 32 years old), which can account for the myopathic features observed, since mitochondrial DNA rearrangements are shown to increase with age. Mitochondrial myopathies display similar features to those seen in this OP-MG case and other reported cases of particularly MuSK positive MG. However, we did not observe any 'ragged red' fibres or mitochondrial paracrystalline inclusions in this OP-MG case, thereby suggesting that age was not a significant factor in this case. The EOMs have been identified as particulary useful tissue for studying the contribution of mitochondrial dysfunction in aging, since they are continuously tonically active in comparison to skeletal muscle, where decreased oxidative phosphorylation could be due to physical inactivity or disease and therefore not a consequence of age per se (Yu-Wai-Man et al. 2010).

Table 3.1.3 Summary of the clinical data and the EOM histopathological & ultrastructural analysis of an MG patient with treatment-resistant ophthalmoplegia and a control patient.

OP-MG		**Control (non MG)**
Middle-aged female (54 years old) Opthalmoplegia with XT Surgery ± 4-5 years after diagnosis of MG Medial rectus muscle – 6.5mm	**Clinical data**	Young adult male (32 years old) Sensory XT (no EOM paresis) – traumatic visual loss Surgery ± 3-4 years after injury Medial rectus muscle – 6.5mm
Myopathic changes	**Histopathology**	Normal myofibre morphology
Myopathic changes • Myofibrillar disarray • Myofibre atrophy • Abnormal mitochondrial accumulations	**Electron microscopy**	Normal EOM ultrastructure • Normal myofibrillar pattern • Normal mitochondria

OP-MG = MG with severe treatment-resistant ophthalmoplegia, MG = myasthenia gravis, EOM = extraocular muscle, XT= exotropia (lateral deviation of the eye)

3.2 DOWNSTREAM TGFβ1 EFFECTS IN PHENOTYPE-SPECIFIC FIBROBLASTS, EOM MYOFIBROBLASTS & C2C12 MOUSE MYOBLASTS

Our group has been exploring the contribution of the cytokine, *TGFβ1,* in the repair and regeneration of EOMs as a result of the MG-associated end-plate complement-mediated damage. We have reported the association of an African-specific *TGFB1* regulatory region polymorphism c.-387 C>T (rs11466316) with juvenile-onset OP-MG patients (Nel et al. 2016). This SNP was shown to be functional with a resultant repression (5-fold) of the basal activity of the *TGFB1* promoter construct in transient transfection experiments using fibroblasts and myotubes (Nel et al. 2016). Since TGFβ1 is upregulated in response to muscle injury, and Cocuzzi et al (2001) demonstrated that TGFβ1 in turn induced DAF up-regulation in orbital fibroblasts, we proposed that OP-MG individuals harbouring functional polymorphisms of the *TGFB1* promoter may have altered downstream Smad-signalling and secondary effects on the *DAF* promoter. We therefore elected to investigate the effect of TGFβ1 on OP-MG specific Smad-pathway activation by using p-Smad3 as a surrogate, and Daf protein expression levels in mouse myotubes.

In the section to follow, we report on the effect of disease-specific sera and rhTFGβ1 on p-Smad3 protein expression in control-MG and OP-MG phenotype-specific fibroblasts (section 3.2.1). Thereafter we investigated the effect of rhTGFβ1 on Daf protein expression in C2C12 myotubes as a proxy for skeletal/extra-ocular muscle (section 3.2.2). Finally we assessed whether there was a differential response in myofibroblast differentiation after rhTGFβ1 stimulation in phenotype-specific EOM myofibroblast cell lines by means of immunofluorescence microscopy for α-smooth muscle actin (α-SMA) and collagen-∝2 type 1 (section 3.2.3).

3.2.1 The effect of rhTGFβ1 or homologous sera on phosphorylated-Smad3 expression in phenotype-specific dermal fibroblasts

In order to assess whether there is a differential activation response of the autocrine TGFβ1 pathway between control-MG versus OP-MG cells in response to stimulation with rhTGFβ1, we determined levels of phosphorylated-Smad3 (p-Smad3), a marker of

the canonical TGFβ1 signalling pathway, by western blotting (see section 2.1.1 for definitions of control MG and OP-MG).

Firstly, we established phenotype-specific fibroblast explant cultures from full-thickness skin biopsies (section 2.2.1). To determine the optimum dose and treatment duration of rhTGFβ1, we performed a dose/duration experiment using concentrations of 1ng/ml and 5ng/ml for periods of 0.5 hours, 1 hour, 6 hours and 24 hours in a single fibroblast cell line (MG7).

The western blot in **Figure 3.2.1** is representative of 2 independent experiments (biological repeats). For densitometric analyses the results were first normalised to p38 MAPK, as background expression, and then normalised to untreated control cells. It is evident that the highest fold increase was seen in band 2, 1ng/ml for 0.5 hours (2-fold upregulation), and band 5, 5ng/ml for 1 hour (≈1.4-fold upregulation. We opted to use the latter dose and duration of 5ng/ml for 1 hour for further experiments based on published reports with similar findings in myoblasts (Meurer et al. 2012).

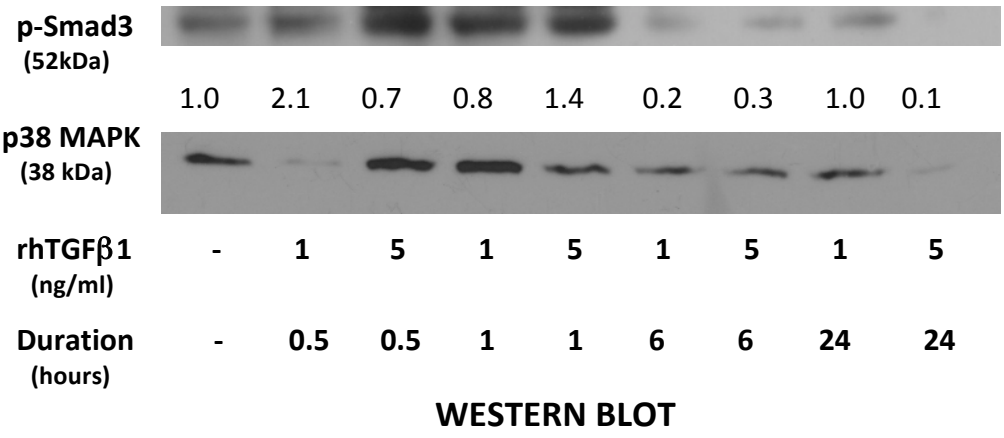

Figure 3.2.1 The effect of different doses and durations of rhTGFβ1 on phosphorylated-Smad3 expression in human dermal fibroblasts (HDF). HDF were treated with 1ng/ml or 5ng/ml of rhTGFβ1 for periods of 0.5 hours, 1 hour, 6 hours and 24 hours. Thereafter cell lysates (35μg) were separated on an 8% SDS-PAGE and analysed by western blotting using antibodies to p-Smad3 and p38 MAPK. The proteins of interest are denoted by their molecular weights as determined by the protein banding pattern in kilodaltons (kDa). The values between the two images represent the average fold change (in arbitary units) in at least two independent western blots based on densitometric readings, first normalised to p38 MAPK expression and then to the respective untreated control cells (band1).

Thereafter we proceeded with stimulation experiments to compare TGFβ1-pathway activation in the different phenotype-specific fibroblasts, control-MG versus partial or complete OP-MG. Phenotype-specific HDF were stimulated with homologous serum (10% dilution in vehicle) from healthy control individuals or from treatment-naïve MG patients, or rhTGFβ1 at 5ng/ml for 1 hour. Thereafter levels of p-Smad3 were determined by western blotting. Fold change of p-Smad3 in response to homologous sera & rhTGFβ1 in phenothype-specific HDF was calculated by means of densitometric readings, first normalised to p38 MAPK and then to untreated control cells.

The pooled data in **Table 3.2.1** demonstrates that there was an almost 9-fold difference in the p-Smad3 levels in the OP-MG versus control-MG HDF in response to rhTGFβ1 stimulation, but this did not reach statistical significance likely due to small sample numbers (p=0.104). Although there appears to be a 2-fold difference in p-Smad3 content of the control-MG cells versus OP-MG cells in response to control and MG sera, there was significant variability in the densitometric readings and the p-values were not statistically significant (p=0.707 for control sera, p=0.699 for MG sera).

Phenotype-specific HDF	**Control serum (10%)**	**MG serum (10%)**	**rhTGFβ1 (5ng/ml)**
	Average ± SD	Average ± SD	Average ± SD
Control-MG (n=2)	**18.10 ± 11.17**	**17.07 ± 15.11**	**18.94 ± 13.17**
Complete OP-MG (n=3)	**10.71 ± 13.14**	**9.6 ± 10.87**	**2.30 ± 2.09***

Table 3.2.1 Phosphorylated-Smad3 protein levels are repressed in response to treatment with rhTGFβ1 in human dermal fibroblasts of complete OP-MG patients. Human dermal fibroblasts were derived from MG patients with specific phenotypes; Control-MG represents patients with no ophthalmoplegia and complete OP-MG refers to MG patients with treatment-resistant ophthalmoplegia affecting all the EOMs. Total protein was isolated from phenotype-specific HDF treated with homologous control (10%) or MG (10%) serum or rhTGFβ1 (5ng/ml) for 1 hour. Cell lysates (35/40 µg) were separated on a 10% SDS-PAGE and analysed by western blotting using antibodies to p-Smad3 and p38 MAPK. Results are expressed as the average fold change in at least two independent western blots based on densitometric readings, first normalised to p38 MAPK expression and then to the respective untreated control cells. Pooled densitometric readings from western blots of control MG (n=2 technical repeats from two individuals) and complete OP-MG fibroblasts (n=3 technical repeats from three individuals) are represented in this table. *p=0.104 ($p<0.05$ statistical significance)

The results of p-Smad3 content of partial OP-MG HDF are not included here because the values were inconsistent with wide standard deviations, and were therefore uninterpretable. These values constituted two technical repeats from a single individual (MG7), who was initially classified as having the control-MG phenotype (with no ophthalmoplegia), but subsequently developed treatment-resistant ophthalmoplegia and was thus reclassified as partial OP-MG during the course of this project.

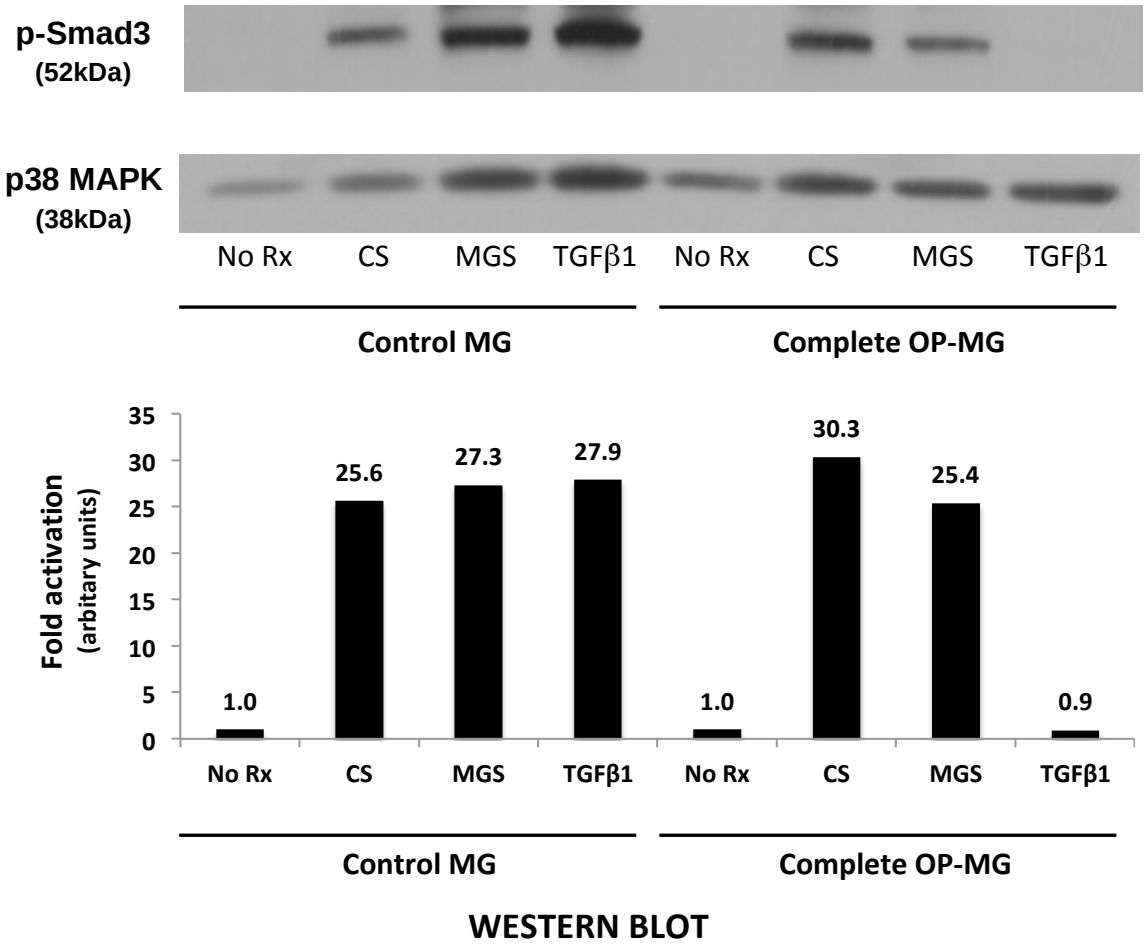

Figure 3.2.2 Western blot demonstrating the repressed levels of phosphorylated-Smad3 protein in complete OP-MG human dermal fibroblasts (HDF) after rhTGFβ1 treatment. Here we show a representative blot of p-Smad3 expression in control-MG versus complete OP-MG HDF, as summarised in Table 3.2.1. Phenotype-specific HDF were treated with 10% control serum (CS), 10% MG serum (MGS) or rhTGFβ1 (5ng/ml) for 1 hour. Cell lysates (35μg) were separated on a 10% SDS-PAGE and analysed by western blotting using antibodies to p-Smad3 and p38 MAPK. The bar graph represents the densitometric readings comparing the intensity of p-Smad3 protein bands normalised to the p38 MAPK 'house-keeping' protein, and then to untreated (No Rx) cells. The positions of the proteins of interest, as determined by the protein marker-binding pattern, are shown on the left in kiloDaltons (kDa).

Figure 3.2.2 is a representative western blot comparing control-MG versus complete OP-MG HDF. Here the repressed response of the OP-MG dermal fibroblasts to stimulation with rhTGFβ1can be clearly seen, as discussed above with reference to **Table 3.2.1**.

In conclusion, we show that there was an inconsistent response to control or MG serum between the OP-MG cells and the control-MG cells. However in response to TGFβ1 there appeared to be a consistent trend (not statistically significant) towards repression of p-Smad3 protein levels in the OP-MG cells compared to control-MG cells.

3.2.2 The effect of rhTGFβ1 on muscle Daf expression

Bioinformatic interrogation showed that the *DAF/CD55* 5' regulatory region (promoter sequence) is predicted to contain a Smad protein-binding element, thereby suggesting that the TGFβ1-Smad signalling pathway might influence the expression of DAF/CD55 (Wenzel et al. 2005). Since we were investigating the role of TGFβ1 and the TGFβ1-Smad pathway in the pathogenesis of OP-MG, and we previously reported an association between a 5' regulatory region *DAF* SNP and OP-MG, we were interested in the effect of rhTGFβ1 on DAF protein expression in a muscle cell line.

We investigated the effect of variable doses and treatment periods of rhTGFβ1 on Daf protein expression in C2C12 mouse skeletal myoblasts. These myoblasts were differentiated into myotubes over a period of at least 6 days by changing the growth medium to differentiation medium supplemented with 2% horse serum. Myotubes were stimulated with either 10ng/ml of rhTGFβ1 for 1 day and 2 days, 1ng/ml of rhTGFβ1 for 3 days and 5 days, or no rhTGFβ1 (vehicle only). Thereafter, cell protein lysates were analysed by western blotting using a polyclonal antibody to murine Daf (sc-9156) and anti-p38 MAPK antibodies (loading control or 'house-keeping' protein).

It is important to note that in these experiments the mouse polyclonal Daf antibody (sc-9156, Santa Cruz Biotechnologies, USA) produced clear and reproducible bands in **Figure 3.2.3**. As specified in the data sheet accompanying the Daf antibody, we used the banding pattern ranging from 70-100kDa as the signature for WT Daf

protein expressed in C2C12 mouse myoblasts.

There was no significant effect on Daf levels in response to 1 and 2 days of rhTGFβ1 at 10ng/ml in mouse myoblasts (p>0.2). However, in **Table 3.2.2** and **Figure 3.2.3** a significant upregulation of Daf in response to 3 and 5 days of rhTGFβ1 at concentration of 1ng/ml (p=0.008 and p=0.004 respectively) was evident.

C2C12 Mouse myoblasts	rhTGFβ1 (10ng/ml) 1 day	rhTGFβ1 (10ng/ml) 2 days	rhTGFβ1 (1ng/ml) 3 days	rhTGFβ1 (1ng/ml) 5 days
Fold activation	Average ± SD	Average ± SD	Average ± SD	Average ± SD
	0.95 ± 0.21	**1.24 ± 0.18**	**1.55 ± 0.28***	**1.47 ± 0.21***

Table 3.2.2 rhTGFβ1 upregulates Daf levels in mouse skeletal muscle cells after 3 and 5 days. Six-day differentiated C2C12 mouse myoblast cells were treated with vehicle (differentiation medium) or rhTGFβ1 at concentrations of 10ng/ml for 1 and 2 days, and 1ng/ml for 3 and 5 days. Cell lysates consisting of 30 μg of total protein were separated on an 8% SDS-PAGE and analysed by western blotting using antibodies to Daf and p38 MAPK. The results are representative of mean densitometric readings of at least 2 independent western blots. All densitometric reading results were first normalised to p38 MAPK expression and then to the respective untreated control cells. *Indicates statistical significance at p<0.01.

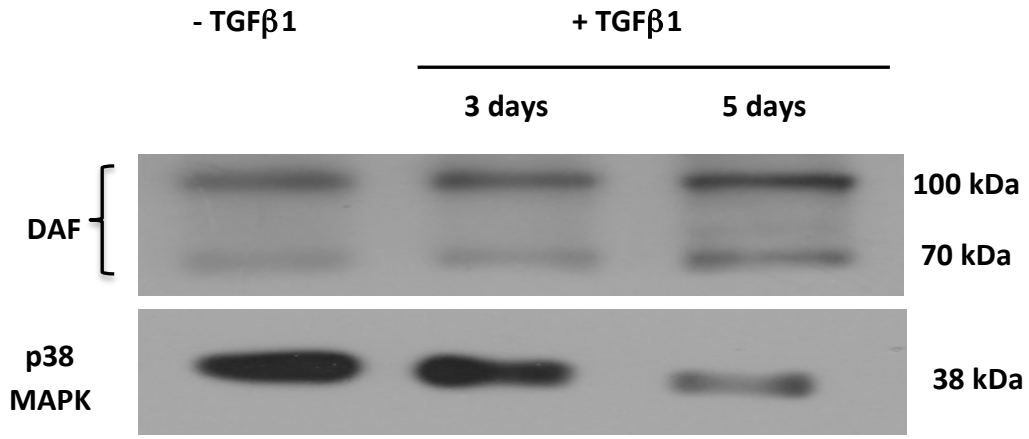

Figure 3.2.3 rhTGFβ1 upregulates Daf levels in mouse skeletal muscle cells after 3 and 5 days. Six-day differentiated C2C12 mouse myotubes were treated with vehicle (differentiation medium) or 1ng/ml of rhTGFβ1 for 3 days and 5 days, after which cell lysates (30 μg) were separated on an 8% SDS-PAGE and analysed by western blotting using antibodies to Daf and p38 MAPK. The positions of the proteins of interest as determined by the protein marker banding-pattern are shown on the right in kiloDaltons (kDa).

In conclusion, there was a consistent and significant increase in TGFβ1-induced Daf expression in C2C12 myoblasts after 3 days of treatment (p<0.01).

3.2.3 The effect of rhTGFβ1 on α-SMA & collagen expression in phenotype-specific EOM perimysial myofibroblasts

Myofibroblasts are critical in the process of healing and repair in almost all tissues, including muscle. TGFβ1 is a crucial cytokine in the transdifferentiation of fibroblasts into myofibroblasts. To evaluate whether there was a differential response between OP-MG and control EOM perimysial myofibroblasts to rhTGFβ1 stimulation, we performed the following:

- Assessment of the basal cell morphology and growth curves of the control and OP-MG cells derived from EOM explant cultures
- Assessment of cell morphology with and without rhTGFβ1 stimulation
- Immunofluorescence microscopic evaluation with/without quantification for the following differentiation proteins, α-smooth muscle actin (α-SMA) and collagen-1A, after stimulation with rhTGFβ1 (1ng/ml).

Fibroblast/Myofibroblast basal cell morphology and growth curves

There were no significant morphological differences observed between the two phenotype-specific (OP-MG & non-MG control) EOM-tendon derived myofibroblasts. Both cell lines demonstrated features consistent with normal myofibroblast morphology including the broad spindle-cell shape, plentiful matrix, the presence of intracellular organelles vital for protein synthesis (collagen, fibronectin and ∝-SMA) and smooth muscle myofilaments. **Figure 3.2.4** represents phase-contrast images of the phenotype-specific cell lines, and reveal almost identical morphology, however there appears to be a greater number of cells per field in the non-MG control patient (MG189) as evidenced by a greater number of visible cell nuclei. The growth curve (**Figure 3.2.5**) also consistently demonstrates more rapid growth of the non-MG control cell line versus the OP-MG cell line over the 14 day period, with a statistically significant greater number of cells on day 4 and day 10 ($p=0.011$ and $p=0.013$ respectively). Doubling time of non-MG control EOM myofibroblasts was calculated to be 14.14 days versus 20.38 days in the OP-MG EOM myofibroblasts. These growth curves were only performed in duplicate, and values therefore represent the mean.

These patients were of the same gender (female) and the control patient was older than the OP-MG patient (55 years versus 42 years) and suffered from diabetes mellitus and systemic hypertension. Nevertheless, the control cells demonstrated significantly faster growth than the OP-MG cells, despite her age and underlying systemic disease.

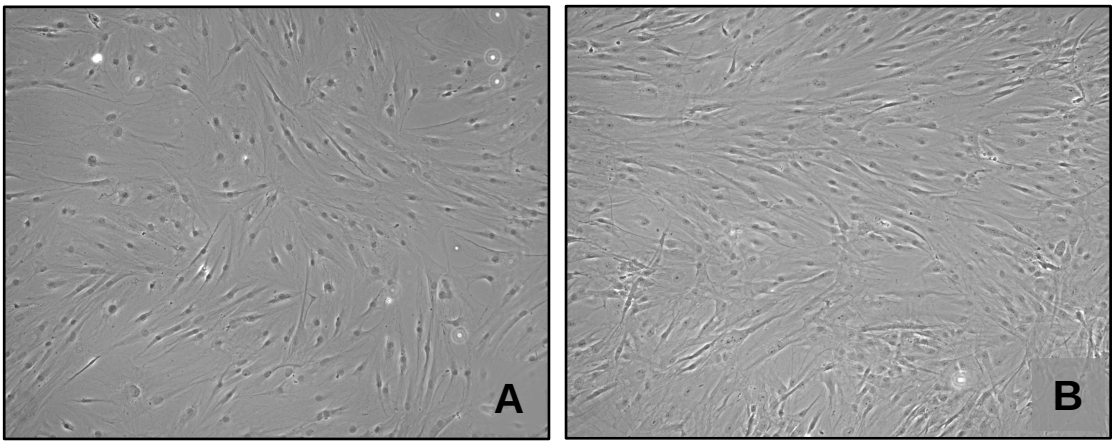

Figure 3.2.4 Phase-contrast microscopy of EOM tendon-derived phenotype-specific fibroblasts/myofibroblasts. (A) OP-MG – Normal fibroblast/ myofibroblast cell morphology. (B) Control (non-MG) – Normal fibroblast/myofibroblast cell morphology, greater cell density than OP-MG cell culture. [10x magnification]

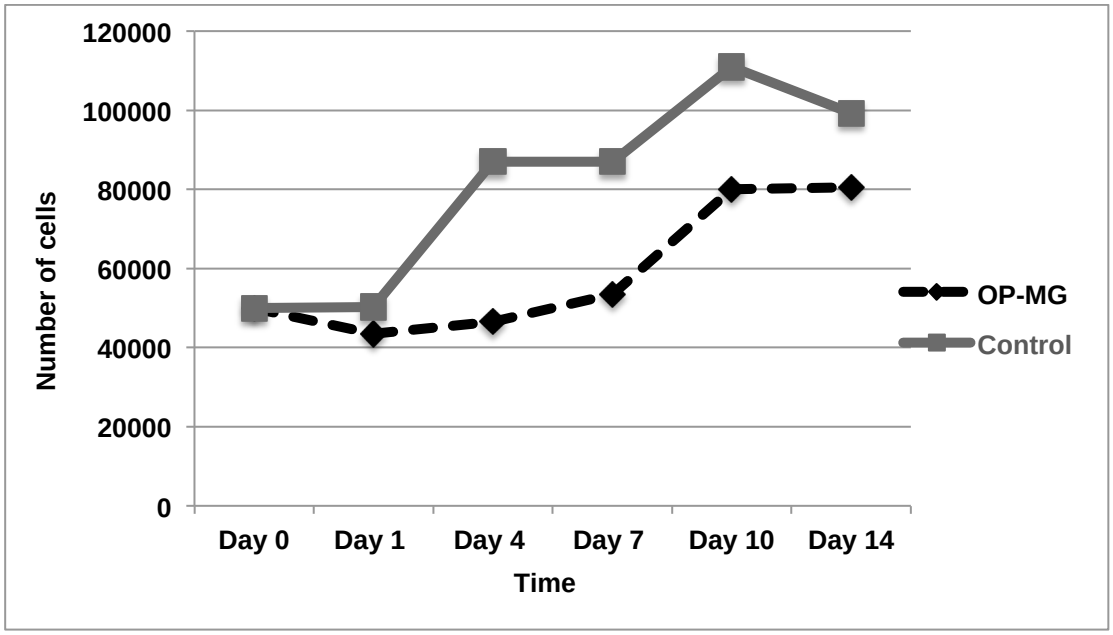

Figure 3.2.5 Graph demonstrating the growth of EOM tendon-derived fibroblast/ myofibroblast cultures of a non-MG control and OP-MG individual. Growth curves were conducted with duplicate samples, therefore values represent the mean.

Fibroblast/myofibroblast cell morphology with and without rhTGFβ1 stimulation

Due to the derivation of these cells from extraocular muscle tendinous insertion, there was some uncertainty as to the exact cell phenotype propagated in explant cell culture. These cells may be primary fibroblasts or myofibroblasts due to their peritendinous origin. Since it has been shown that fibroblasts differentiate into myofibroblasts upon stimulation of the TGFβ1 pathway (Lehmann et al. 2011), care was taken to compare the cell morphology before and after the stimulation experiments in addition to comparing treated and untreated cells.

There were no apparent differences in the morphological appearance of these cells on phase-contrast microscopy prior to the experiments, or after 96 hours of exposure to vehicle with and without rhTGFβ1. This was true for both the OP-MG and control EOM tendon-derived cell lines. This therefore suggests that the cells were myofibroblasts to begin with. The cell phenotype was further scrutinised in the next section when comparing ∝-smooth muscle actin staining across these experimental groups and cell lines.

The effect of TGFβ1 on ∝-smooth muscle actin (∝-SMA) expression in phenotype-specific EOM perimysial myofibroblasts with fluorescence microscopy.

Patient-derived phenotype-specific myofibroblast cell lines were established from the tendinous insertions of excised extraocular muscle by standard explant culture techniques described in section 2.2.1.1. Cells were cultured to 80-85% confluence on coverslips, then treated with vehicle or rhTGFβ1 (1ng/ml) for 96 hours. Thereafter the cells were fixed, stained with primary antibodies to ∝-SMA (#ab7817, Abcam, UK), followed by the addition of HRP-conjugated secondary antibodies. Coverslips were mounted with Mowiol® and observed with the Zeiss Axiovert fluorescence microscope (detailed in section 2.2.7).

There was a consistent difference in ∝-SMA expression observed between the OP-MG and non-MG control myofibroblasts irrespective of TGFβ1 treatment, with considerably more ∝-SMA staining in the control myofibroblasts (**Figure 3.2.6**). In response to treating the cells with TGFβ1, there was only a modest increase in ∝-

SMA staining in both OP-MG and control cells, with the control line possibly showing a slightly greater increase than the OP-MG cells (**Figure 3.2.6**).

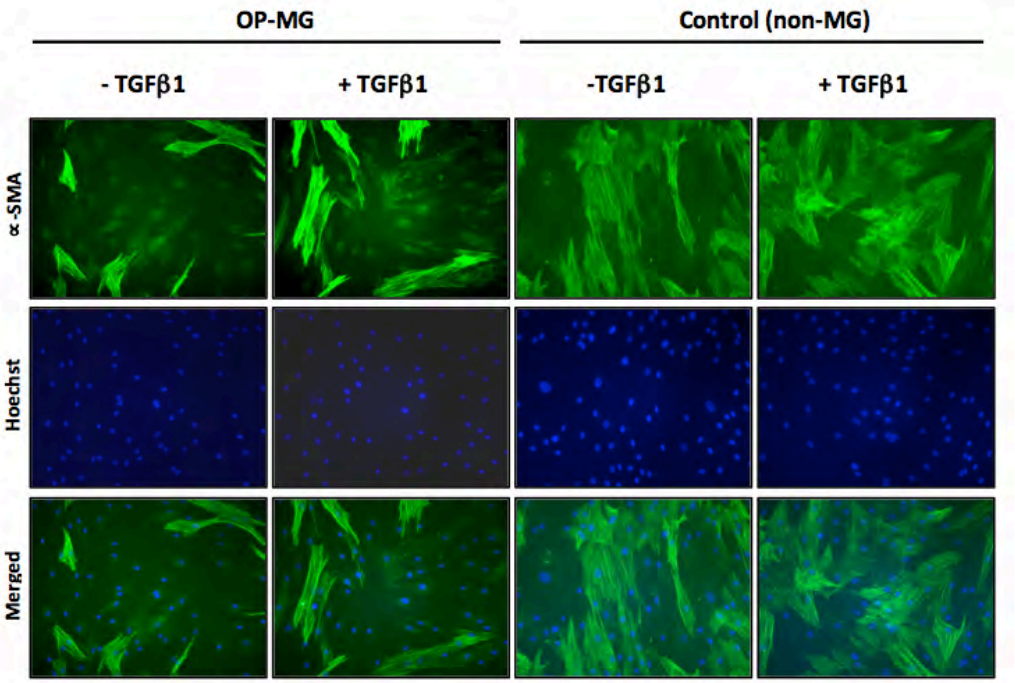

Figure 3.2.6 Immunofluorescence microscopy of OP-MG & control (non-MG) EOM tendon-derived phenotype-specific myofibroblasts after 96 hours of exposure to vehicle with and without rhTGFβ1 (1ng/ml). The OP-MG cell line expresses considerably less ∝-SMA than the control cell line with and without TGFβ1 treatment. Both cell lines demonstrated a modest increase in ∝-SMA staining after 96 hours of TGFβ1 stimulation. (Analysis of ≥4 slides at 20x magnification, and ≥2 slides at 10x magnification for each cell line with and without TGFβ1). [20x magnification]

We attempted to crudely quantify any enhanced staining by counting the number of cells per representative microscope field (at 10x magnification) that stained positive for ∝-SMA as a percentage of all the cells with Hoechst-stained nuclei in that field. This proved to be difficult due to the density of cells in the field and the difficulty to discern individual cells, with cells often overlapping or overlying one another as seen in **Figure 3.2.4** and **Figure 3.2.6**. It was therefore not possible for us to reliably quantify our findings or to objectively determine differences between cell lines and experimental groups by means of simple visualisation alone. Ideally, we would have liked to perform imaging flow cytometry for cells labelled for ∝-SMA as described by

Lehmann et al. (2011) to better quantify the potential staining differential of each cell, as the differences in cell growth/density between OP-MG and non-MG control cells may be confounding these results.

The effect of TGFβ1 on collagen-∝2 type 1 (Col1A2) expression in phenotype-specific EOM perimysial fibroblasts/myofibroblasts with flourescence microscopy.

Here we assessed collagen-∝2 type 1 (Col1A2) expression after specimen preparation and stimulation as for ∝-SMA detailed above and in section 2.2.7.

Unfortunately immunoflourescence staining for collagen with the Col1A2 antibody (sc-8786, Santa Cruz Biotechnology, USA) was less successful than for ∝-SMA. We had significant non-specific staining or 'background' in these slides, despite attempts to optimise the procedure by modifying the blocking solution(s) and the simultaneous incubation of cell cultures with both ∝-SMA and collagen antibodies. As a result the staining and consequent microscopy images were of poor quality, with very little specific antibody binding apparent. We can therefore not make any worthwhile observations in these slides. Slightly better quality images could be obtained with the confocal microscope, most likely due to better fluorescence filters in this microscope. Again, there were insufficient images of suitable quality to make any meaningful or valid observations.

In summary, we found the basal cell morphology of the OP-MG and control (non-MG) EOM-derived cells to be the same and compatible with that of myofibroblasts, and this basal morphology remained largely unchanged after TGFβ1 exposure, suggesting that the cells were myofibroblasts at the outset. Growth curves of the OP-MG and control cells were comparable, but increased growth was evident in the non-MG control cells ($p=0.011$ on day 4, $p=0.013$ on day 10) with limited interpretability due to limitations discussed above. Due to technical constraints we cannot make valid inferences with respects to ∝-SMA and collagen expression in the treated and untreated cells and control and OP-MG lines. These findings are certainly intriguing and warrant further investigation by means of better quantifiable methods to allow for more robust data and conclusions.

3.3 GENERATING PATIENT-DERIVED PHENOTYPE-SPECIFIC INDUCED PLURIPOTENT STEM CELLS

Due to the paucity of muscle tissue, especially extraocular muscle tissue, available for study in MG-related complications such as OP-MG, one of my objectives was to establish patient-specific induced pluripotent stem (iPS) cells that could later be used to differentiate into OP-MG or control-MG muscle cells. These muscle cell lines would provide limitless cells for *in vitro* work and potential drug testing or development. In the development of a muscle line from iPS cells, the first step is to reprogramme somatic cells into iPS cells and then to redirect the differentiation of these iPS cells into muscle cells. Here I describe the results of the first stage of establishing iPS cells from patient-derived dermal fibroblasts.

3.3.1 Reprogramming of HDF with SeVdp (Figure 3.3.1)

We simultaneously infected two phenotype-specific human dermal fibroblast (HDF) cell lines (MG822 – control-MG, MG7 – partial OP-MG) with transgene-containing SeVdp to generate phenotype-specific iPS cells. Thirty days after infecting 1.5 x 10^5 of the MG7 HDF with 75µl of SeVdp (MOI > 5), no promising iPS colonies were observed. A few colony-like structures were manually passaged but these could not be successfully maintained or propagated in feeder-dependent culture beyond p1 and the cells were frozen down for later retrieval.

In contrast, the cells from MG822 (control-MG, female, African-genetic ancestry) were successfully reprogrammed, with iPS cell colonies emerging from day 17 post infection. In total, seven iPS cell clones were picked from the original p0-plate for a period of up to 37 days, at which time the residual undifferentiated colonies were lifted with TrypLE Express™ and cryopreserved at -80°C (as described in section 2.3.1).

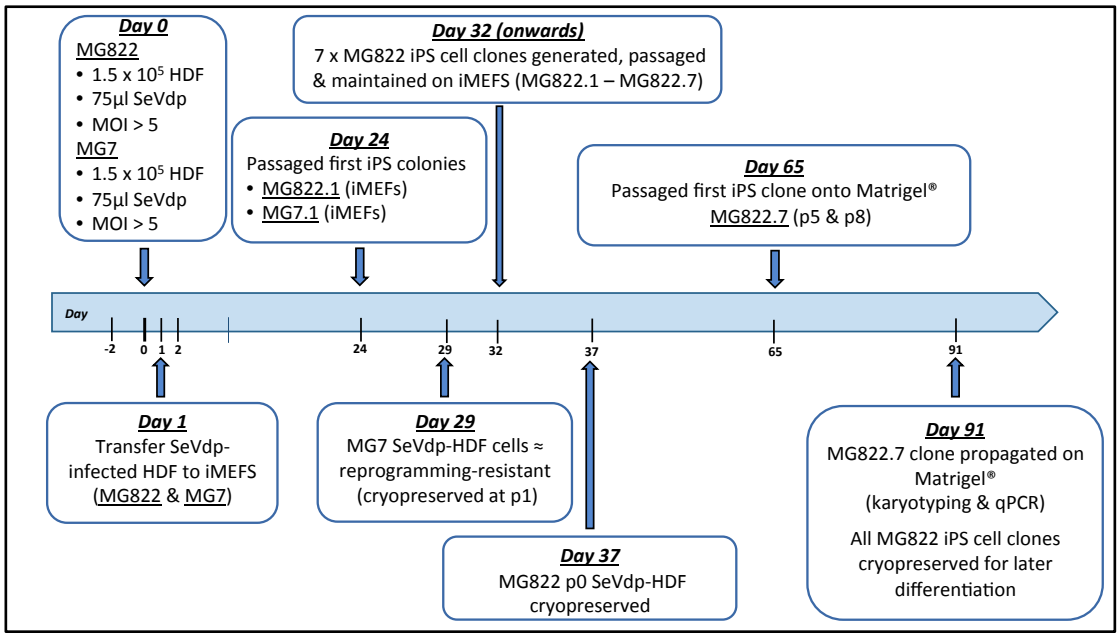

Figure 3.3.1 A timeline representing key events in the generation and maintenance of patient-specific (MG822 & MG7) induced pluripotent stem (iPS) cells from human dermal fibroblasts (HDF). Day 0 represents the day of fibroblast infection with the reprogramming gene-loaded Sendai viral vector (SeVdp).

3.3.2 Culture & maintenance of iPS cells in feeder-dependent culture (iMEFs) & feeder-free culture (Matrigel®)

Undifferentiated iPS cell colonies were maintained and propagated on feeder cell monolayers (iMEFs – locally outbred E14.5 iMEFs & commercially obtained ATCC® iMEFs) for 91 days. During this period, seven clones of MG822 HDF-derived iPS cells up to a maximum of nine subpassages were established and cryopreserved at regular intervals.

Approximately 40 iPS colonies, with good morphology and little or no differentiation, were present in each 35mm well for each MG822 clone at various passages in co-culture with iMEFs. The ideal feeder cell density to enable iPS colony propagation without differentiation was 0.3 x 10^6 E14.5 iMEFs/35mm well and 0.15 x 10^6 ATCC® iMEFs /35mm well.

For the purposes of karyotyping and RNA extraction for q-PCR characterisation, MG822.7 (p4 + p7) were enzymatically treated with TrypLE™ Express & transferred onto Matrigel® coated dishes in Essential 8™ medium (Gibco™, Life Technologies,

USA) . We continued to enzymatically passage these clones with TrypLE™ Express or EDTA (100µl of 0.25M EDTA pH8.0 in 50ml 1x PBS) and daily complete medium changes with the addition of Y-27632 dihydrochloride (Sigma-Aldrich®, USA). Initially the iPS cells formed abundant adherent colonies with good morphology and little/no differentiation (**Figure 3.3.2** and **Figure 3.3.3**), but after approximately eleven days and three passages these iPS cells started lifting from the substrate. Questioning the Essential 8™ medium quality, we transferred the remaining adherent cells onto Matrigel® in conjunction with mTeSR1™ Complete kit for hESC and hiPSC Maintenance (Stemcell technologies™, Canada) supplemented with Y-27632 dihydrochloride (Sigma-Aldrich®, USA). The mTeSR medium was refreshed daily and cells were passaged three more times to confluency. Sufficient cells were obtained for RNA extraction for the purposes of q-PCR, and a confluent 25cm^2 flask was transferred to the NHLS Cytogenetics laboratory at Groote Schuur Hospital for karyotype analysis.

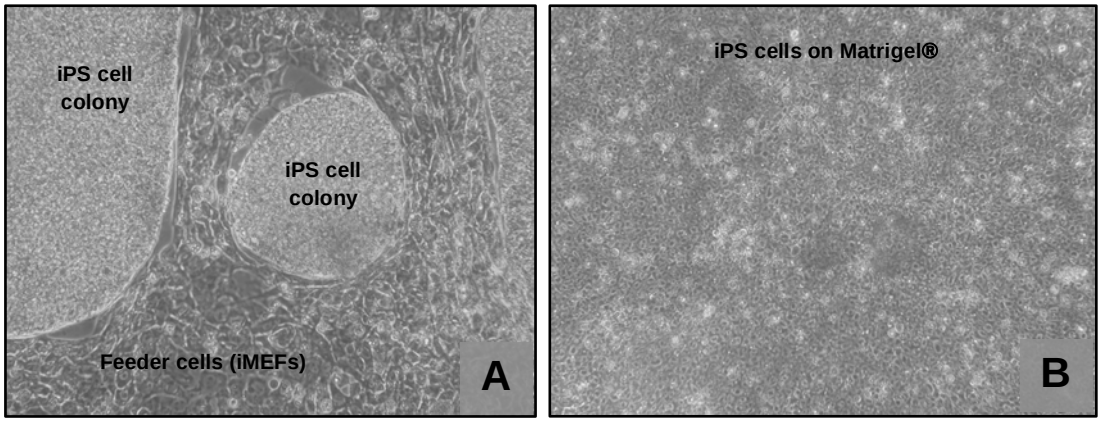

Figure 3.3.2 (A) Induced pluripotent stem (iPS) cell colonies (MG822.7 p4) in co-culture with inactivated mouse embryonic fibroblast (iMEF) feeder cells demonstrating tightly packed cells with high nucleus-to-cytoplasm ratio and distinct borders. [20x magnificaiton] **(B) iPS cells (MG822.7 p10) in feeder-free culture on Matrigel® substrate with Essential 8 medium demonstrating tightly-packed cells with a high nucleus-to-cytoplasm ratio.** [20x magnification]

The iPS cell clones generated from MG822 HDF cells were cryopreserved in specialised iPS cell freezing medium at various intervals during the course of this project. The iPS cells are all stored in clearly labeled cryovials in a dedicated MG822 iPS cell box in liquid nitrogen. These cells were not further differentiated during the

course of my project for numerous reasons, which will be elaborated upon in the discussion.

3.3.3 Characterisation of iPS cells

Morphology

A distinguishing feature of iPS colonies is a distinct morphology which appeared after the repeated subpassage of early colonies picked from the p0-plate. The colonies were flat with distinct borders, and contained tightly packed cells with a high nucleus-to-cytoplasm ratio (**Figure 3.3.2** and **Figure 3.3.3**).

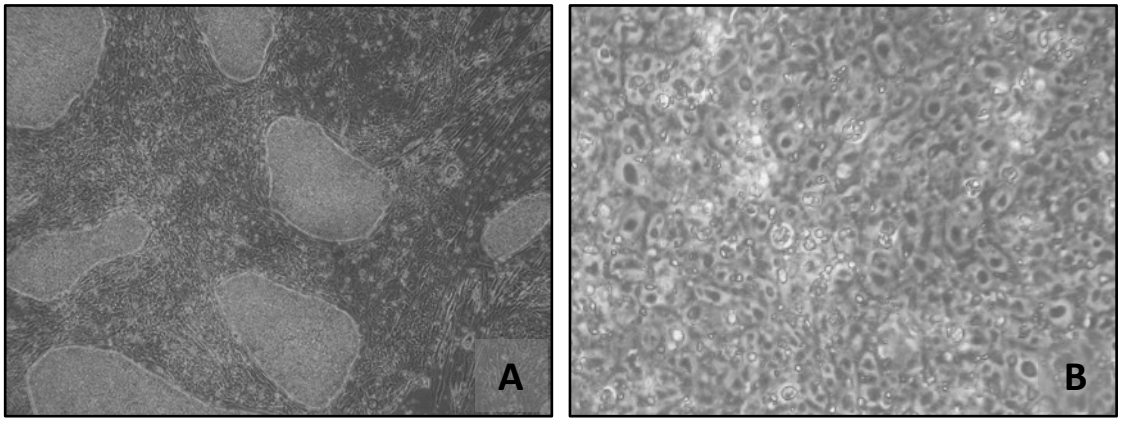

Figure 3.3.3 Morphology of induced pluripotent stem (iPS) cell colonies (MG822.7 p4) in co-culture with inactivated mouse embryonic fibroblast (iMEF) feeder cells. (A) The iPS colonies had distinct borders that separated the iPS cells from the surrounding iMEFs [10x magnification]**. (B) iPS colonies (MG822.7 p4) could be seen as groups of tightly packed cells with a high nucleus-to-cytoplasm ratio.** [200x magnification]

Expression of pluripotency markers

To determine whether each MG822 iPS cell clone expressed markers associated with pluripotency, each line was subjected to immunocytochemistry (ICC) and q-PCR. Immunocytochemical analysis was performed at 3 different time points, with optimisation of the procedure and outcome by the final event. At initial ICC on day 38, 3 clones of MG822 (MG822.1, MG822.2, MG822.5) at low passage (p2-p3) were manually passaged onto iMEFs (E14.5) on gelatin-coated coverslips in a 12-well plate. While the iPS cells were positive for all 3 pluripotency markers (OCT4, NANOG

and TRA-1-60), the morphology and size of the iPS cell colonies were poor due to the loss of cells during the ICC preparation process which requires numerous cell washes. On subsequent ICC (day 59), 2 clones (MG822.2, MG822.7) at passage 6 were enzymatically passaged with TrypLE™ Express from E14.5 iMEFs and from Matrigel®. The hES++ medium was only replenished after 48 hours to ensure better cell adherence and PFA fixation was delayed by a further 24 hours. The colonies were larger and greater care was taken to ensure gentle cell washes. There was a degree of differentiation evident in these colonies, and the antibody-antigen staining pattern was non-specific with marked cytoplasmic staining for both nuclear (OCT4, NANOG) and cell surface markers (TRA-1-60). Similar staining patterns have been reported and attributed to variability in the different commercially available antibodies (Zuk et al. 2009). However, we attribute our non-specific staining to a technical factor related to permeabilisation of the cells during enzymatic passage or the methods and reagents (possibly degraded/expired PFA) used in cell fixation. In repeat ICC experiments on MG822 iPS cell lines, and iPS cells derived by other investigators, specific nuclear and cell membrane staining was demonstrated using the same batch of commercial antibodies.

Finally, for ICC on day 104, we manually passaged many patches (> 10/well) of a single clone of MG822.7 (p5) from ATCC & E14.5 iMEFs to the prepared wells with iMEFs on coverslips. Again the iPS cell patches were left undisturbed in the incubator for 48 hours, without hES++ medium change on the first day after passage. Care was taken to perform all cell washes gently so as not to dislodge any of the colonies and fixation took place 3 days after the manual passage. The iPS cell line (MG822.7) revealed iPS cell colonies demonstrating distinct nuclear-specific staining for OCT4 and NANOG, compared to the surrounding iMEFs (**Figure 3.3.4**). The iPS cell colonies also stained positive for TRA-1-60, a cell surface antigen expressed by undifferentiated human embryonic stem cells. Therefore, we confirmed the expression of all three pluripotency markers, OCT3/4, NANOG, and TRA-1-60, in at least one iPS cell clone generated from the reprogrammed fibroblasts derived from patient MG822.

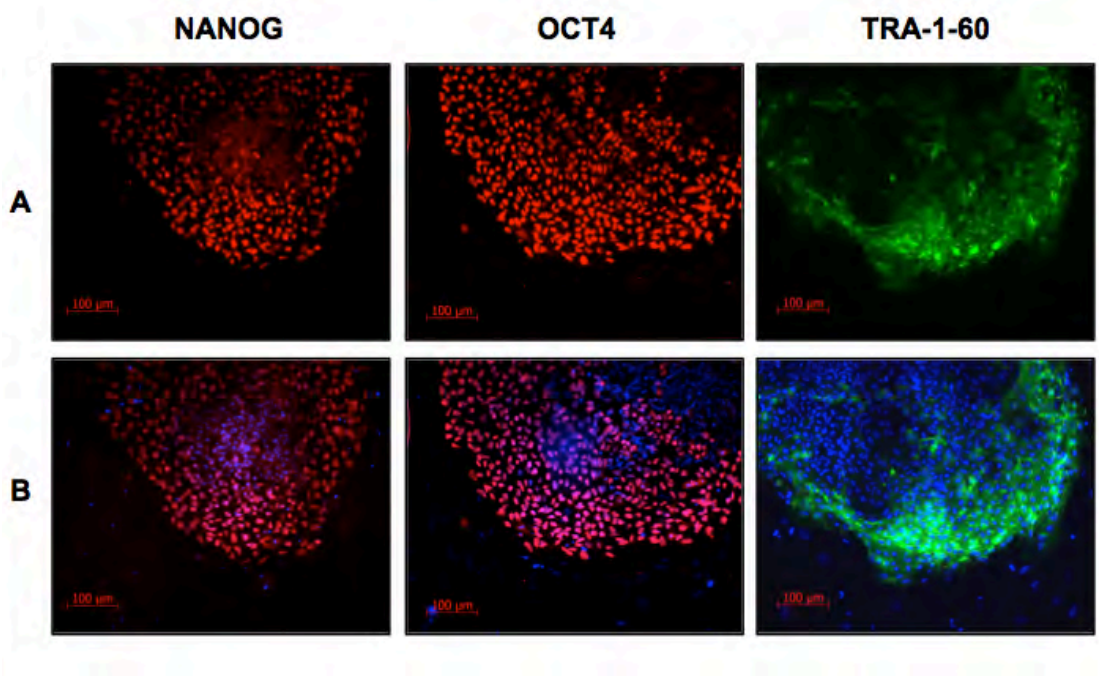

Figure 3.3.4 Immunocytochemistry for pluripotency markers in induced pluripotent stem (iPS) cells in co-culture with inactivated mouse embryonic fibroblasts (iMEFs). Images in the left column demonstrate positive nuclear staining for NANOG (red) in the iPS cell colonies of cell line MG822.7 with Cy3 filter (A) and Cy3 & DAPI filters (B). Images in the middle column show staining for the nuclear marker NANOG (red) in the iPS cell colony of cell line MG822.7 with Cy3 filter (A) and Cy3 & DAPI filters (B). Images in the column on the right show expression of the cell surface marker TRA-1-60 (green) in cell line MG822.7 with Alexa488 filter (A) and Alex488 & DAPI filters (B). Nuclei in blue. [20x magnification].

The expression of pluripotency genes was confirmed by qPCR. The iPS cell lines MG822.4 and MG822.7 (p11 and p10 respectively) expressed high levels of *OCT3/4, SOX2* and *NANOG* (**Figure 3.3.5**). The expression of these pluripotency genes was also comparable to that of another unrelated control iPS cell line established by Dr Robea Ballo. The expression levels of *OCT3/4, SOX2* and *NANOG* were similar across the two iPS cell lines. Little or no expression of *OCT3/4*, *SOX2* and *NANOG* was evident in HDF since these are already terminally differentiated cells. Furthermore qPCR for *COL1A1*, a gene expressed in differentiated fibroblasts, demonstrated very little or no expression in both our iPS cell lines (MG822.4 & MG822.7). Together these results confirmed that these MG822 iPS cell lines were indeed pluripotent.

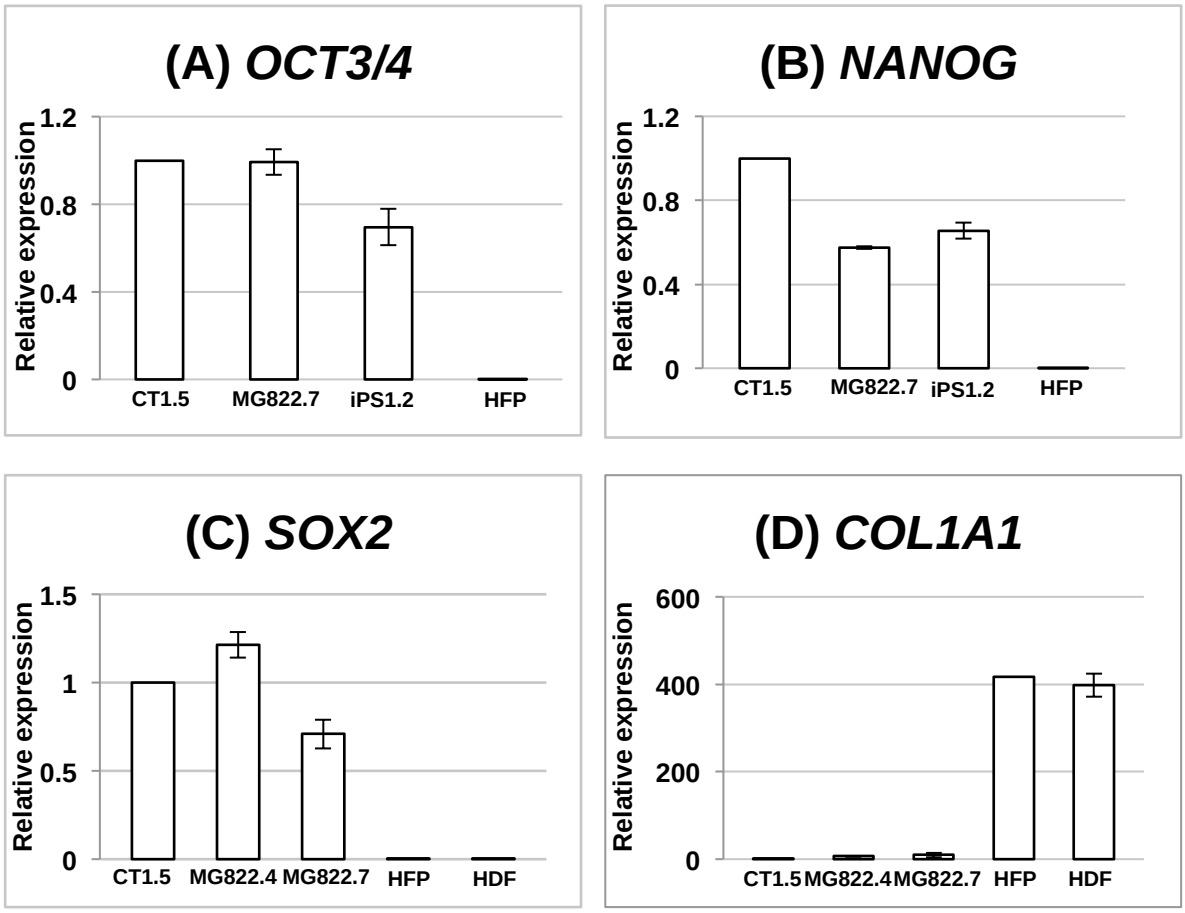

Figure 3.3.5 Expression of pluripotency markers in iPS cell lines, determined by qPCR. iPS cell lines CT1.5 & MG822.7 expressed *OCT3/4* (A), *NANOG* (B), and *SOX2* (C), while MG822.4 was only subjected to qPCR for *SOX2* expression (C). This is compared to low expression levels in the control fibroblasts (two different fibroblast lines – HFP & HDF). (D) Demonstrates the lack of *COL1A1* expression in all iPS cells lines (CT1.5, MG822.4 & MG822.7) and thereby indicates that they are reprogrammed and undifferentiated versus expression in the donor fibroblasts (HFP & HDF). All levels are normalised to β-glucuronidase (GUSB), and expression is relative to CT1.5 (unrelated control iPS cell line) expression. Error bars show standard deviation from the mean. iPS cell qPCR data courtesy of Dr Robea Ballo.

Silencing of SeVdp

To determine whether the iPS cell lines could demonstrate growth and maintenance independent of reprogramming gene expression, immunocytochemistry and qPCR were used to confirm that the iPS cell lines did not contain traces of the reprogramming Sendai viral vector. The SeVdp used for reprogramming contained an miRNA target site to enable silencing of reprogramming gene expression in

pluripotent cells (Nishimura et al. 2011). The vector was also replication-defective, and would therefore be diluted with subsequent cellular divisions. The MG822.7 iPS cell colonies were co-stained with primary antibodies against the pluripotency marker OCT4 and the nucleocapsid protein of the virus (anti-NP). This iPS cell line was assessed after passage 5. iPS cell colonies showed no evidence of SeVdp NP staining (**Figure 3.3.6 B**), compared to intense cytoplasmic staining in newly infected fibroblasts (**Figure 3.3.6 A**), indicating that the Sendai virus had been effectively silenced in the iPS cell colony.

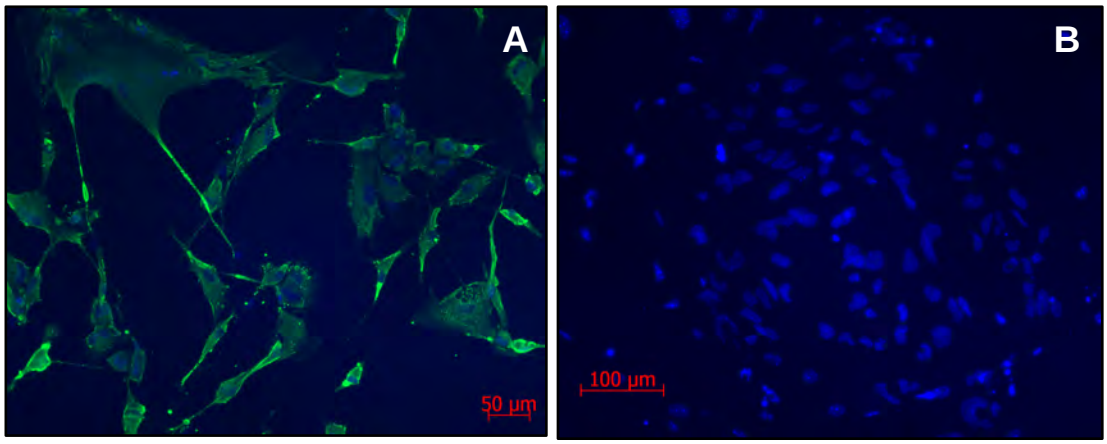

Figure 3.3.6 Silencing of the reprogramming Sendai virus (SeVdp) on immunocytochemistry. (A) Newly infected fibroblasts demonstrating positive staining for SeVdp NP (green) [40x magnification] **and (B) induced pluripotent stem (iPS) cell colonies stained with primary antibodies against the viral nucleocapsid protein (green)** [20x magnification]**. Nuclei in blue.** Image of SeVdp-positive fibroblasts (A) courtesy of Dr Lauren Watson.

Gene expression analysis of the SeVdp gene demonstrated very high expression of the viral vector in cells that had recently been infected with the virus compared to our MG822-derived iPS cell line(s), showing effective silencing of the Sendai viral vector during the reprogramming process (**Figure 3.3.7**).

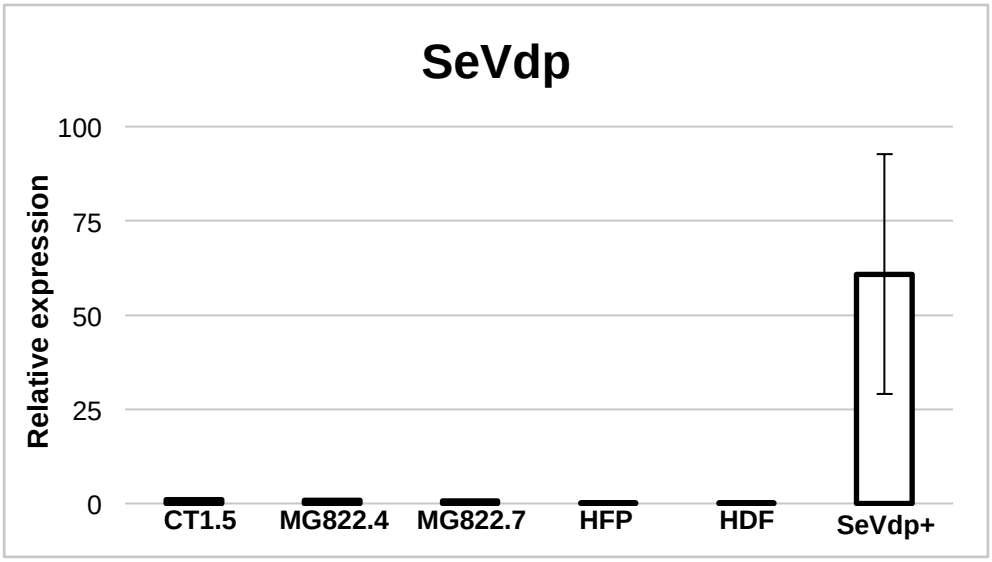

Figure 3.3.7 Absent expression of the reprogramming Sendai virus (SeVdp) in iPS cell lines, determined by qPCR. iPS cell lines CT1.5, MG822.4 & MG822.7, and control fibroblasts (HFP & HDF) did not express SeVdp. Newly-infected fibroblasts demonstrate expression of SeVdp. All levels are normalised to β-glucuronidase (GUSB), and expression is relative to CT1.5 (unrelated control iPS cell line) expression. Error bars show standard deviation from the mean. iPS cell qPCR data courtesy of Dr Robea Ballo.

Karyotyping

While propagating 2 of our iPS cell clones in feeder-free culture (Matrigel® with Essential 8™ medium or mTeSR1™ Complete kit for hESC and hiPSC Maintenance), the original patient-specific (MG822) parent HDF cells for karyotyping at the NHLS Cytogenetics Laboratory at Groote Schuur Hospital. This sample served as an indicator as to the number of cells required to submit in order to have sufficient cells in metaphase to enable karyotyping; one confluent 25cm^2 flask of cells. Chromosome analysis of 10 metaphase cells revealed the karyotype: 46, XX, which is consistent with a normal female pattern. No gross structural abnormalities were detected on Giemsa-banded metaphase spreads, and the chromosome band resolution was approximately 400 G-bands.

The first MG822 HDF-derived iPS cells (MG822.7, p9) evaluated in the cytogenetics laboratory revealed that metaphase was present, but the chromosomes could not be properly identified and karyotype analysis was therefore not possible. The metaphases had a very unusual morphology, with the chromosomes described as 'broken' into their short and long arms, with the appearance of acrocentric chromosomes. A thorough review of culture and laboratory procedures could not identify any specific technical factors in our laboratory or the NHLS Cytogenetics Laboratory that may have contributed to this unusual phenomenon. We suspect that it may be attributable to culture failure and/or toxicity associated with the feeder-free substrate (Matrigel®) and/or the medium (Essential 8™) used to maintain and propagate these cells, and not a function or characteristic of the iPS cell itself.

Further investigation of the observed cytogenetic abnormality using a different clone (MG822.4 – p8) could not be performed due to culture failure in the cytogenetics laboratory. The genomic integrity of these iPS cells has therefore not yet been established, since 2 attempts at karyotype analysis on these cells were unsuccessful. Prior to the use of these iPS cells for any future differentiation experiments or models, this process will have to be repeated to ensure that there are no induced karyotype abnormalities, the most common of which are copy number variation, and trisomy 12 and 8 (Hussein et al. 2011; Taapken 2011).

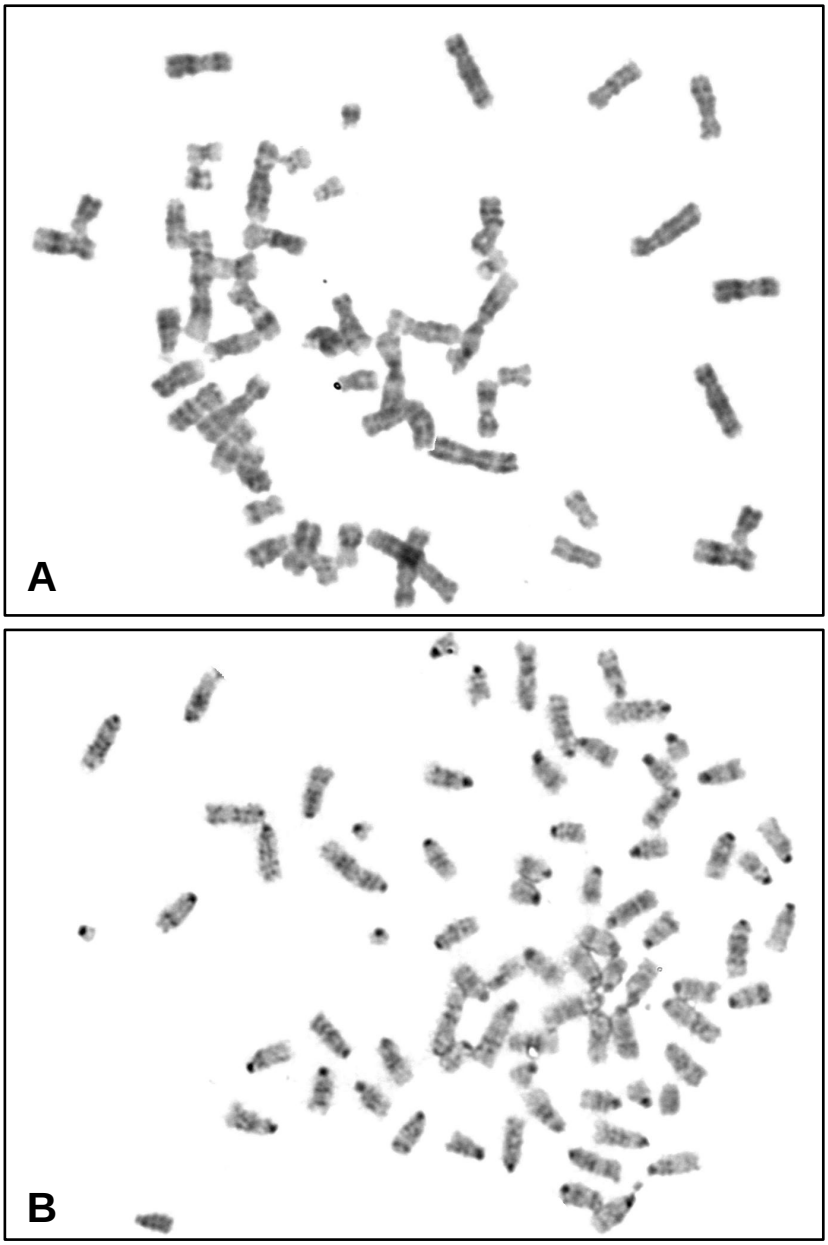

Figure 3.3.8 Karyotype analysis - photographs of chromosomes in metaphase. (A) Normal chromosomes of adult human dermal fibroblasts (MG822) – karyotype = 46,XX. (B) Abnormal chromosome appearance (appear broken into long and short arms) of induced pluripotent stem cells (MG822.7), karyotype analysis not possible.

In summary, we have successfully established iPS cells from a control MG patient's (MG822) dermal fibroblasts and these cells have been partially characterised demonstrating markers of pluripotency and silencing of the viral vector. However, the karyotyping needs to be repeated for these MG822 HDF-derived iPS cells to exclude cytogenetic abnormalities which could restrict the use of the iPS clones for differentiation into useful disease models.

CHAPTER 4

DISCUSSION, LIMITATIONS AND CONCLUDING REMARKS

DISCUSSION

In an attempt to better understand the pathophysiology of treatment-resistant ophthalmoplegia in a specific subset of MG patients, this study contains various components centred around the cellular and molecular investigation of this complication and the development of a potential *in vitro* disease model for OP-MG. Firstly I describe the clinical, imaging and pathological findings, and their correlation, in selected patients with OP-MG in whom EOM tissue was available for study versus EOM from a healthy control.

All three OP-MG patients had complete or near-complete ophthalmoplegia (≈100% pareses) and variable degrees of blepharoptosis. Forced duction testing revealed no restriction or resistance to movement, and active force generation testing demonstrated marked paresis with virtually no clinically detectable power in all the EOMs. A manifest deviation, exotropia and hypotropia, was present and warranted surgical intervention for intractable diplopia in two cases. The two cases with juvenile onset OP-MG also had additional clinical features demonstrating anatomical variation in globe stucture and/or position .

There is little reported on the imaging of the EOMs in MG specifically; with three of seven cases of 'CT-proven' bilateral EOM atrophy attributable to underlying MG in one report (Okamoto et al. 1996), while in another single MG case EOM volumes were reported normal and comparable to those of CPEO subjects on high-resolution MRI (Ortube et al. 2006). The latter study found that CPEO, a mitochondrial myopathy, can be associated with normal or near-normal EOM volumes on orbital MRI despite clinically severe ophthalmoplegia in patients who had been symptomatic for between 9 months and 22 years (Ortube et al. 2006).

The normal orbital imaging excluded the entity known as 'heavy eye syndrome', which describes the herniation of the globe between the lateral rectus and superior rectus muscles and can be attributed to degeneration of the connective tissue band between these two muscles with resultant inferior sagging of the LR pulley and consequent strabismus (Fresina et al. 2014). This condition has been predominantly described in the presence of axial myopia, which was present in both juvenile-onset OP-MG cases, however neither of these cases had LR or SR muscle displacement on orbital imaging. Another variant of this condition, 'sagging eye syndrome', is seen in elderly patients without axial myopia, and can be ascribed to the age-related degeneration of orbital connective tissue (Rutar & Demer 2009). While the two juvenile OP-MG cases did not have radiological evidence of muscle displacement and/or globe herniation, they did appear to exhibit anatomical variations in globe stucture and/or position, which may be secondary to chronic functional 'denervation' and/or antibody-mediated complement endplate damage in the EOM.

I describe the histopathological and ultrastructural features of extraocular muscle in a triple-seronegative OP-MG case. Our OP-MG case showed similar histopathological findings in her EOM to a previously reported AChR positive MG case (Gratton et al. 2014). However the ultrasctructural features that we describe here are novel. The pathological characteristics in the EOMs of MG patients are very poorly reported in the literature due to EOM tissue rarely being available for analysis, since this is not an accessible site for biopsy and re-alignment surgery is seldom indicated in patients with MG. Due to the paucity of OP-MG cases requiring and undergoing EOM resections, our case description of OP-MG is of significance.

Myopathic features predominated in the EOM of our OP-MG case, with replacement of muscle by fatty connective tissue, wide variation in myofibre size, myofibrillar disarray, mitochondrial abnormalities, but no ragged red fibres being the most striking features. No clustered or group atrophy, angulated fibres, target formations or nuclear clumping were evident in the OP-MG muscle. In chronic denervation and in the absence of fibre type grouping, certain features on muscle histology (excess endomysial connective tissue, presence of internal nuclei in some hypetrophic fibres) may make it difficult to distinguish this from a myopathy (Dubowitz et al.

2013). Indeed, it is generally recommended that profoundly weak or atrophic muscle not be biopsied for diagnostic purposes as specific abnormalities may be obscured by the replacement of muscle by fatty tissue and fibrosis. The latter representing chronic secondary myopathic changes (Dubowitz et al. 2013).

The changes that we observed in the OP-MG EOM tissue mirror those reported in limb skeletal muscle biopsies of MG patients. For example, AChR positive MG is associated with a broad spectrum of muscle pathology, ranging from normal morphological features to the presence of marked myofibre atrophy (non-specific or type II fibre atrophy), increased variability in muscle fibre diametre, and myofibrillar disarray with Z-line streaming; a non-specific finding that may be present to a variable degree in normal muscle (Padua et al. 2006; Martignago et al. 2009; Cenacchi et al. 2011; Dubowitz et al. 2013). In MuSK positive MG, cases demonstrated myopathic changes and frequent mitochondrial abnormalities with/without ragged red fibres on limb muscle biopsies (Rostedt Punga et al. 2006; Canacchi et al. 2011).

The case and control EOMs displayed different clinical and ultrastructural features, probably due to the underlying pathogenic mechanisms, although age may be a contributing factor to these findings since the OP-MG case was 54 years of age versus our 32 year old control. Mitochondrial DNA point mutations and deletions accumulate with age in various tissues, including muscle, and result in mitochondrial dysfunction observable as COX-deficiency on histochemistry (Yu-Wai-Man et al. 2010). COX-negative fibres are evident much earlier and at higher levels in EOMs than in skeletal muscle (3.34% versus <1% respectively in individuals over 60 years of age), with a significant age-related increase in COX-deficiency (from 0.05% under 30 years of age to 3.34% over 60 years of age) in EOMs (Yu-Wai-Man et al. 2010).

As comparator EOM, we selected a control EOM sample from a donor who had a similar period of ocular malalignment (3-4 years) and had the same muscle (medial rectus) resected and donated for study. The control case had a sensory exotropia in a non-seeing eye, and had normal motility in all his EOMs. In this case the deviation was due to a reduced central drive for fusion, resulting in altered supranuclear outflow and unequal tonic innervation of the horiontal recti with a consequent

malaligment. No EOM paresis was evident on motility testing, however, it can be assumed that the innervation to the medial rectus muscle was reduced in comparison to that of its antagonist muscle (lateral rectus). Interestingly, after approximately 36-40 months of reduced tonic innervation of the medial rectus muscle, this muscle did not demonstrate clinically-detectable paresis or any abnormal features on histology/ultrastructure.

The clinical findings of complete or near-complete ophthalmoplegia in the OP-MG case, and the inability to elicit a generated force in the EOMs on clinical testing correlated well with the degree of generalised atrophy and 'myopathy' observed in the EOM. Forced duction testing in this OP-MG case, and others (personal communication Professor A Murray), revealed no resitance to movement in any direction, thereby indicating that the absence of eye movement was not due to a mechanical restriction and thereby implying no underlying fibrosis and consequent EOM shortening. While the EOMs are reported to not exhibit the massive denervation atrophy that characterises other skeletal muscles (Porter & Baker 1996), in our case and the case reported by Gratton et al., we demonstrated marked replacement fibrosis with abundant adipose and collagen deposition in EOM tissue (Gratton et al. 2014). This pathological intermyofibrillar network of collagen and adipose tissue was reported in conjunction with mitochondrial abnormalities in limb skeletal muscle biopsies in all MuSK positive MG cases (100%), and less frequently in double seronegative MG (22%) and AChR positive MG (26%)(Rostedt Punga et al. 2006).

In summary, EOM tissue from an OP-MG individual with AChR- and MuSK-antibody negative MG, demonstrated predominantly myopathic pathology and ultrastructural evidence of mitochondrial stress. The OP-MG EOM findings differ from the control EOM, which showed normal muscle histopathology in a patient with a sensory exotropia and a similar duration of deviation. These OP-MG findings appear to better correlate with previously reported histology/ultrastructure in limb muscle in MuSK-positive MG rather than AChR-positive MG. Imaging by means of STIR sequence MRI and CT did not reveal any alterations in EOM appearance in all three of our reported OP-MG cases. The two reported cases with juvenile onset OP-MG, had additional

clinical features demonstrating anatomical variation in globe stucture and/or position, which may be attributable to aberrant processes in orbital connective tissue.

Transforming growth factor beta-1 (TGFβ1) plays a critical role in muscle injury and repair, and its expression is upregulated by both muscle and the secondary inflammatory cell infiltrates in/around the muscle. Several polymorphisms in the *TGFB1* regulatory region are functional and impact on TGFβ1 tissue expression levels (Nel et al. 2016). In addition, Nel et al. found that an African-specific functional *TGFB1* regulatory region variant, that associated with South Africans with juvenile OP-MG, resulted in five-fold repression of TGFB1 mRNA levels compared wild-type fibroblasts (Nel et al. 2016). Here I had an opportunity to undertake and complete investigations into the effect of exogenous TGFβ1 on the protein expression levels of TGFβ1/p-Smad3 in phenotype-specific fibroblasts (dermal- and EOM-derived) and mouse muscle cells.

We observed a non-significant, but consistent trend towards a differential response in TGFβ1-induced Smad3 phosphorylation, with lower p-Smad3 levels in OP-MG dermal fibroblasts compared to control-MG fibroblasts (p=0.104) (**Table 3.2.1** and **Figure 3.2.2**). My work focussed on the phenotype of the cases (OP-MG versus control-MG), while Nel et al. extended this work by studying the *TGFB1* promoter genotype underlying the phenotype, and found that the disease-specific differences that I observed where underpinned by the individual's *TGFB1* regulatory region genotype (Nel et al. 2016).

Based on previous work by Heckmann et al. (2010) and Auret et al. (2014) that showed some OP-MG individuals have lower inducable DAF expression due to a functional regulatory variant in their *DAF* promoter, and the prediction of a Smad binding site in that vicinity by Wenzel et al. (2005), we proceeded to assess the effect of exogenous TGFβ1 on muscle DAF expression levels. A more relevant approach would have been to study the effect of TGFβ1 on human EOM muscle cells, however such EOM cell lines were not available. However, we did demonstrate a significant (p=0.008 and p=0.004 for 3 and 5 days respectively) increase in Daf protein expression in C2C12 mouse myotubes after TGFβ1 treatment (**Figure 3.2.2 & Figure**

3.2.3). This TGFβ1-induced upregulation of Daf in skeletal muscle is consistent with the reported upregulation of Daf in orbital fibroblasts in response to TGFβ1 (Cocuzzi et al. 2001). My results suggest that in OP-MG, fibroblasts and possibly EOM muscle cells, are likely to be more susceptible to complement-mediated damage and abnormal myofibrogenesis due to their lower TGFβ1 tissue levels and therefore secondary drive to adequately upregulate DAF. In light of these findings, and lower intrinsic DAF expression levels in EOMs, a possible mechanism was proposed for the pathogenesis of OP-MG in susceptible individuals – **Figure 4.1** (Nel et al. 2016).

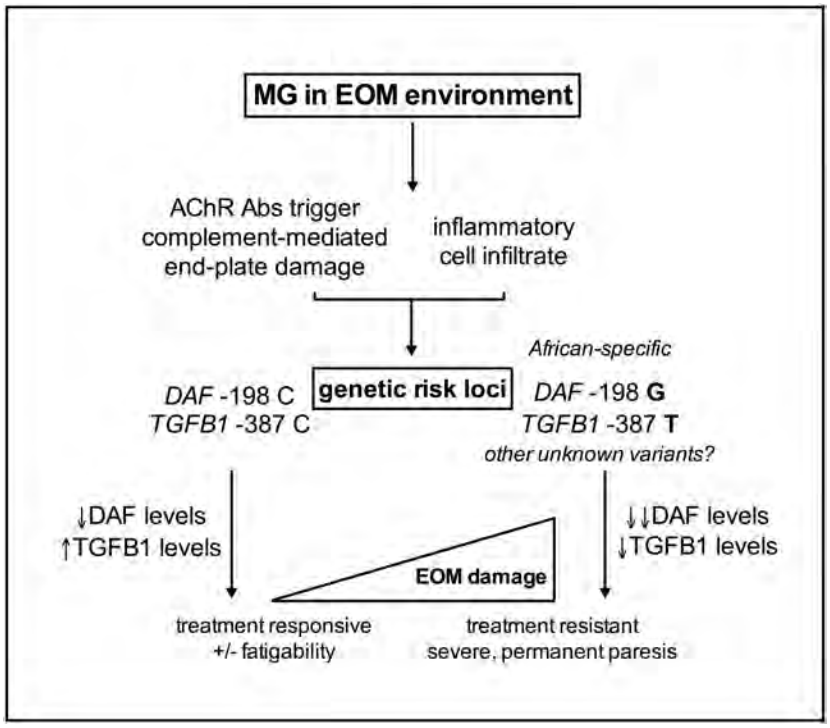

Figure 4.1 Proposed model for pathogenesis of disease in OP-MG. MG results in inflammatory cell infiltrates and antibody-activated complement-mediated endplate damage in the EOM environment. In susceptible individuals, with *DAF* and/or *TGFB1* risk haplotypes, this results in lower basal TGFβ1 activity and inadequate DAF upregulation, making the EOMs even more susceptible to complement-mediated damage. Severe and permanent EOM paresis ensues as a consequence of critically low EOM DAF expression levels, due either to MG-induced DAF repression (in genetically susceptible individuals) and/or repressed TGFβ1-Smad3 canonical signalling. (Nel at al. 2016)

Myofibroblasts in muscle most often arise via direct differentiation of a resident progenitor cell (satellite cell) or by means of partial myogenic differentiation of a fibroblast. TGFβ1 stimulation resulted in myofibroblast differentiation in almost 80% of cultured human fibroblasts via the canonical TGFβ1-Smad pathway (Lehmann et al. 2011). Eyden described the ultrastructure of the myofibroblast and emphasised the following defining features of this cell: a spindled cell morphology, an abundant matrix, immunostaining for ∝-smooth muscle, peripherally located smooth-muscle type myofilaments, rough endoplasmic reticulum, a Golgi apparatus producing collagen-secretion granules, and gap fibronexus junctions (Eyden 2005).

The patient-specific myofibroblasts derived from EOM tendon explant cell cultures from our OP-MG & non-MG control possessed the characteristics of myofibroblasts. The basal morphology of these cells remained largely unaltered after stimulation with TGFβ1, thereby indicating that the cells may have been myofibroblasts to begin with. In comparison to the OP-MG patient's EOM-derived myofibroblasts, the control myofibroblasts demonstrated more rapid growth consistently over a 14 day period (**Figure 3.2.3**), with a greater number of cells on day 4 and day 10 (day 4, p=0.011; day 10, p=0.013). These growth curves were performed to assist with the interpretation of the expression end-products, ∝-SMA and collagen, and represent basic cell count data (in duplicate), which is inappropriate for statistically meaningful comparison. In order to correctly analyse growth curve data, multiple independent cultures must be analysed over time, and data for each cell line at each time point should be plotted with error bars (Wang & Bushman 2006).

A consistent difference in ∝-SMA expression was observed between the OP-MG and non-MG control myofibroblasts irrespective of TGFβ1 treatment; considerably more staining for ∝-SMA was evident in the control myofibroblasts (**Figure 3.2.6**). In response to treating the cells with TGFβ1, there was only a modest increase in ∝-SMA staining in both OP-MG and control cells, with the control line possibly showing a slightly greater increase than the OP-MG cells (**Figure 3.2.6**). It was, however, not possible for us to reliably quantify our findings or to objectively measure differences in ∝-SMA expression between cell lines and experimental groups by means of simple visualisation alone. Ideally, we would have liked to perform imaging flow cytometry

for cells labelled with ∝-SMA as described by Lehmann et al. (2011) to better quantify the potential staining differential per cell, as the differences in cell growth/density between OP-MG and non-MG control cells may be confounding these results. Nevertheless, the reduced cell growth observed in OP-MG myofibroblasts coupled with the above observations of reduced responsiveness in the TGFβ1-Smad3 pathway, is intriguing and requires further investigation.

At the time of starting this project, iPS cell technology was new to our university and offered the possibility of 'disease-in-a-dish' modeling. The utility and advantages of such patient-specific, and therefore phenotype-specific models of disease are extensive and would result in more accurate models and unlimited patient-specific material for study. This is a particularly exciting and valuable prospect in OP-MG patients, where the tissue of interest, extraocular muscle, is inaccessible for biopsy and study.

We successfully reprogrammed a single patient's dermal fibroblasts to pluripotency over a period of approximately four months. These patient-specific iPS cell lines demonstrated growth and maintenance independent of reprogramming gene expression; ICC and qPCR of the MG822 iPS cell lines confirmed silencing of the reprogramming Sendai viral vector. The MG822-derived iPS cells were partially characterised by means of ICC and qPCR for markers of pluripotency and differentiation, allowing us to conclude that these iPS cells were not only completely reprogrammed to pluripotency, but also remained undifferentiated.

Although pioneering methods have demonstrated the reprogramming of adult somatic cells to iPS cells (Takahashi & Yamanaka 2006; Takahashi et al. 2007), there are still many challenges associated with this technique. While we successfully generated iPS cell clones from the dermal fibroblasts of one individual, we experienced low efficiency of fibroblast conversion to iPS cells as well as resistance to reprogramming or incomplete reprogramming in another cell line (MG7) that we attempted to reprogramme. The reprogramming rate of somatic cells into iPS cells was 0.01–0.1% in the original mouse study (Takahashi & Yamanaka 2006), and is reported to be higher with the use of the Sendai viral vector (up to 16.8% with the SeVdp used in this project – Nakanishi et al. 2012). The low efficiency rate may be

related to timing, absolute reprogramming gene expression levels, and possibly other genetic and/or epigenetic alterations in the original somatic cell.

Our iPS cells were in culture for approximately four months, during which time the maintenance and expansion of these cells required daily changes of specialised media and frequent passaging onto feeder layers or expensive substrates. The prolonged culture of these cells puts them at significant risk of contamination or infection despite antibiotic prophylaxis, especially since our tissue culture facility is a shared one. Due to the expense, the specialised knowledge and skill required, and the long duration of iPS cells in culture, we would recommend that iPS cell technology be undertaken in dedicated and highly-specialised facilities for this exclusive purpose.

The application of our MG822-derived iPS cells was limited by the aforementioned factors, as well as the lack of an appropriate and efficient differentiation protocol for muscle/EOM. As a result our group is exploring an alternative method of establishing a 'disease-in-a-dish' model that is more cost-effective and practically feasible than the iPS cell route. Another approach to achieve myogenic differentiation is the use of genetic modifications to directly activate myogenic signalling pathways. Forced expression of MyoD is known to transform fibroblasts into skeletal muscle cells (Tapscott et al. 1988; Cooper et al. 2007). There is significant potential for MyoD-forced differentiation of non-muscle cells for research of human muscle disease, a field severely constrained by the paucity of human tissue available for study. This method is highly efficient, with transduction efficiencies of > 70% and a six day differentiation protocol, and is therefore less expensive and labour-intensive. However, unlike iPS cells where the cells divide indefinitely providing an infinite supply of study material, here the supply of patient-specific fibroblasts is limited. There is also uncertainty as to whether such a model can or will replicate the specialised EOM allotype with its distinct morphology, muscle gene expression profile, and unique physiological and immunological microenvironment. A concern with disease models derived in this manner is whether a single cell type will be sufficient to manifest the full spectrum of pathogenesis, since interaction among

different cell types may be important to reconstruct the disease phenotypes faithfully (Colman & Dreesen 2009a; 2009b).

Table 4.1 The advantages and disadvantages of iPS cell technology (reprogramming of an adult somatic cell into an induced pluripotent stem cell by means of a reprogramming gene-loaded viral vector) versus transdifferentiation (MyoD forced myogenesis with transdifferentiation of fibroblasts into myoblasts).

Reprogramming somatic cells to iPS cells		**Transdifferentiation** (MyoD forced myogenesis)
• Patient-specific cells • Non-integrating viral vector • Infinite supply of cells • Regenerative potential	**Advantages**	• Patient-specific cells • Highly efficient (>70%) • Shorter culture periods (differentiation – 6 days) • Defined differentiation protocol
• Expensive • Low efficiency (≤16.8%) • Long-term cultures (4 months) • High contamination risk • No defined EOM differentiation protocol	**Disadvantages**	• Limited supply of cells • Potential viral vector integration

LIMITATIONS

There are several limitations of this work; firstly the descriptive clinical-pathological data represents a solitary MG case with treatment-resistant ophthalmoplegia, and while she does have the clinical OP-MG phenotype, she is caucasian with triple seronegative MG and therefore not a typical case. Unfortunately this OP-MG case was also an older patient (54 years of age), a factor that we cannot eliminate as a contributor to her pathology, particularly since somatic mitochondrial DNA point mutations and deletions accumulate in human EOMs with aging (Yu-Wai-Man et al. 2010). While we excluded mtDNA deletions in this patient's serum, we would suggest analysing any remaining OP-MG extraocular muscle tissue for mtDNA rearrangements in future.

In our resource-limited setting, it was not technically possible or feasible to perform multiple (17) contiguous fine (2mm) cuts of the EOMs on high-resolution orbital MRI as described by Ortube et al. (2006) in all MG or OP-MG cases. Also, the value of imaging in detecting EOM atrophy in MG remains uncertain, with very variable results reported in the literature to date.

Due to the small size of the excised EOM tissue sample and its processing, a limited number of histological investigations were possible on this tissue, and no histochemical or enzyme studies were performed for reasons elaborated upon in the methodology. Histochemical techniques are advantageous as they can reveal the biochemical properties of the specific muscle fibre types and their selective involvement in certain disease processes, expose structural changes in the muscle that may not be apparent with routine histological stains, and may demonstrate the absence of a particular enzyme or an excess of a particular substrate in certain disorders. Cytochrome oxidase (COX) deficiency in muscle fibres is an important biomarker of mitochondrial dysfunction, and would have been valuable in the assessment of the OP-MG EOM sample. We attempted to overcome one of these limitations by performing immunohistochemistry staining for fast and slow myosin on the archived wax-embedded sections from 2012, but the quality of our results was disappointing and the findings non-specific.

The histological and ultrastructural findings in this OP-MG case should be regarded as qualitative, and therefore do not allow for firm inferences or conclusions in light of the low number of observations we were able to make due to limited study material. Ideally one would like to have had a greater number and spectrum of patients and patient material (EOM) to compare, including AChR positive versus AChR negative MG patients, but as previously mentioned these cases seldom require surgery, which also explains the paucity of published scientific matter on this subject. Nonetheless we did make some meaningful observations (see below in concluding remarks).

We successfully generated and characterised iPS cells for one individual with MG over a peroid of approximately four months. However, the genomic integrity of these iPS cells has not yet been established, since two attempts at karyotype analysis

on these cells were unsuccessful. Karyotyping needs to be repeated for these MG822 HDF-derived iPS cells to exclude cytogenetic abnormalities which could restrict the use of the iPS cell clones for differentiation into useful *in vitro* disease models.

CONCLUDING REMARKS

In conclusion, EOM tissue from an OP-MG individual with AChR- and MuSK-antibody negative MG, demonstrated predominantly myopathic pathology and ultrastructural evidence of mitochondrial dysfunction. These EOM ultrastructural findings are novel, and appear to best correlate with MuSK-antibody associated MG, where non-ocular muscle demonstrated myopathic changes and frequent mitochondrial abnormalities with/without ragged red fibres.

In light of the repressed TGFβ1-induced phosphorylation of Smad3 in OP-MG fibroblasts, and the apparent lower basal ∝-SMA expression in OP-MG EOM-derived myofibroblasts, we propose that there is abnormal myofibrogenesis in the EOMs in OP-MG. The TGFβ1 pathway appears to be differentially regulated in OP-MG compared to control-MG cases and may impact DAF upregulation in the EOMs in MG patients, thereby making the EOMs even more susceptible to MG antibody-mediated complement damage.

Finally, our group is exploring an alternative method of establishing a 'disease-in-a-dish' model that is more cost-effective and practically feasible.

REFERENCES

Alshekhlee, A. et al., 2009. Incidence and mortality rates of myasthenia gravis and myasthenic crisis in US hospitals. *Neurology*, 72(18), pp.1548–1554.

Auret, J. et al., 2014. The effects of prednisone and steroid-sparing agents on decay accelerating factor (CD55) expression: Implications in myasthenia gravis. *Neuromuscular Disorders*, 24(6), pp.499–508.

Awaya, T. et al., 2012. Selective development of myogenic mesenchymal cells from human embryonic and induced pluripotent stem cells. *PLoS One*, 7(12), e51638.

Barberi, T. et al., 2007. Derivation of engraftable skeletal myoblasts from human embryonic stem cells. *Nature Medicine*, 13(5), pp.642-8.

Benton, G. et al., 2009. Advancing science and technology via 3D culture on basement membrane matrix. *Journal of Cellular Physiology,* 221(1), pp.18-25.

Blobe, G.C. et al., 2000. Role of transforming growth factor beta in human disease. *New England Journal of Medicine*, 342(18), pp.1350-8.

Brown, P.D. et al., 1990. Physiochemical activation of recombinant latent transforming growth factor-beta's 1,2, and 3. *Growth Factors*, 3(1), pp.35-43.

Burks, T.N. & Cohn, R.D., 2011. Role of TGF-β signaling in inherited and acquired myopathies. *Skeletal Muscle*, 1(1), pp.19.

Carlow, T.J. et al., 1998. MR of extraocular muscles in chronic progressive external ophthalmoplegia. *American Journal of Neuroradiology*, 19(1), pp.95–99.

Carr, A.S. et al., 2010. A systematic review of population based epidemiological studies in Myasthenia Gravis. *BMC Neurology*, 10, p.46.

Carroll, M.C., 2004. A protective role for innate immunity in systemic lupus erythematosus. *Nature Reviews Immunology*, 4, pp.825-831.

Cauvi, D.M. et al., 2006. Constitutive expression of murine decay-accelerating factor 1 is controlled by the transcription factor Sp1. *Journal of Immunology*, 177, pp.3837-3847.

Cenacchi, G. et al., 2011. Comparison of muscle ultrastructure in myasthenia gravis with anti-MuSK and anti-AChR antibodies. *Journal of Neurology*, 258(5), pp.746–752.

Chan, J.W. & Orrison, W.W., 2007. Ocular myasthenia: a rare presentation with MuSK antibody and bilateral extraocular muscle atrophy. *British Journal of Ophthalmology*, 91(6), pp.842-3.

Cocuzzi, E.T. et al., 2001. Upregulation of DAF (CD55) on orbital fibroblasts by cytokines. Differential effects of TNF-beta and TNF-alpha. *Current Eye Research*, 23, pp.86-92.

Colman, A. & Dreesen, O., 2009a. Pluripotent stem cells and disease modeling. *Cell Stem Cell*, 5(3), pp.244-7.

Colman, A. & Dreesen, O., 2009b. Induced pluripotent stem cells and the stability of the differentiated state. *EMBO Reports*, 10(7), pp.714-721.

Cooper, S.T. et al., 2007. Dystrophinopathy .carrier determination and detection of protein deficiencies in muscular dystrophy using lentiviral MyoD-forced myogenesis. *Neuromuscular Disorders*, 17, pp.276-284.

Dityatev, A. et al., 2010. Compartmentalization from the outside : the extracellular matrix and functional microdomains in the brain. *Trends in Neurosciences*, 33(11), pp.503–512.

Dubowitz, V. et al., 2013. Muscle Biopsy: A Practical Approach (4th Edition). Elsevier Health Sciences.

Eyden, B., 2005. THe myofibroblast: a study of normal, reactive and neoplastic tissues, with an emphasis on ultrastructure. *Journal of Submicroscopic Cytology and Pathology*, 37(3-4), pp.231-96.

Fischer, M.D. et al., 2005. Definition of the unique human extraocular muscle allotype by expression profiling. *Physiological genomics*, 22(3), pp.283–91.

Fresina, M. et al., 2014. Equatorial Loop Myopexy in "Sagging Eye" Syndrome: A Case Report. *Journal of Clinical and Experimental Ophthalmology*, 5:3.

Gasperi, C. et al., 2014. Anti-agrin autoantibodies in myasthenia gravis. *Neurology*, 82(June), pp.1976–1983.

Gratton, S.M. et al., 2014. Atrophy and Fibrosis of Extra-Ocular Muscles in Anti-Acetylcholine Receptor Antibody Myasthenia Gravis. *Open Journal of Ophthalmology*, 4, 117-119.

Guyon, T. et al., 1998. Regulation of Acetylcholine Receptor Gene Expression in Human Myasthenia Gravis Muscles. *Journal of Clinical Investigation*, 102(1), pp.249–263.

Heckmann, J.M. et al., 2010. A functional SNP in the regulatory region of the decay-accelerating factor gene associates with extraocular muscle pareses in myasthenia gravis. *Genes and Immunity*, 11(1), pp.1–10.

Heckmann, J.M. et al., 2011. A single-blinded trial of methotrexate versus azathioprine as steroid-sparing agents in generalized myasthenia gravis. *BMC Neurology*, 11(1), p.97.

Heckmann, J.M. et al., 2012. The characteristics of juvenile myasthenia gravis among South Africans. *South African Medical Journal*, 102(6), pp.532–6.

Heckmann, J.M., Owen, E.P. & Little, F., 2007. Myasthenia gravis in South Africans: racial differences in clinical manifestations. *Neuromuscular disorders*, 17(11-12), pp.929–34.

Hoh, H.B. et al., 1994. The STIR sequence MRI in the assessment of extraocular muscles in thyroid eye disease. *Eye*, 8(5), pp.506–510.

Huda, S., et al., 2016. Characteristics of AChR-antibody-negative myasthenia gravis in a South African cohort. *Muscle & Nerve*, accepted manuscript online 22 April 2016.

Hughes, C. et al., 2010. Matrigel: a complex protein mixture required for optimal growth of cell culture. *Proteomics* 10(9), 1886-90.

Hussein, S.M. et al., 2011. Copy number variation and selection during reprogramming to pluripotency. *Nature*, 471(7336), pp.58-62.

Jacob, S. et al., 2009. Myasthenia gravis and other neuromuscular junction disorders. *Practical Neurology*, 9(6), pp.364–371.

Kallestad, K.M. et al., 2011. Sparing of extraocular muscle in aging and muscular dystrophies: a myogenic precursor cell hypothesis. *Experimental Cell Research*, 317(6), pp.873–885.

Kaminski, H.J. et al., 2004. Complement regulators in extraocular muscle and experimental autoimmune myasthenia gravis. *Experimental Neurology*, 189(2), pp.333–342.

Kaminski, H.J. et al., 2003. Susceptibility of ocular tissues to autoimmune diseases. *Annals of the New York Academy of Sciences*. pp.362–374.

Kaminski, H.J. et al., 1995. The gamma-subunit of the acetylcholine receptor is not expressed in the levator palpebrae superioris. *Neurology*, 45(3 Pt 1), pp.516–518.

Kaminski, H.J., Kusner, L.L. & Block, C.H., 1996. Expression of acetylcholine receptor isoforms at extraocular muscle endplates. *Investigative Ophthalmology and Visual Science*, 37(2), pp.345–351.

Kang, J.S. & Krauss, R.S., 2010. Muscle stem cells in developmental and regenerative myogenesis. *Current Opinion in Clinical Nutrition & Metabolic Care*, 13(3), pp.243–248.

Kim, D.D. & Song, W.C., 2006. Membrane complement regulatory proteins. *Clinical Immunology*, 118(2-3), pp.127-36.

Kohl, J., 2006. Self, non-self, and danger: a complementary view. *Advances in Experimental Medicine and Biology*, 586, pp.71-94.

Kubiczkova, L., 2012. TGF-β - An excellent servant but a bad master. *Journal of Translational Medicine*, 10, pp.183.

Kusner, L.L. et al., 2010. Perimysial Fibroblasts of Extraocular Muscle, as Unique as the Muscle Fibers. *Investigative Ophthalmology & Visual Science*, 51(1), pp.192–200.

Lehmann, G.M. et al., 2008. Immune mechanisms in thyroid eye disease. *Thyroid : Official Journal of the American Thyroid Association*, 18(9), pp.959–965.

Lehmann, G.M. et al., 2011. The Aryl Hydrocarbon Receptor Ligand ITE Inhibits TGFβ1-Induced Human Myofibroblast Differentiation. *American Journal of Pathology*, 178, pp.1556-1567.

Liu, Y. et al, 2006. Effects of basic fibroblast growth factor microspheres on angiogenesis in ischemic myocardium and cardiac function: analysis with dobutamine cardiovascular magnetic resonance tagging. *European Journal of Cardiothoracic* Surgery, 30(1), pp.103-7.

Mahmood, A. et al, 2010. Enhanced differentiation of human embryonic stem cells to mesenchymal progenitors by inhibition of TGF-beta/activin/nodal signaling using SB-431542. *Journal of Bone and Mineral Research*, 25(6), pp.1216-33.

Martignago, S. et al., 2009. Muscle histopathology in myasthenia gravis with antibodies against MuSK and AChR. *Neuropathology and Applied Neurobiology*, 35(1), pp.103–110.

Mendias, C.L. et al., 2012. Transforming growth factor-beta induces skeletal muscle atrophy and fibrosis through induction of atrogin-1 and scleraxis. *Muscle & Nerve*, 45(1), pp.55-59.

Meuer, S.K. et al., 2012. BMP-7/TGF-β1 signalling in myoblasts: Components involved in signalling and BMP-7-dependent blockage of TGF-β1-mediated CTGF expression. *European Journal of Cell Biology*, 91, pp.450-463.

Mombaur, B. et al., 2015. Incidence of acetylcholine receptor-antibody-positive myasthenia gravis in South Africa. *Muscle & Nerve*, 51(4), pp.533–7.

Nakanishi, M. & Otsu, M., 2012. Development of Sendai virus vectors and their potential applications in gene therapy and regenerative medicine. *Current Gene Therapy*, 12(5), pp.410-6.

Nakano, S. & Engel, A.G., 1993. Myasthenia gravis: quantitative immunocytochemical analysis of inflammatory cells and detection of complement membrane attack complex at the end-plate in 30 patients. *Neurology*, 43(6),pp.1167-72.

Nel, M. et al., 2016. The African-387 C>T TGFB1 variant is functional and associates with the ophthalmoplegic complication in juvenile myasthenia gravis. *Journal of Human Genetics*, 61(4), pp.307-16.

Nishimura, K. et al., 2011. Development of Defective and Persistent Sendai Virus Vector. *Journal of Biological Chemistry*, 286(6), pp.4760–4771.

Okamoto, K. et al., 1996. Atrophy of bilateral extraocular muscles. CT and clinical features of seven patients. *Journal of Neuro-ophthalmology*, 16(4), pp.286-8.

Oosterhuis, H. & Bethlem, J., 1973. Neurogenic muscle involvement in myasthenia gravis A clinical and histopathological study. *Journal of Neurology, Neurosurgery, and Psychiatry*, 36(2), pp.244–254.

Ortube, M., Bhola, R. & Demer, J., 2006. Orbital Magnetic Resonance Imaging of Extraocular Muscles in Chronic Progressive External Ophthalmoplegia: Specific Diagnostic Findings. *Journal of American Association for Pediatric Ophthalmology and Strabismus*, 10(5), pp.414–418.

Pacheco-Pinedo, E.C. et al., 2009. Transcriptional and functional differences in stem cell populations isolated from extraocular and limb muscles. *Physiological Genomics*, 37(1), pp.35–42.

Padua, L. et al., 2006. Seronegative myasthenia gravis: Comparison of neurophysiological picture in MuSK+ and MuSK- patients. *European Journal of Neurology*, 13(3), pp.273–276.

Peter, J.G., Heckmann, J.M. & Novitzky, N., 2014. Recommendations for the use of immunoglobulin therapy for immunomodulation and antibody replacement. *South African Medical Journal*, 104(11), p.796.

Plath, K. & Lowry, WE., 2011. Progress in understanding reprogramming to the induced pluripotent state. *Nature Reviews Genetics*, 12(4), pp.253-265.

Porter, J.D. et al., 2006. Distinctive morphological and gene/protein expression signatures during myogenesis in novel cell lines from extraocular and hindlimb muscle. *Physiological Genomics*, 24(3), pp.264–275.

Porter, J.D. et al., 2001. Extraocular muscle is defined by a fundamentally distinct gene expression profile. *Proceedings of the National Academy of Sciences of the United States of America*, 98(21), pp.12062–12067.

Porter, J.D. & Baker, R.S., 1996. Muscles of a different ' color ': The unusual porperties of the extraocular muscles may predispose or protect them in neurogenic and myogenic disease. *Neurology*, 46, pp.30–37.

Prince, S. et al., 2003. Stimulation of Melanogenesis by Tetradecanoylphorbol 13-acetate (TPA) in Mouse Melanocytes and Neural Crest Cells. *Pigment Cell Research*, 16(1), pp.26–34.

Rostedt Punga, A. et al., 2006. Neurophysiological and mitochondrial abnormalities in MuSK antibody seropositive myasthenia gravis compared to other immunological subtypes. *Clinical Neurophysiology : Official Journal of the International Federation of Clinical Neurophysiology*, 117(7), pp.1434–43.

Rostedt Punga, A., 2011. Myasthenia Gravis: New Insights into the Effect of MuSK Antibodies and Acetylcholinesterase Inhibitors, Autoimmune Disorders - Current Concepts and Advances from Bedside to Mechanistic Insights, Dr. Fang-Ping Huang (Ed.), InTech, DOI: 10.5772/20425.

Rutar, T. & Demer, J.L., 2009. "Heavy Eye" Syndrome in the Absence of High Myopia: A Connective Tissue Degeneration in Elderly Strabismic Patients. *Journal of American Association for Pediatric Ophthalmology and Strabismus,* 13(1), pp.36–44.

Sahashi, K. et al., 1980. Ultrastructural localization of the terminal and lytic ninth complement component (C9) at the motor end-plate in myasthenia gravis. *Journal of Neuropathology and Experimental Neurology*, 39(2), pp.160-172.

Sanders, D.B. et al., 2003. Clinical aspects of MuSK antibody positive seronegative MG. *Neurology*, 60(12), pp.1978–1980.

Shah, R. et al., 2006. Allelic diversity in the TGFB1 regulatory region: characterization of novel functional single nucleotide polymorphisms. *Human Genetics,* 119, pp.61–74.

Shah, A.K., Goldenberg, W.D. & Lorenzo, N., 2015. Myasthenia Gravis Workup: Histologic Findings. *Medscape*, p.Histologic Findings. Available at: http://emedicine.medscape.com/article/1171206-workup#c12.

Silvestri, N.J. & Wolfe, G.I., 2012. Myasthenia gravis. *Seminars in Neurology*, 32(3), pp.215–26.

Soltys, J. et al., 2008. Extraocular muscle susceptibility to myasthenia gravis: unique immunological environment? *Annals Of The New York Academy Of Sciences*, 1132, pp.220–224.

Soltys, J. et al., 2009. Novel complement inhibitor limits severity of experimentally myasthenia gravis. *Annals of Neurology*, 65(1), pp.67–75.

Stadtfeld, M. & Hochedlinger, K., 2010. Induced pluripotency: history , mechanisms , and applications. *Genes & Development*, pp.2239–2263.

Taapken, S.M. et al., 2011. Karyotypic abnormalities in human induced pluripotent stem cells and embryonic stem cells. *Nature Biotechnology*, 29(4), pp.313-314.

Takahashi, K. & Yamanaka, S., 2006. Induction of Pluripotent Stem Cells from Mouse Embryonic and Adult Fibroblast Cultures by Defined Factors. *Cell*, 126(4), pp.663–676.

Takahashi, K. et al., 2007. Induction of pluripotent stem cells from adult human fibroblasts by defined factors. *Cell*, 131(5), pp.861-72.

Tapscott, S.J. et al., 1988. MyoD1: a nuclear phosphoprotein requiring a Myc homology region to convert fibroblasts to myoblasts. *Science*, 242(4877), pp.405-11.

Thomas, D.J. & Lublin, D.M., 1993. Identification of 5'-flanking regions affecting the expression of the human decay accelerating factor gene and their role in tissue-specific expression. *Journal of Immunology,* 150(1), pp.151-60.

Tüzün, E., Huda, R. & Christadoss, P., 2011. Complement and cytokine based therapeutic strategies in myasthenia gravis. *Journal of Autoimmunity*, 37(2), pp.136–43.

Valamehr, B. et al., 2011. Developing defined culture systems for human pluripotent stem cells. *Regenerative Medicine*, 6(5), pp.623-634.

Vaphiades, M., Bhatti, M. & Lesser, R., 2012. Ocular myasthenia gravis. *Current Opinion in Ophthalmology*, 23, pp.537–542.

Villa-Diaz, L.G. et al., 2013. Concise review: The evolution of human pluripotent stem cell culture: From feeder cells to synthetic coatings. *Stem Cells*, 31(1), pp.1-7.

Vincent, A. & Drachman, D.B., 2002. Myasthenia gravis. *Advances in Neurology*, 88, pp.159–188.

Walport, M.J., 2001. Complement. First of two parts. *New England Journal of Medicine*, 344(14), pp.1058-66. Complement. Second of two parts. *New England Journal of Medicine*, 344(15), pp.1140-4.

Wang, G.P. & Bushman, F.D., 2006. A statistical method for comparing viral growth curves. *Journal of Virological Methods*, 135, pp.118–123.

Watanabe, K. et al., 2007. A ROCK inhibitor permits survival of dissociated human embryonic stem cells. *Nature Biotechnology*, 25(6),pp.681-6.

Wenzel, K. et al., 2005. Increased susceptibility to complement attack due to down-regulation of Decay-Accelerating Factor/CD55 in Dysferlin-deficient muscular dystrophy. *Journal of Immunology*, 175, pp.6219-6225.

Yu Wai Man, C.Y., Chinnery, P.F. & Griffiths, P.G., 2005. Extraocular muscles have fundamentally distinct properties that make them selectively vulnerable to certain disorders. *Neuromuscular Disorders*, 15(1), pp.17–23.

Yu-Wai-Man, P. et al., 2010. Somatic Mitochondrial DNA Deletions Accumulate to High Levels in Aging Human Extraocular Muscles. *Investigative Ophthalmology and Visual Science*, 51(7), pp.3347-3353.

Zacharias, AL. et al, 2011. *Pitx2* is an upstream activator of extraocular myogenesis and survival. *Developmental Biology*, 349(2), pp.395-405.

Zhang, B. et al., 2014. Autoantibodies to agrin in myasthenia gravis patients. *PLoS ONE*, 9(3), pp.4–9.

Zhou, Y. et al., 2014. RNA expression analysis of passive transfer myasthenia supports extraocular muscle as a unique immunological environment. *Investigative Ophthalmology and Visual Science*, 55(7), pp.4348–4359.

Zouvelou, V. et al., 2013. Double seronegative myasthenia gravis with anti-LRP 4 antibodies. *Neuromuscular Disorders*, 23(7), pp.568–570.

Zuk, P.A., 2009. The Intracellular Distribution of the ES Cell Totipotent Markers OCT4 and Sox2 in Adult Stem Cells Differs Dramatically According to Commercial Antibody Used. *Journal of Cellular Biochemistry*, 106(5), pp.867-877.

APPENDICES

A.1 HEALTH RESEARCH ETHICS COMMITTEE DOCUMENTS & CONSENT FORMS

UNIVERSITY OF CAPE TOWN

Faculty of Health Sciences
Faculty of Health Sciences Human Research Ethics Committee
Room E52-24 Groote Schuur Hospital Old Main Building
Observatory 7925
Telephone [021] 406 6338 • Facsimile [021] 406 6411
e-mail: sumayah.ariefdien@uct.ac.za
www.health.uct.ac.za/research/humanethics/forms

21 February 2013

HREC REF: 121/2013

Dr M Nel & Dr R Raytenbach
c/o Prof J Heckmann
Neurology
E-8/74
NGSH

Dear Drs Nel & Rautenbach

PROJECT TITLE: LINKED TO 257/2012: INVESTIGATING THE ROLE OF TGF-B IN THE DEVELOPMENT OF SEVERE OCULAR MUSCLE FIBROSIS AS A COMLICATION IN MYASTHESIA GRAVIS

Thank you for submitting your sub-study to the Faculty of Health Sciences Human Research Ethics Committee for review.

It is a pleasure to inform you that the HREC has **formally approved** the above mentioned sub- study.

Approval is granted for one year till the 28 February 2014.

Please submit a progress form, using the standardised Annual Report Form, if the study continues beyond the approval period. Please submit a Standard Closure form if the study is completed within the approval period.

Please note that the ongoing ethical conduct of the study remains the responsibility of the principal investigator.

Please quote the REC. REF in all your correspondence.

Yours sincerely

PROFESSOR M BLOCKMAN
CHAIRPERSON, HSF HUMAN ETHICS

Federal Wide Assurance Number: FWA00001637.
Institutional Review Board (IRB) number: IRB00001938

sAriefdien

UNIVERSITY OF CAPE TOWN
Faculty of Health Sciences
Human Research Ethics Committee

Room E52-24 Old Main Building
Groote Schuur Hospital
Observatory 7925
Telephone [021] 406 6338 • **Facsimile** [021] 406 6411
Email: shuretta.thomas@uct.ac.za
Website: www.health.uct.ac.za/research/humanethics/forms

24 October 2013

Prof J Heckmann
Neurology
E8-74
NGSH

Dear Prof Heckmann

Re: HREC Ref 320/2009, 257/2012, 121/2013

"Identifying the molecular basis for treatment resistance in a subset of Myasthenia Gravis patients of African ancestry"

Thank you for your letter to the Faculty of Health Sciences Human Research Ethics Committee dated 22 October 2013.

The HREC has **noted and approved** the following documentation on the above mentioned study:

- UCT Surgical Control Skin Biopsy Informed Consent Form version 3 dated 22 October 2013 (clean copy & track changes)
- Advertisement: Volunteers wanted for Myasthenia Gravis Research
- UCT OP-MG/MG Control Skin Biopsy Informed Consent Form dated 08 October 2013
- UCT Healthy Control Skin Biopsy Informed Consent Form dated 08 October 2013

Please note that the ongoing ethical conduct of the study remains the responsibility of the principal investigator.

Please quote the HREC REF in all your correspondence.

Yours sincerely

PROFESSOR M BLOCKMAN
CHAIRPERSON, FHS HUMAN ETHICS

Investigating the role of TGF-B in the development of severe ocular muscle fibrosis as a complication in Myasthenia Gravis.

REC REF 257/2012

Prof J Heckmann, Dr Melissa Nel, Dr Robyn Rautenbach and the Neuroscience group collaborators.

Division of Neurology, Department of Medicine, University of Cape Town.

Summary for patients:

The overall aim of the study is to investigate the susceptibility of certain individuals with myasthenia gravis (MG) to develop ***severe*** eye muscle involvement. You may be one of the individuals who have severe ophthalmoplegic MG with severe eye involvement or you may be approached because you do not have MG, but will be undergoing corrective squint surgery by Prof. Murray's eye team. Here is an explanation of why we want to study the TGF-B gene and the importance of this project.

Myasthenia Gravis is a disease where a subset of an individual's immune cells, for reasons yet unknown, starts attacking the muscles. This results in fatigable weakness of the muscles. Typically MG affects the eye muscles early on in the disease process, but in Africa we find a group of patients who develop long-lasting and severe eye muscle involvement in MG that does not appear to respond to the standard MG therapies. The aim of the project is to understand why these eye muscles a) develop the problem and b) how we can respond and treat the problem.

We know that in MG the complement system is involved in damaging the muscle cells. Complement is activated by either infections or antibodies. In MG, a subset of antibodies actually causes the illness and therefore complement proteins are activated resulting in muscle damage. The TGF-B protein is a chemical that is important in starting the healing process in muscles after damage, BUT interestingly, it can very easily switch to form scar tissue instead of normal muscle tissue. We are wondering whether this is what happens in the eye muscles of some of our MG patients- the MG/complement damages the eye muscle but instead of normal healing the muscles develop scar tissue and never really return to normal working order. Other scientific work by our group suggests that certain individuals, who happen to have inherited a slightly different genetic code in their TFG-B gene, may be producing higher levels of TGF-B under certain conditions. This may have been an advantage in certain circumstances, but we are supposing that if you have MG and this altered code, you may have a higher risk of developing eye muscle problems. We wish to understand this so that ultimately we may alter the course of events. Also, it may improve our general understanding of MG as well.

In order to study these events in the laboratory we have asked MG patients who undergo corrective surgery for severe eye squint to donate eye muscle which may be cut and "discarded in to waste". If there are no muscles that are discarded then we will not have any tissue donated to the project. If you are someone who has been booked for squint corrective procedure but the eye muscle is otherwise normal, we

would appreciate such a donation to be used as a “normal control eye muscle”-if available. Again, we understand that you may say yes to a donation of excess material but the surgeon may not cut excess material and therefore we may not receive any excess eye muscle.

Once we have the eye muscle we wish to do several things; 1) use some for histological examination under a microscope 2) to grow cells from the discarded muscles in a dish. There are 2 types of cells that we anticipate growing a) eye socket/orbital fibroblasts and b) eye muscle (if we are lucky). These cells from the eye muscle are very different to ordinary skeletal muscle and we wish to study how these cells respond to the MG therapies. Also, we will study the differences in TGF-B production between these cells obtained from our MG patients and those obtained from “normal controls”.

It is important to realize that you have been asked to participate in this study to help in the understanding of this process. You may not have the eye problem and may never develop it, but your participation will still be hugely beneficial in the understanding of this problem. If you do agree to potentially donate excess eye muscle/tendon if it becomes available during your surgery, you will be asked to sign this consent form. Consent for this procedure is voluntary and you may refuse. If you refuse this will not affect your standing or care in the MG clinic or by Prof Murray’s team.

Signature

Signing below indicates that you have been informed about the research study in which you voluntarily agree to participate.

I also give permission for my “excess” eye muscle sample to be used for research purposes, subject to the approval of the University of Cape Town Research Ethics Committee, provided that any information from such research will remain confidential.

_____Date_____ _____

Signature of Participant Printed Name of Participant

_____ Date_____ _____

Signature of Investigator obtaining consent Printed Name of Person obtaining consent

Neuroscience research group

Division of Neurology

Department of Medicine

University of Cape Town

Research ethics committee REC/REF 257/2012

Consent for donating removed extra-ocular muscle for research

Prof. Heckmann and her collaborators are involved in a research project in which they are investigating the susceptibility of certain individuals with myasthenia gravis (MG) to develop ***severe treatment-resistant*** external ocular muscle paralysis – see TGFβ1 study patient information sheet.

Prof. Heckmann has requested that I donate any extra-ocular muscle which ***may*** be cut and discarded during a corrective oculoplastic procedure that Prof. A. Murray will be performing at Groote Schuur Hospital on _____, 2013.

I understand that the decision to cut any ***"excess"*** muscle will only be made at the time of the surgery by the surgeon (Prof. Murray); if no muscle needs to be removed then there will be no donation to Prof. Heckmann and the research laboratory.

I hereby voluntary consent for this donation and understand that the result of the muscle histology or protein expression studies that will be performed on my muscle may not necessarily result in any direct benefit to the management of my condition (either Myasthenia Gravis or squint corrective surgery) and will not affect my future medical management and that there will be no costs involved nor any financial reward.

Ms/Mr ……. …… Date…….

Witness: ……Date …….

Consent taken by : Dr ……Date…….

Signature of Dr. ……

Information and Consent Document for MG Participants:

Study Title: INVESTIGATING THE MOLECULAR BASIS OF TREATMENT RESISTANT OPHTHALMOPLEGIA IN A SUBSET OF MYASTHENIA GRAVIS PATIENTS OF AFRICAN ANCESTRY.

Project Leader: Prof. Jeannine Heckmann

Investigators: Dr Melissa Nel, Dr Robyn Rautenbach, Dr Robea Ballo, Prof. Sharon Prince

Neurology Research Group, Division of Neurology, Department of Medicine, Groote Schuur Hospital and University of Cape Town.

Summary:

Myasthenia gravis (MG) is a neuromuscular auto-immune disease. This means that, for unknown reasons, the body's immune system attacks an MG individual's own muscle fibres. This process causes inflammation and muscle damage; it interferes with the muscle's ability to receive nerve impulses which normally instruct the muscle to contract. The result is muscle weakness. Most patients do well on chronic medication to control the disease and a proportion of patients go into remission (not requiring treatment) after a variable period.

The exception is a group of African individuals with MG who develop **severe** eye muscle weakness which does not respond to our treatment. Many have drooping eyelids and are not able to move their eyes which significantly impairs their vision. We refer to these individuals as having ophthalmoplegic MG or **OP-MG**.

We have been studying this problem for several years because we want to find out why it develops. We observe OP-MG frequently in South Africa because a large proportion of MG patients are of African genetic ancestry (Black or Mixed-Ancestry). Since OP-MG occurs almost exclusively in these racial groups we believe that there must be certain differences in their genes which make them vulnerable to the damage that occurs in MG.

Genes are found inside all the cells of the body and hold all the instructions necessary for our organs and systems to function. Genes contain a coding sequence

which is read by specialized machinery in the cell. This allows the many different messages on our genes to be interpreted by the cell to make different proteins. These proteins are the building blocks of the body. There are also special signals which the cell uses to decide which genes are read and which proteins are made. These “switches” can turn a gene on and off depending on the needs of the body.

Our genes are unique and give us the individual characteristics that make us different from one another. Genes are inherited from each parent (half from the mother and half from the father). In this way, our genes will therefore be similar in some ways to those of our parents. Similarly, the genes of African individuals may be similar since these individuals share common African ancestors. It is possible that through many sets of African parents and offspring, certain genes have been passed on through the generations.

It is these unique “African genes” that we are interested in because we think that this may explain why the eye muscles of some African patients with MG react differently to those with European (White) ancestors. The “African genes” may have slightly different coding sequences. When the cell reads these messages it could affect which proteins it makes, when these proteins are made and how much of them are made.

When MG affects the body it causes a shock to the muscle system, especially the eye muscles. The body releases chemical signals which can trigger repair genes to “turn on” so that the body can heal itself. The MG medication that we prescribe assists this process so that most patients with MG can have a good outcome.

We think that OP-MG develops when African individuals have certain differences in their muscle repair genes. When MG strikes the eye muscles the chemical signals do not result in healing. Certain of their eye muscles genes may carry mistakes in the coding sequence (message) so that when they are “switched on” they make proteins which do not work properly.

The overall aim of this study is to investigate the reason why certain African individuals with myasthenia gravis (MG) develop ***OP-MG*** which does not respond to our treatment. We hope that if we can really understand what is causing this complication we may have a chance of developing treatments for OP-MG patients.

In order to study OP-MG we will need to perform experiments in the laboratory. OP-MG affects the eye muscles, but we cannot get eye muscle tissue to study. As an

alternative, we want to use a small piece of skin, measuring 3mm x 3mm, to grow skin cells in a dish in the laboratory. These skin cells are called fibroblasts. From this small piece of skin we can grow many, many fibroblasts which we can freeze and store for later use. This means that we only need to perform the skin biopsy once.

Once we have the fibroblasts, we will deliver special signals inside these cells which can turn on “muscle genes”. Once these “muscle genes” are switched on the fibroblast will be tricked into becoming a muscle cell. This means that we can grow muscle tissue in the lab without actually taking a piece of muscle from an individual.

We want to take skin biopsies from African MG patients so that we can grow fibroblasts and turn these into muscle cells. The fibroblasts need to come from some patients that have OP-MG and some that don’t so that we can compare them and see what the differences are. The MG patients that don’t have OP-MG are called the “controls”. You may be approached to donate a skin biopsy for this study because you are an African MG patient who may or may not have OP-MG.

Once we have made muscle cells from OP-MG and control fibroblasts, we will break them up and remove all their genes. We will send the genes to a laboratory abroad. There they will use a very specialized computer to read and check the coding sequence on all the genes and see which proteins they can make. This technique is called RNAseq. Once we have this information we will be able to see whether the message on OP-MG muscle genes is different to control muscle genes.

It is important to remember that participation in this research is voluntary; this means that you may decline to donate a skin biopsy. If you are approached and you feel uncomfortable undergoing this minor “procedure” after reading this document, you may refuse. Your decision to participate will have no influence on your routine medical care in the MG clinic.

If you choose to participate in our study, the fibroblasts that we grow from your skin biopsy will only be used for this project. If we ever want to use them for a different project, we would have to obtain permission from the UCT research ethics committee. Once your skin biopsy is taken to the lab it will be assigned a unique code. All cells that we grow from this biopsy and any other material we generate in the lab will bear this same code and not your name or other personal details. In this way your confidentiality will be maintained.

Though MG affects you personally, it is important for you to realize that you are unlikely to derive any personal benefit from participation in this study. However, using your cells in experiments may help us to understand OP-MG better and thereby help us to think about which treatment may change the course of this complication for others. You will not receive any personalized feedback or any other results from this study although, if you wish, we can send you a summary of our findings when we have completed the study. Please indicate how we can contact you if this is the case.

With this consent form we are asking you to consider giving us a skin biopsy. This circular piece of skin measuring 3mm x 3mm will be obtained from the skin site over your shoulder area. Dr Melissa Nel (Departments of Medicine and Human Biology) will be performing the procedure (detailed below):

The skin biopsy will be performed in a private consulting room in E7 (Department of Neurology) at Groote Schuur Hospital (GSH). While you are lying on your stomach, a small area over your shoulder area will be anaesthetized using an injection of local anaesthetic. Once the area is numb, a circular piece of skin measuring 3mm x 3mm (see image below) will be removed using a special punch biopsy needle.

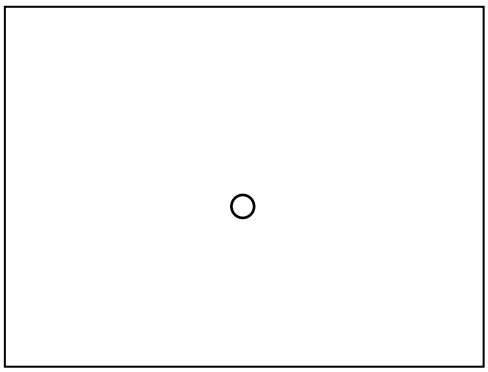

Size of skin punch biopsy (to scale)

You will only require a plaster to cover the area and no stitches. You will be advised to keep the biopsy site clean and dry and to remove the plaster after 24 hours.

You should feel only minor discomfort during this procedure. All individuals heal differently so it is not possible to predict what the biopsy site will look like once it has healed. For most individuals, no scar will be noticeable. Complications are uncommon following this simple procedure but can occur with any surgical procedure. Some of the complications associated with skin punch biopsy include local bleeding and bruising, pain, infection and allergic reaction to the local anaesthetic used in the procedure.

This consent form asks for:

1) a skin biopsy to grow fibroblasts

2) permission to convert these fibroblasts into muscle cells

3) permission to perform RNAseq on the muscle cell genes by reading their coding sequence (the messages for making proteins)

What if Something Goes Wrong?

The University of Cape Town (UCT) undertakes that in the event of you suffering any significant deterioration in health or well-being, or from any unexpected sensitivity or toxicity, that is caused by your participation in the study, it will provide immediate medical care. UCT has appropriate insurance cover to provide prompt payment of compensation for any trial-related injury according to the guidelines outlined by the Association of the British Pharmaceutical Industry, ABPI 1991. Broadly-speaking, the ABPI guidelines recommend that the insured company (UCT), without legal commitment, should compensate you without you having to prove that UCT is at fault. An injury is considered trial-related if, and to the extent that, it is caused by study activities. You must notify the study doctor immediately of any side effects and/or injuries during the trial, whether they are research-related or other related complications.

UCT reserves the right not to provide compensation if, and to the extent that, your injury came about because you chose not to follow the instructions that you were given while you were taking part in the study. Your right in law to claim ompensation for injury where you prove negligence is not affected. Copies of these guidelines are available on request.

If you do agree to participate in this research you will be asked to sign the consent form. If you are willing to give a sample so that we can establish a control line for this study and you are willing for us to re-use the cells for other MG studies once authorized by the UCT research ethic committee, you may indicate that option on the form. Consent for this procedure is voluntary and you may refuse. If you refuse this will not affect your standing at UCT. You will be given a copy of this signed form for your own records.

To contact Prof Heckmann, the local principal investigator, phone 021-404 3198 or -3263. If you have questions about your rights and welfare in the study you can contact Prof Blockman, the chairman of UCT, Faculty of Health Sciences Human Research Ethics Committee at 021 406 6411.

Signature

Signing below indicates that you have been informed about our research in which you voluntarily agree to participate and provide a skin biopsy for this MG research study.

Yes ☐

I understand that I will be participating in the study in the following capacity:

OP-MG Case ☐ MG Control (no OP-MG) ☐

I also give permission for my cells (fibroblasts or muscle cells) to be used for Myasthenia Gravis research purposes, subject to the approval of the University of Cape Town Research Ethics Committee, provided that any information from such research will remain confidential.

☐ Yes

_____Date_____ _____

Signature of Participant Printed Name of Participant

_____ Date_____ _____

Signature of PI Obtaining Consent Printed Name of Person

A.2 SUPPLEMENTARY DATA – CASES & CONTROLS

	Clinical phenotype	Sample type	Use(s) in project
MG86	OP-MG (complete) Juvenile-onset AChR+	Skin (fibroblasts)	Clinical data Western blot
MG64	OP-MG (complete) Juvenile-onset AChR+	EOM (myofibroblasts)	Clinical data EOM myofibroblast IF/ICC
MG82	OP-MG (complete) Adult-onset AChR-/MuSK-/LRP4-	EOM	Clinical data EOM histopathology & EM
MG189	No MG	EOM (myofibroblasts)	EOM myofibroblast IF/ICC
C8	No MG	EOM	Clinical data EOM histopathology & EM
C9	No MG	EOM	Clinical data EOM histopathology
MG7	OP-MG (partial) Adult-onset AChR+	Skin (fibroblasts)	Western blot Pluripotent stem cells
MG822	MG - no OP Juvenile-onset AChR+	Skin (fibroblasts)	Western blot Pluripotent stem cells
MG182	MG – no OP Adult-onset AChR+	Skin (fibroblasts)	Western blot
MG188	OP-MG (complete) Juvenile-onset AChR+	Skin (fibroblasts)	Western blot
MG70	OP-MG (complete) Juvenile-onset AChR+	Skin (fibroblasts)	Western blot

A.3 HISTOPATHOLOGY & ULTRASTRUCTURAL ANALYSIS

EOM tissue sample cryoprotection & freezing

- EOM collected in ice cold saline on ice (theatre)
- Soak in 4% PFA/PBS x 2 hrs
- 1x PBS washes – 10 minutes x3
- Soak in 30% sucrose/PBS x >6 hrs/overnight (until tissue floats)
- Tissue pinned to cork & 'flash' frozen in iso-pentane cooled in liquid nitrogen
- Transferred to -80°C

Scott's tap water substitute

3.5g $NaHCO_3$
20g $MgSO_4$
1 litre dH_2O
Mix salts separately
Add 1% formalin (to prevent growth of mould)

Gadsdon's Haematoxylin

5.5g Haematoxylin
100ml Absolute alcohol (100% Ethanol)
60g Saturated aqueous potassium alum [$KAI(SO_4)_2$]
20ml Glacial acetic acid
0.5g $NaIO_3$
300ml Glycerol
Dissolve the haematoxylin in 100ml of absolute alcohol
Make the saturated potassium alum solution
Dissolve 0.5g sodium iodate in 10ml of dH_2O
Mix the haematoxylin and potassium alum solutions together
Add the diluted sodium iodate to this mixture
Add 20ml of acetic acid and leave at RT for 1 hour
Add 300ml glycerol
Mix well and filter through 0.22 µM filter
Store in dark cupboard
Staining time = 5 minutes, with differentiation in 1% acid alcohol

Eosin/Phloxine solution

Stock solution (frozen sections & cytology)
1% Aqueous Eosin Y
1% Aqueous Phloxine B
Mix 2 parts of Eosin to 1 part Phloxine
Store in dark cupboard
Working solution
Mix equal quantities of the stock solution and tap water and allow to stand for ≥48 hours before use.
Store in labeled bottle.
Discard and replace (from stock solution) after 2 months

Control (C8) EOM histopathology – H&E stain

H&E stained longitudinal (not transverse) section of the control EOM (C8) displayed artefactually separated muscle fibres with no associated collagen and adipose deposition, this finding was therefore attributed to the mechanical separation of fibres during the cutting of these sections. [100x magnification]

Modified Gomori trichrome stain

0.6g Chromotrope 2R
0.3g Fast green FCF
0.6g Phosphotungstic acid
1ml Glacial acetic acid
100ml dH_2O
Adjust the pH to 3.4 with 1M NaOH.
Prepare new stain every week or when pale.

Oil red O stain

Stock solution
Saturated solution of Oil Red O in iso-propyl alcohol (±2.7g per litre)
Working solution
30ml of stock solution and 20ml of dH_2O
Filter through a 0.22µM filter and use immediately.

Immunohistochemistry – slow & fast myosin
Slow and fast myosin antibodies (Novocastra, UK, Dilution 1:40)

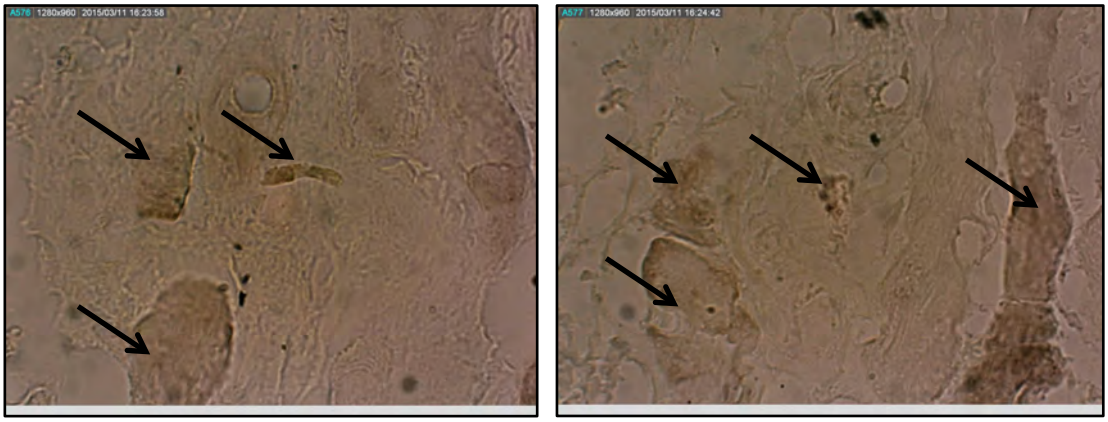

Immunohistochemistry for fast (type II) and slow (type I) myosin (antigen-retrieval) on archived (2012) wax-embedded formalin-fixed EOM sections of OP-MG case. Slow (type I) myosin did not stain at all, while fast (type II) myosin only stained focally with an apparent mixture of stained fast/type II fibres (arrows) and unstained slow/type I fibres. [100x magnification]

Glutaraldehyde in Sodium cacodylate buffer (tissue fixative for EM specimens)
For 500ml of 3% Glutaraldehyde in 0.2M Cacodylate buffer:
25% Glutaraldehyde (60ml/120ml)
0,2M Sodium cacodylate buffer up to 250ml/500ml
Add dH_2O up to 500ml/1000ml
Divide into aliquots of 4ml and store at 4°C.
Sodium cacodylate buffer:
Solution A
8.56g Sodium cacodylate [$Na(CH_3)_2AsO_23H_2O$]
20ml dH_2O
Solution B (0.2M HCl)
10ml Concentrated HCl
603ml dH_2O
0.2M Working solution pH7.2 (per 200ml)
50ml Solution A
4.2ml Solution B
Make up to 200ml with dH_2O

Saturated uranyl acetate in sterile water
6.25 g uranyl acetate
100 ml dH_2O

Spurr resin (Spurr resin Premix Kit, TAAB, UK)
Resin stored in fridge at 4°C.
Add premix resin to the premix hardener.

Mix by inverting the bottle – take care not to introduce bubbles.
Break acceleration vial, remove fluid with a pipette and add to resin/hardener mixture. Mix as before.

Toluidine Blue stain
Borax Tetra (sodium tetraborate)
Toluidine Blue O
dH_2O
Combine the following ingredients (in order) in a 150ml beaker

- 1g sodium tetraborate
- 100ml dH_2O
- 0.5-0.7g Toluidine Blue

Filter through a 0.22µM filter
Store at RT

Lead citrate
2,66g lead nitrate
3,52g trisodium citrate
60ml dH_2O
Add lead nitrate and trisodium citrate to the dH_2O
Place on a mixer for several hours
Add 16ml 10N NaOH (4g/100ml dH_2O) – solution should clear
Make up to 100ml with dH_2O
Filter and allow to stand overnight
Just before use, centrifuge at 3000rpm for 5 minutes to remove any precipitate

Template for viewing & analysis – histology

* Modified – small EOM sample & archived wax-embedded formalin-fixed sections reviewed

MUSCLE HISTOLOGY

Morphology
Variation in myofibre size:
Atrophic fibres:
Variation in myofibre shape:
Increase in internal nuclei:
Necrotising fibres:
Regenerative fibres:
Increased endomysial connective tissue:
Inflammatory infiltrate

Special stains
Modified Gomori:
PAS:
Oil red O:

Histochemistry:
NADH:
SDH:
COX:

Immunohistochemistry:
Dystrophins (N, C, R):
Sarcoglycans (a, b, g):
Caveolin:
Dysferlin:
Emerin:
MHC Class 1:
Slow and fast myosin:

A.4 GENERAL CELL CULTURE

Dulbucco's Modified Eagle's Medium
13.55g DMEM
3.7g $NaHCO_3$
Make up to 1 litre with autoclaved ddH_2O
pH to 7.2
Filter through a 0.22µM filter
Store at 4°C
Medium older than 3 weeks was re-supplemented with L-glutamine because of its instability

Differentiation medium for C2C12 mouse myoblasts
48.5ml DMEM
1ml Horse serum
500µl P/S
Start with differentiation medium the day after plating cells
Change medium every 2-3 days during differentiation
Differentiate for 6 days before drug treatments

Penicillin/Streptomycin (P/S)
900mg penicillin
1500mg streptomycin
Make up to 150ml in sterile 1x PBS
Filter through a 0.22µM filter
Store at -20°C

10x Phosphate Buffered Saline (PBS)
160g NaCl
4g KCl
25.2g anhydrous $Na_2HPO_4.12H_2O$
4.8g KH_2PO_4
Make up to 2 litres with dH_2O
pH to 7.4 then autoclave
Store at RT

Trypsin-EDTA
8g NaCl
1.26g Na_2HPO_4
0.2g KCl
0.2g KH_2PO_4
0.5g Trypsin
0.2g EDTA
Make up to 1 litre with dH_2O
pH to 7.4
Filter sterilize through 0.22µM filter
Store at 4°C

Hoechst Stain Working Solution (0,5µg/ml)
1ml Hoechst 33258
100ml Hanks balanced salt solution
Wrap in tin foil and store at 4°C.

Mounting Fluid
22.2ml 0.1M Citric acid
27.8ml 0.2M $Na_2HPO_4.2H_2O$
50 ml Glycerol
Make up to 100 ml and pH to 5.5
Store at 4°C

A.5 STIMULATION EXPERIMENTS

Serum-free medium (HDF)
49.25ml DMEM
250µl FBS
500µl P/S

Serum-free medium (C2C12)
49.25ml DMEM
250µl Horse serum
500µl P/S

10% MG serum (heated to activate latent TGFβ1)
100µl MG serum
900µl Serum-free medium (HDF)
Heat activate at 80°C x 5 minutes
Allow to cool to RT before administering to cells

10% Control serum (heated to activate latent TGFβ1)
100µl Pooled control serum 1:1 (50µl from two different donors)
900µl Serum-free medium (HDF)
Heat activate at 80°C x 5 minutes
Allow to cool to RT before administering to cells

Recombinant human transforming growth factor β1 (rhTGFβ1)
(#240-B, R & D Systems, USA)
Stock solution
Reconstitute at 20µg/ml in sterile 4mM HCl containing 1mg/ml of BSA
After reconstitution; solution is stable at -20°C/-70°C for 3 months or 2-8°C for 1 month
Working solution
Dilute with 4mM HCl containing 1mg/ml BSA to 5µg/ml
(5µl of stock solution @20µg/ml + 995µl of 4mM HCl, 1mg/ml BSA)
Use within 1 month

A.6 PROTEIN ISOLATION & WESTERN BLOTTING

RIPA buffer with SDS
150mM NaCl
1% Triton X-100
0.1% SDS
20mM Tris pH 7.5
1% deoxycholate
Make up to 50ml with dH_2O
Store at 4°C

Supplement with 1 μg/ml aprotinin, 1 μg/ml pepstatin A, 2mM phenylmethanesulfonyl fluoride (PMSF) protease inhibitors (Sigma, USA) and 25x Proteinase Inhibitor Cocktail (Roche, Germany) just before use.

RIPA Buffer without SDS
150mM NaCl
1% Triton X-100
50mM Tris pH 8.0
Make up to 10 ml with ddH_2O.
Filter sterilize with 0.45μm filter
Store at 4°C

Supplement with 1 mg/ml aprotinin, 1 mg/ml pepstatin A, 2 mM phenylmethanesulfonyl fluoride protease inhibitors (Sigma, USA) and 25x Proteinase Inhibitor Cocktail (Roche, Germany) just before use.

RIPA Buffer for phospho-Smad
50mM TRIS-HCl (pH=7.2)
250mM NaCl
2% NP-40
0.1% SDS
0.5% Na-deoxycholate
Make up to final 50ml with ddH_2O
Aliquot into 12ml tubes & store @ 4°C

BCA Protein Determination (Pierce)
Preparing working reagent
Formula
(number of samples) x 2 (duplicate) x 0.2ml (volume of working reagent) = χ ml
Make 50:1 ratio @ A : B (eg. 15ml = 15ml A : 0.3ml B)

- Add 25μl of each standard in duplicate to 96-well plate
- Add 25μl of each sample in duplicate to 96-well plate
- Add 200μl of working reagent
- Cover plate with parafilm
- Incubate at 37°C for 30 minutes
- Cool plate at room temperature
- Read plate @ OD 595nm on plate reader

Sodium Dodecyl Sulphate (SDS)-polyacrylamide gels

Resolving gel

	8%		**10%**	
dH_20	4.6ml	9.3ml	4ml	7.9ml
30% Acrylamide	2.7ml	5.3ml	3.3ml	6.7ml
1,5M Tris (pH=8,8)	2.5ml	5ml	2.5ml	5ml
10% SDS	100µl	200µl	100µl	200µl
10% APS	100µl	200µl	100µl	200µl
TEMED	10µl	20µl	10µl	20µl
Total volume	**10ml**	**20ml**	**10ml**	**20ml**

Stacking gel

	5%	
dH_2O	2.75ml	5.5ml
30% Acrylamide	650µl	1.3ml
1,5M Tris (pH=6.8) / 0,5M Tris (pH=6.8)	500µl	1ml
10% SDS	40µl	80µl
10% APS (make new if >2/3 days old)	40µl	80µl
TEMED	4µl	8µl

Running buffer

10x Running buffer (1000ml)
- 144g Glycerine
- 30g TRIS powder
- 10g SDS
- Make up to volume with dH_20
- pH solution to 8.3

1x Running buffer (1000ml)
- 100ml 10x Running buffer
- 900ml dH_2O
- Store at RT

Transfer buffer

10x Transfer buffer (1000ml)
- 144g Glycine
- 38g Tris powder
- Make up to volume with dH_20

1x Transfer buffer (1000ml)
- 100ml 10x Transfer buffer
- 700ml dH_20
- 200ml Isopropanol/Methanol
- Store in fridge (4°C)

1x PBS/0.1% Tween
1x PBS made up to 1 litre
1 ml Tween 20
Mix well with stirrer bar
Store at 4°C

1x TBS/0.1% Tween
1x PBS made up to 1 litre
1ml Tween 20
Mix well with stirrer bar
Store at 4°C

5% Skim-milk Blocking Buffer
5% powder skim milk (w/v)
Make up to 50 mls with 1x TBS(pSmad3) or 1xPBS(other)/0.1% Tween
Store at 4°C
Use within 7 days

Incubating buffer for 1° Antibody (pSmad3) = 5% BSA in TBS-Tween
2.5g BSA powder
Make up to 50ml with TBS-Tween
Mix well & sore at 4°C
Use within 7 days

Membrane Stripping Buffer
100ml nM β-Mercaptoethanol
2% SDS
62.5ml mM Tris-HCl (pH 6.7)
Fill up to final volume with dH_2O
Cover in foil and store at room temperature

Antibodies

1° Antibodies	**Rabbit monoclonal anti-phospho-Smad3** (#9520, Cell Signalling Technology, USA)	**1:1000**
	Rabbit polyclonal anti-Daf antibody (sc-9156, Santa Cruz Biotechnologies, USA)	**1:200**
	Rabbit polyclonal anti-P38 MAPK (M0800, Sigma, USA)	**1:500**
2° Antibodies	**HRP-conjugated goat-anti-rabbit polyclonal antibody** (BioRad, USA)	**1:4000 -5000**

A.7 IMMUNOFLUORESCENCE & IMMUNOCYTOCHEMISTRY

MYOBFIBROBLAST IF & ICC

1° Antibodies	**Anti-alpha smooth muscle Actin mouse monoclonal antibody [1A4]**, #ab7817, Abcam, UK	**1:100**
	Anti-Collagen alpha2 Type 1 goat polyclonal antibody [COL1A2 (C-19), #sc-8786, Santa Cruz Biotechnology, USA	**1:50**
2° Antibodies	**Alexa Fluor® 488 AffiniPure F(ab')$_2$ Fragment Goat Anti-Mouse IgG (H+L)**, #115-546-146, Jackson ImmunoResearch Laboratories, USA	**1:500**
	Alexa Fluor® 488 AffiniPure F(ab')$_2$ Fragment Donkey Anti-Mouse IgG (H+L), #115-546-150, Jackson ImmunoResearch Laboratories, USA	**1:500**
	Cy™3 AffiniPure F(ab')$_2$ Fragment Donkey Anti-Goat IgG (H+L), #705-166-147, Jackson ImmunoResearch Laboratories, USA	**1:500**

INDUCED PLURIPOTENT STEM (IPS) CELL ICC

Blocking solution for iPS cell ICC
0.5ml FBS (5%)
1µl 0.25% Triton-X stock solution (0.01%)
9.5ml 1x PBS

Antibodies

1° Antibodies	**Rabbit polyclonal to OCT4** #ab19857 Abcam, UK	**1:200**
	Rabbit polyclonal to NANOG #ab21624, Abcam, UK	**1:200**
	Anti-TRA-1-60, Alexa Fluor®488 conjugate (no 2° antibody) MAB4360A4, Merck Millipore, Germany	**1:200**
	Anti-SeVdp NP Kind gift from Professor Mahito Nakanishi, Japan	**1:1000**
2° Antibodies	**Alexa Fluor® 488 AffiniPure F(ab')$_2$ Fragment Donkey Anti-Mouse IgG (H+L)**, #115-546-150, Jackson ImmunoResearch Laboratories, USA	**1:500**
	Cy™3 AffiniPure F(ab')$_2$ Fragment Donkey Anti-Rabbit IgG (H+L), #711-166-152, Jackson ImmunoResearch Laboratories, USA	**1:500**

Hoechst solution for iPS cell ICC
Need 0.5µg/ml
Stock solution = 10mg/ml = 10000µg/ml
Prepare 5µg/ml of stock by diluting 0.5µl in 1ml of block.
Then prepare 0.5µg/ml stock by diluting 200µl in 2ml of block

A.8 STEM CELL CULTURE

HDF (human dermal fibroblast) medium (500ml)
500ml Advanced DMEM (Gibco 12491)
56ml FBS (Gibco or PAA)
5.6ml GlutaMAX 100X (Gibco 35050)
1% penicillin/streptomycin

iMEF (inactivated mouse embryonic stem cell) medium (500ml)
444.5ml Advanced DMEM (Gibco 12491)
50ml Stem cell grade FBS (PAA/Gibco)
5ml 100x GlutaMAX (Gibco 35050)
500µl 1000x 50mM β-mercaptoethanol
Supplemented with P/S at concentration of 1% (5ml P/S per 500ml of iMEF medium)

hES (human embryonic stem cell) medium (500ml)
389.5ml Knockout DMEM (Gibco 10829)
100ml Knockout serum replacement (KOSR) (Gibco 10828)
5ml 100x non-essential amino acids (PAA/Gibco)
5ml 100x GlutaMAX (Gibco 35050)
500µl 1000x β-mercaptoethanol
Filter through a 0.22µm sterile filter & aliquot into 50ml tubes
Aliquots of 40ml stored at -20°C
Thaw overnight at 4°C
Bring to RT before use
Supplement aliquots with 1% P/S (0.4ml of 100x stock/40ml aliquot of hES) and b-FGF (10-20ng/ml of 10µg/ml stock; 40/80µl per 40ml aliquot of hES)

MEF conditioned medium (MCM)
Day 1 Seed 4 x 10^6 iMEFS/T75 flask in 13ml MEF medium at 37°C overnight
Day 2 Replace medium with 13ml hES medium at 37°C overnight
Day 3-8 Collect supernatant into a sterile container every 24 hours for 8-9 days and replenish with a fresh 13ml of hES medium after each harvest
Filter the pooled supernatant through a 0.22µm sterile filter
Store at -20°C
Thaw overnight at 4°C when required
Add 1x penicillin/streptomycin & βFGF (10-20ng/ml) before use

Knockout™ DMEM (KODMEM)
#10828, Gibco, Thermo Fisher Scientific, USA

Knockout™ Serum Replacement (KOSR)
#10829, Gibco, Thermo Fisher Scientific, USA

TrypLE™ Express
#12605-010, Gibco,Thermo Fisher Scientific, USA
Human bFGF (#130-093-839, MACS, Miltenyi Biotec, Germany)

Supplement with 4ng/ml
Dissolve 10µg FGF-2 in 1000ul sterile (0.1%BSA in 1x PBS) = 1,000x concentrate.
Because we freeze hES in 40ml aliquots we freeze 40ul b-fgf aliquots as working stock. Use one aliquot of b-fgf per tube of hES.
OR
Dissolve 50µg FGF-2 in 500ul sterile (SABAX) water = 10,000x concentrate.
For working stock – dilute 1/10 in 0.1% BSA in PBS
Store aliquots at -20°C (up to six months) or long term at -80°C.

ROCK inhibitor (Y-27632, Merck Millipore, Germany)
MW 338.3g/mol/l
Add 10ul (of stock 1mM solution) /ml medium = 10uM/ml
Add ROCK inhibitor to final concentration of 10µM (=10µl of 1mM stock per 1ml of medium)

Gelatine (Sigma G1393)
0.1% in dH_2O

EDTA dissociation solution
500µl of 0.5M EDTA ph=8.0 (stock solution)
500ml of calcium- & magnesium-free PBS
0.9g of NaCl (to adjust osmolarity to 340mOsm)
Filter sterilise through 0.22 µM filter
Store at 4°C
Use within 6 months

100µl of 0.25M EDTA (pH8.0) in 50ml 1x PBS
Filter sterilise through 0.22 µM filter
Store at 4°C
Use within 6 months

Matrigel® preparation
- ≥1 day before passage – put 1x bottle of Matrigel® & 2x 15ml conical tubes on ice in fridge at 4°C overnight
- Aliquot 2mg of Matrigel® into each pre-chilled tube and freeze immediately
- Matrigel® concentration usually 7-10mg/ml (check product sheet for specific batch details)

  Details of Matrigel® in use with our iPS cells

  330µl + 165µl aliquots frozen and stored at -80°C
  Used 1x 165µl aliquot with 12.5ml of DMEM-F12
- 2mg usually sufficient for 2x 6-well plates
- Store aliquots of Matrigel® at -80°C for up to 1 year
- Keep everything cold while preparing Matrigel® to prevent it from setting/hardening
- Use 12ml of cold DMEM-F12 to reconstitute each 2mg aliquot of Matrigel®
- Use 1.5ml of this to thaw and resuspend Matrigel®

- Take this 1.5ml of medium with thawed and resuspended Matrigel® and return it to the rest of the 12 ml of DMEM-F12 in the tube
- Rinse Matrigel® tube again with the same medium
- Mix the Matrigel® well
- Plate 1ml/well in 2x 6-well plates & shake/rock plate to ensure that the entire well surface is covered
- Leave plate at room temperature for ≥30 minutes/coat overnight at 4°C

iPS cell freeze-down/cryopreservation medium
20% DMSO
60% Stem-cell grade FBS/FCS (@-20°C)
20% KODMEM/ADMEM
Keep on ice with basal ADMEM

DNAse
1U/µl
Promega

Mitomycin C
Stock solution = 1mg/ml – Mix 2mg vial with 2ml of dH_2O
Add 100µl of 10x dilution of stock solution of MMC for every 1ml of medium
Recommended dose for inactivation of MEFs = 10µg/ml

Class II biosafety precautions (*Biosafety in Microbiological and Biomedical Laboratories)*
- Working in a biohazard class II cabinet with an ultra-violet (UV) light
- Using only disposable pipettes, gloves and instrumentation which are discarded into a separate plastic waste bag
- Discarding all media and liquids directly into a plastic beaker containing a 1-2% solution of Virkon (Antec International, UK) in dH2O
- Ensuring that the UV light remains on in the hood for at least 30 minutes when work within the hood is completed and all cells have been transferred to the incubator.

Derivation of Primary Mouse Embryonic Fibroblasts or Feeders (Dr Robea Ballo, 2012)

<u>In General lab (Work in a quiet space and minimise talking):</u>
- Dissect mouse embryos 12.5-14.5 p.c. (preferably13.5 or 14.5), Remove each uterine horn as a long "sausage tube" and place in a petri dish of sterile PBS. Remove the individual yolk sacs and place them all in a single dish of PBS.
- Remove head and internal organs from each embryo. Rinse the trunks in DMEM only about three times. Transfer to a 10cm dish lid without transferring the medium. Mince the trunks as finely as possible with surgical blades.
- Transfer the sludge into 10-15 ml of **0.25%** trypsin (1 mL trypsin per embryo) in a 50 mL conical tube. You may have to use some trypsin to transfer the sludge.
- Pull the sludge a few times through a 16 or 18 gauge needle into a 20 ml syringe to disaggregate further.

- Rock cells gently at 37°C for 20-30 minutes. If you don't have a warm rocker, you can also use waterbath and then invert the tube every 3-5 minutes.
- During this time, prepare the 10cm dishes that your cells will be plated onto by coating them with 5ml of 0.1% gelatine in TC. For 13.5 and 14.5pc embryos use one 10cm plate per harvested embryo (for 12.5pc use one dish for two embryos). The cells are accustomed to being packed together in the embryo, so they are happiest very confluent at first.
- Pull everything through the syringe 1 more time, discard blades, syringes and needles in sharps bin.
- Add 20 ml DMEM/FBS/PS medium and 20units of DNAse. Pipette up and down aggressively with a 10cm disposable pipette. You want to try to break up the genomic DNA because it can interfere with the procedure. Some people like to make the mix "foamy" to help – it won't hurt the cells.
- Remove the floating gloop or cartilage bits - be careful, because you could also suck off your cells. This floating stuff is usually no more than 10% of the volume.
- Incubate in this trypsin/medium/DNase solution for 15 minutes.

In Tissue Culture Room:

- Spin down your cells at 1500+ rpm for 5 minutes.
- Remove the supernatant. Wash the pellet once by pipetteing a few times with 20ml medium to get rid of trypsin and DNase. You will find larger bits of cartilage also come floating off into the medium. Try to remove these with a Gilson pipette without removing your cells.
- Spin once more at 1500rpm for 5mins.
- Remove the gelatin and plate cells onto the 10 cm dishes. These cells are passage 0 (p0). Change medium the next day. Cells should be growing nicely, andmay be ready to split already.

The following are the steps to then make your MEFs into Feeders for ES cells:

- When confluent, split each dish onto 2x T75 flasks or 2x15cm dishes. This is a 1:6 split.
- When confluent, freeze down about half of the cells at $3x10^6$ cells/vial. This will be passage 2 (passage 0 on the 10 cm dish, passage 1 in the T75 or 15 cm, and now passage 2 in the vials. Each vial can be thawed later onto one 15cm dish as P2). Take the other half of your batch and split them 1:6 again. They are happy, actively growing cells now, but they will stop growing at passage 4 or 5 if they are simply primary fibroblasts.
- To make MEFs into Feeders, inactivate them for 2.5-3hrs with 10ug/ml Mitomycin C.
- Rinse the **iMEFS** at least 3x with PBS.
- Trypsinise as usual and count the cells (2ml TE/ T75 flask).
- Freeze down as $2x10^6$ and $0.3x10^6$ cells/vial.

$0.3x10^6$ iMEFs are sufficient for 1x 35mm dish or 1 well of a 6 well plate.
$2 x\ 10^6$ iMEFs are sufficient for 6x35mm dishes or 1x 6 well plate.

Preparation of mitomycin C inactivated MEF feeders for hES culture (Kidson lab, 2013)

Note: Make sure new stocks are made well in advance of previous stock running out, as it takes 1 week to prepare the cells, and they need to be tested for at least 3 hES cell passages to ensure that they support growth of hES cells.

- ATCC MEFs are inactivated at p6 / E14.5 MEFs are inactivated at p4-5 [E14.5 outbred mice are harvested from PO mice embryos at 13.5-E14.5d (= Cape Town outbred).
- **Day 1:** Thaw frozen E14.5 cells, resuspend in 10ml PBS, spin at 400g, discard supernatant, resuspend in 20ml MEF medium and plate into a T175 flask.
- **Day 3-4:** Split MEFs when they are ~80% confluent into 3 T175 flasks. Do not allow to get 100% confluent as may induce quiescence. Remove medium, rinse with 10ml PBS, add 3ml TrypLE, incubate at 37^{o}C for about 5mins/until cells have detached, add complete medium and divide into 3 new flasks, total volume 30ml/flask.
- **Day 6-7:** Split again when 80% confluent as described above, into 12 x T175 flasks

Inactivation for ATCC and local outbred Mouse fibroblasts**:**

- **Day 9-10:** Treat cells with mitomycin C. Resuspend 2mg vial in 2ml dH2O = 1mg/ml stock (=100x). NB: It a powerful mutagen, so handle with gloves, be careful of spills, inactivate before throwing away, etc. Add this to 200ml warm MEF medium. Remove medium flasks and add 16.5ml medium with mitomycin C to each, incubate for 2.5 – 3 hours at 37 ^{o}C.
- Harvest cells by removing medium, wash with 10ml PBS, then add 2-3ml TrypLE, incubate for 3mins at 37 ^{o}C. Loosen cells by knocking flask. Remove cells into PBS (diluting TrypLE x10), or into medium, pool cells from all flasks, remove aliquot for cell count, and spin at 400g. Resuspend pellet in freeze medium by triturating thoroughly, aliquot into precooled, labelled, cryovials. Freeze in cryobomb at -80^{o}C. (Rate is -1 deg/min, takes 1.5hrs to get to -80 ^{o}C).

Expected yield: 10-20 x 10^6 cells per flask.
Freeze most at 0.3x10^6, 0.6x10^6, 1 x10^6 cells per vial for passaging into 1-3wells;
About 10 vials at 2 x 10^6/vial for p0 6-well plate for derivation

Reprogramming of HDF to iPS cells using SeVdp (Dr Robea Ballo, 2013)
UCT Stem Cell Lab (modification of WSJ lab in Oxford and Nakanishi lab in Japan)

Day 0:Set up wells for infection
Seed low passage HDF onto wells of 6 well plates @ 0,75 x $10^{5;}$ 1 x 10^5; 1,5x10^5; 2x10^5 /well in HDF medium

Day 1: Infection with SeVdp virus
Take full class II precautions as working with infectious virus. Have extra gloves; bleach/vircon beaker; plastic waste bag; plastic pipettes. Work in virus hood and leave u-v light on for at least 15mins when complete.

Choose the well with cells @ 80-90% confluency for infection
Replace medium before infection with 2ml HDF – P/S
Add 50-100ul virus to well dropwise
Mix through by shuffling L/R, side to side
Stand 2hrs at RT in the TC hood.
Culture O/N @ 37^{o}C and 5% CO_2
Prepare iMEF wells for next day
Gelatinise all wells of a 6 well plate (1ml/well) for 1hr or longer at 37^{o}C.
Thaw iMEFs and seed in MEF medium @ 0.4x10^{6} cells/ gelatinised well.
Leave to settle O/N.

Day 2: Transfer infected cells to iMEFs
Take full class II precautions as working with infectious virus. Take full class II precautions as working with infectious virus. Have extra gloves; bleach/vircon beaker; plastic waste bag; plastic pipettes. Work in virus hood and leave u-v light on for at least 15mins when complete.
iMEFs
Remove MEF medium. Replace with 1ml warm NHDF medium. Return to incubator.

Infected cells
Check under microscope that cells are attached and still okay.
Remove viral medium with plastic pipette.
Discard all viral supernatants into virkon beaker
Wash cells once with 2ml of 1xPBS.
Add 0.5ml TryPLE and incubate 5mins at 37^{o}C.
Aspirate cells and TryPLE into 4.5ml 1xPBS and transfer to 15ml tube. Mix well.
Count the cells.
Meanwhile spin 3mins at 1000rpm.
Remove PBS and resuspend in HDF medium. Adjust medium for 16000cells/ml.
Add cells to iMEFs in wells. Mix well by shuffling plate.

Check the seeding efficiency
Also plate 1ml cells/well onto a well without iMEFs to act as plating check as it is not possible to distinguish between MEFs and HDF when co-culturing the cells.

Day 3: Medium change (Thursday)
Check under microscope that cells have stuck down in seeding efficiency plate.
Remove medium from cells on iMEF feeders.
Rinse feeders 1 x with 1ml warm KODMEM.
Replace with 2ml warm hES medium.
Replace hES medium every 2nd day for the next 6-8 days.
Small 'colonies' should start emerging by this time.
Replace medium every 2nd day with MEF conditioned medium (MCM) thereafter.

Day 15-20 onwards
Observe wells carefully for emergence of stem cell like colonies

Picking iPS colonies

Choose colonies with tightly packed morphology and distinct edge.

When starting, only pick one colony per well and label the colony by marking the lid. Name the colony eg. for patient MG2.3 (family 2, person3) call the first colony MG2.3.1 and the 2nd colony MG2.3.2 etc.

Have 1x 6well plate per colony and label the plates well.
Label the wells when you've plated iMEFs/ date and when you passage the colony.
Do not use feeder layers older than 3days.

Manually passage onto one gelatinised well of iMEFs in hES medium and maintain as normal stem cell, changing 50% hES medium every day and manually passage every 4-5 days for the first few passages.Freeze down or discard colonies as you go along from week to week

Pick colonies from p0 plate if your clones are not growing well.

Bulk up the colonies until you have about 150 good, undifferentiating, colonies per well. Passage half the colonies onto matrigel and passage 2x more on matrigel until there is sufficient for characterisation.

A.9 POLYMERASE CHAIN REACTION (PCR)

Conventional PCR

Conventional PCR was used to check the quality of the synthesised cDNA (and to test the specificity of the primer sets before use in qRT-PCR).

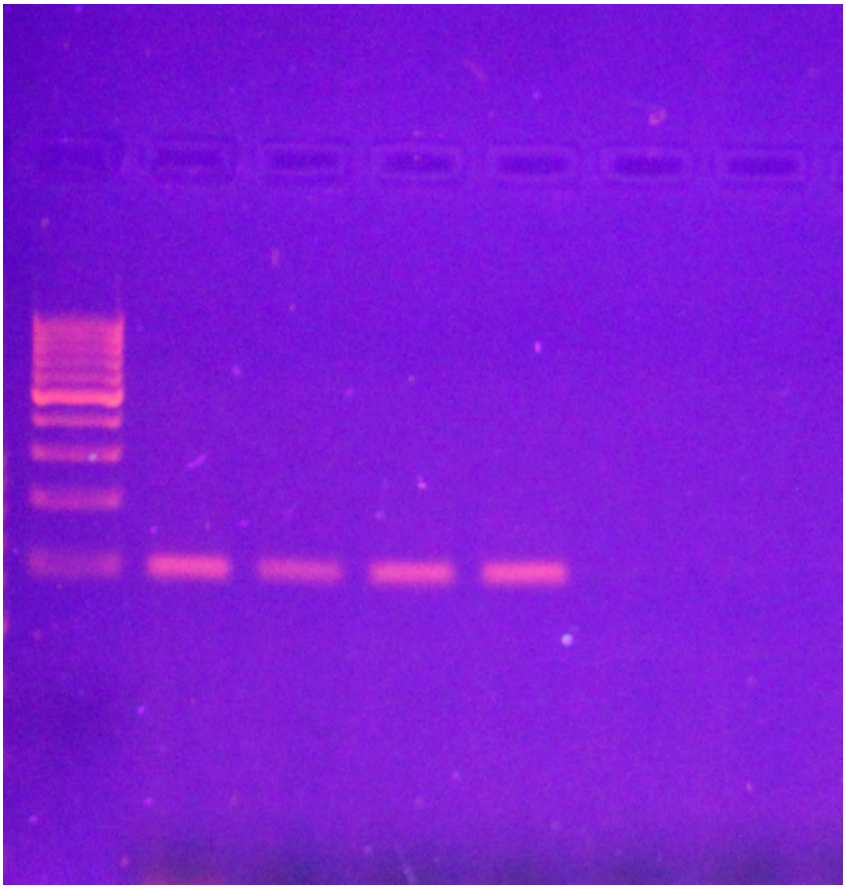

1% agarose gel with molecular marker
Lane 1 = Molecular weight marker
Lane 2 = CT1.5 (comparison iPS cell line)
Lane 3 = HDF (dermal fibroblasts – differentiated)
Lane 4 = MG 822.7 (iPS cell line)
Lane 5 = MG 822.4 (iPS cell line)
Lane 6 = No template control
Lane 7 = Water blank

Primers

Gene	Sequence (5' -3')	Melting Temperature (°C)	Annealing Temperature (°C)	Product size (bp)
OCT3/4	Forward primer – hOCT3/4-S1165 GAC AGG GGG AGG GGA GGA GCT AGG	82	60	143
	Reverse primer – hOCT3/4-AS1283 CTT CCC TCC AAC CAG TTG CCC CAA AC	82		
SOX2	Forward primer – hSOX2-	82	60	150
	Reverse primer – hSOX2	80		
NANOG	Forward primer – ECAT4-macaca-968S CAG CCC CGA TTC TTC CAC CAG TCC C	82	60	388
	Reverse primer – ECAT4-macaca-1334AS CGG AAG ATT CCC AGT CGG GTT CAC C	80		
COL1A1	Forward primer – AAC AGC CGC TTC ACC TAC AG	82	60	
	Reverse primer – AAG CCG AAT TCC TGG TCT G	80		
SEVDP	Forward primer – AGA CCC TAA GAG GAC GAA GAC AGA	72	60	693
	Reverse primer – ACT CCC ATG GCG TAA CTC CAT AG	70		

Components of qPCR cocktail (for one sample)

Component	Manufacturer	Final concentration	Reaction volume
cDNA		50ng/µl	2µl
PowerUp™ SYBR® Green Mastermix	Life Technologies, USA		5µl
Forward primer (10µM)		4µM	0.2µl
Reverse primer (10µM)		4µM	0.2µl
Sabax sterile distilled water	Adcock Ingram, RSA		2.6µl
TOTAL VOLUME			10µl

Cycling conditions for qPCR

StepOnePlus™ Real-Time PCR System cycling conditions

Times & Temperatures			
Initial Steps		Each of 40 Cycles	
		Denature	Anneal/Extend
HOLD	HOLD	CYCLE	
2 minutes 50°C	10 minutes 95°C	15 seconds 95°C	1 minute 60°C

Procedure (concise)

- 1 µg of RNA combined with 0.5 µg of Oligo (dT)15 primer in a 5-10µl volume & denatured at 70°C for 5 minutes
- Chilled on ice and combined with a reverse transcription reaction mix
    - 1X M-MLV RT reaction buffer
    - 2.5mM MgCl2
    - 0.5mM dNTP mix
    - 20 units RNasin® ribonuclease inhibitor
    - 1µl of MMLV- RT) to a final volume of 20µl
- The reactions were incubated at 42°C for 1 hour, followed by 15 min incubation at 70°C to inactivate the reverse transcriptase prior to PCR.
- The plates were sealed with a MicroAmp™ optical adhesive film (Applied Biosystems, USA)
- Centrifuged at 2500 rpm for 20 seconds in an Eppendorf 5810R centrifuge (Eppendorf, Germany)
- Loaded into the StepOnePlus™

Relative Quantification of Gene Expression (Qiagen manual, 2004)

- To interpret data from the reactions and to determine the relative expression of each gene, the crossing threshold values (C_T) were analysed.
- The C_T value represents the cycle number, at which the amplification plot crosses a threshold, indicating that there is a significant detectable increase in fluorescence.
- A mean C_T value was obtained from each target gene, as they were run in duplicate.

- A comparative $\Delta\Delta C_T$ method was used to determine the fold expression for each target gene relative to a callibrator sample
- The endogenous reference gene, β-glucuronidase (GUSB), was used to allow for the normalisation of gene expression for each target gene, to the amount of cDNA.
- Calculation of $\Delta\Delta C_T$ was obtained first by subtraction the C_T value for each target gene from the mean C_T value for the refernce range (C_T target gene – C_T endogenous refernce gene).
- The obtained value, termed ΔC_T, was then used to determine the $\Delta\Delta C_T$ value.
- The $\Delta\Delta C_T$ describes the difference between the average ΔC_T value of the sample of interest and the average ΔC_T value of a reference sample.
- This sample, known as the calibrator sample, is usually obtained from unstimulatied or untreated cells and is used to normalise all other (stimulated) samples.
- Thus $\Delta\Delta C_T$ = average ΔC_T (sample of interest) – average ΔC_T (reference sample). Relative expression levels for each target gene were calculated by the following formula; 2^ ($-\Delta\Delta C_p$) and represented graphically via bar graphs plotted in Microsoft® Excel® for Mac 2011 version 14.4.6 (141106).